HOMEOSTATIC ROLE OF ACID SPHINGOMYELINASE IN MTOR SIGNALING AND AUTOPHAGY

Matthew Jose Justice

Submitted to the faculty of the University Graduate School
in partial fulfillment of the requirements
for the degree
Doctor of Philosophy
in the Department of Biochemistry & Molecular Biology,
Indiana University
April 2017

Accepted by the Graduate Faculty, Indiana University, in partial fulfillment of the requirements for the degree of Doctor of Philosophy.

Doctoral Committee

_____
Irina Petrache, M.D., Co-Chair

_____
Ronald C. Wek, Ph.D., Co-Chair

_____
Peter J. Roach, Ph.D.

_____
X. Charlie Dong, Ph.D.

_____
Xiao-Ming Yin, M.D., Ph.D.

January 19, 2016

Dedication

This thesis is dedicated to all of those who have helped me during my graduate studies. The one person whom this work would not be possible without is my loving wife, LaDonna Marie Justice, a.k.a., Superwoman. To my three girls, Savana, Karianne, and Eliana who have helped me learn that the little things in life are usually just as important as the big things. To my mother who always told me, “Matthew, you can do anything if you put your mind to it.” She was correct–thanks, Mom. To my father who instilled the discipline and logic needed to succeed in this environment. I am appreciative for the monetary supplements along the way as well (all of them)–thanks, Dad. I would also like to thank Dr. Richard Gelderman for inspiring me to do well.

Acknowledgements

First, I would like to thank my mentor, Irina Petrache, for making this degree possible and for taking on the grueling task of furthering my education, professionalism, and mental capacity–no small feat. I would like to thank all of my committee members, Janice Blum, Ronald Wek, Zhong-Yin Zhang, Peter Roach, Charlie Dong, and Xiao-Ming Yin for their critiques, suggestions, advice, and support. I would like to thank both the Indiana University School of Medicine as well as National Jewish Health for providing outstanding environments that are conducive to research and collaborations. I would like to thank the National Institutes of Health for their support through the National Heart, Lung, and Blood Institute in the form of a Ruth L. Kirschstein National Research Service Award Individual Predoctoral Fellowship as well as funding secured through Irina Petrache through the National Institutes of Health. I would like to thank Kelly Schweitzer for her guidance over the years. I would like to thank all of the Petrache lab members, present and former, for all of their help with assays, critiques during lab meetings, fun outings and moral support along the way. I would like to thank my former mentor, Horia Petrache, for impressing upon me the importance of documentation and what it means to be “serious.” I would like to thank Martha Zettlemoyer for all of the good food, in-depth discussions about how biomedical science translates to real-world practices, and, of course, the edits.

Funding Sources: RO1HL077328 (IP), F31HL126459 (MJ)

Matthew Jose Justice

HOMEOSTATIC ROLE OF ACID SPHINGOMYELINASE IN MTOR SIGNALING AND AUTOPHAGY

Key regulatory decisions of protein synthesis and autophagy are controlled by the lysosomal nutrient sensing complex (LYNUS). To engage protein synthesis signaling, LYNUS requires cellular availability of amino acids, adenosine triphosphate (ATP), growth factors, and docking at the lysosomal membrane. The molecular determinants of LYNUS signaling and docking are not completely elucidated and may involve regulators of the lipid membrane structure and function of the lysosome. Since ceramides are both bioactive second messengers and determinants of lipid membrane stiffness, we investigated the role of the ceramide-producing lysosomal acid sphingomyelinase (ASM) in the homeostatic function of mammalian target of rapamycin (mTOR) signaling and autophagy. Using ASM inhibition with either imipramine or siRNA against *SMPD1*, in primary human lung cells or *Smpd1*$^{+/-}$ mice, we demonstrated that ASM is an endogenous inhibitor of autophagy. ASM was necessary for physiological mTOR signaling and maintenance of sphingosine levels. Whereas overstimulation of ASM has been shown to trigger autophagy with impaired flux, inhibition of ASM activity during homeostatic, non-stressed conditions triggered autophagy with degradative potential, associated with enhanced transcription factor EB (TFEB), a master regulator of autophagy and lysosomal biogenesis genes, translocation to the nucleus and decreased sphingosine levels. These findings suggest LYNUS signaling and autophagy are partially regulated by ASM.

Irina Petrache, M.D., Co-Chair

Ronald C. Wek, Ph.D., Co-Chair

Table of Contents

Figures

Abbreviations

4E-BP	4E binding protein
ADP	adenosine diphosphate
AM	alveolar macrophage
AMPk	adenosine monophosphate-activated kinase
ASM	acid sphingomyelinase
ATG	autophagy-related protein
ATP	adenosine triphosphate
BEAS2b	bronchial epithelial cells
Cer	ceramide
COPD	chronic obstructive pulmonary disease
DHS1P	dihydrosphingosine-1-phosphate
DMEM	Dulbecco’s Modified Eagle’s Medium
eIF4E	eukaryotic initiation factor 4E
eIF4F	eukaryotic initiation factor 4F
eIF4G	eukaryotic initiation factor 4G
ER	endoplasmic reticulum
ESI	electron spray ionization
FBS	fetal bovine serum
FFT	fast Fourier transform
FIASMA	functional inhibitor of ASM
GAP	GTPase-activating protein
GDP	guanine diphosphate

GEF	guanine nucleotide exchange factor
GTP	guanine triphosphate
HLMVEC	primary human lung microvascular endothelial cells
HPAEC	primary human pulmonary artery endovascular cells
HUVEC	primary human umbilical vein endothelial cells
LAMP1	lysosome-associated membrane protein 1
LC	liquid chromatography
LC3B	microtubule-associated protein light chain 3 beta
LYNUS	lysosomal nutrient sensing complex
M-6-P	mannose 6 phosphate
MA-NSM	mitochondria-associated neutral sphingomyelinase
MLV	multilamellar vesicle
MRM	multiple reaction monitoring
mRNA	messenger RNA
MS/MS	tandem mass spec
mTOR	mammalian target of rapamycin
mTORC1	mammalian target of rapamycin complex 1
mTORC2	mammalian target of rapamycin complex 2
NMR	nuclear magnetic resonance
NPD	Niemann-Pick disease
NSM	neutral sphingomyelinase
PBS	phosphate-buffered saline
PC	phosphorylcholine

PE	phosphoethanolamine
PGK	phosphoglycerate kinase
PI(4,5)P2	phosphatidylinositol 4,5-bisphosphate
PI3k	phosphoinositide 3-kinase
PIP3	phosphatidylinositol (3,4,5)-trisphosphate
PKB	protein kinase B
PABP	poly A binding protein
POPC	1-palmitoyl-2-oleoyl-*sn*-glycero-3-phosphocholine
PS	phosphatidylserine
RAPTOR	Regulatory-associated protein of mTOR
RHEB	Ras homolog enriched in brain
RICTOR	rapamycin-insensitive companion to mTOR
S1P	sphingosine-1-phosphate
S1PL	S1P lyase
SAXS	small-angle x-ray scattering
siRNA	small interfering RNA
SMPD	sphingomyelin phosphodiesterase
TFEB	transcription factor EB
TSC	tuberous sclerosis protein
ULK	Unc-51-like kinase
ULV	unilamellar vesicle

Chapter 1. Introduction

1.1 Relevance

Acid sphingomyelinase (ASM), a phosphodiesterase that hydrolyzes sphingomyelin to produce ceramide and phosphorylcholine, is most notably known for its role in Niemann-Pick disease (NPD), a lysosomal storage disorder that has recently been shown to involve aberrant autophagy as part of its pathogenesis (Figure 1).[1] Niemann-Pick type A patients have little to no ASM activity and usually die during infancy, while type B patients have about 10% of normal ASM activity and may survive into the second decade of life.[2] Sphingomyelin buildup in lysosomes due to decreased hydrolysis by ASM leads to permeabilization of the lysosomal encapsulating membrane and subsequent release of cathepsin B (a lysosomal cysteine protease) thereby digesting cytosolic proteins needed for cellular function.[1] Sphingomyelin overload also causes dysregulated autophagy, a process that degrades a portion of the cytoplasm in order for the cell to survive during times of nutrient-deprivation—this process will be explained in depth later in the introduction.[1, 3] In the last decade, it has come to light that a number of other diseases exhibit dysregulation of ASM coupled with altered autophagy [4-8]. However, outside of the context of hypo- or hyper-activation of ASM in disease states, very little is known about the homeostatic function of ASM.[5] This thesis sets out to understand the basal role of ASM in homeostatic conditions as it pertains to autophagy. Since autophagy is a process that is signaled by complexes that are anchored to the lysosome, a

Figure 1.

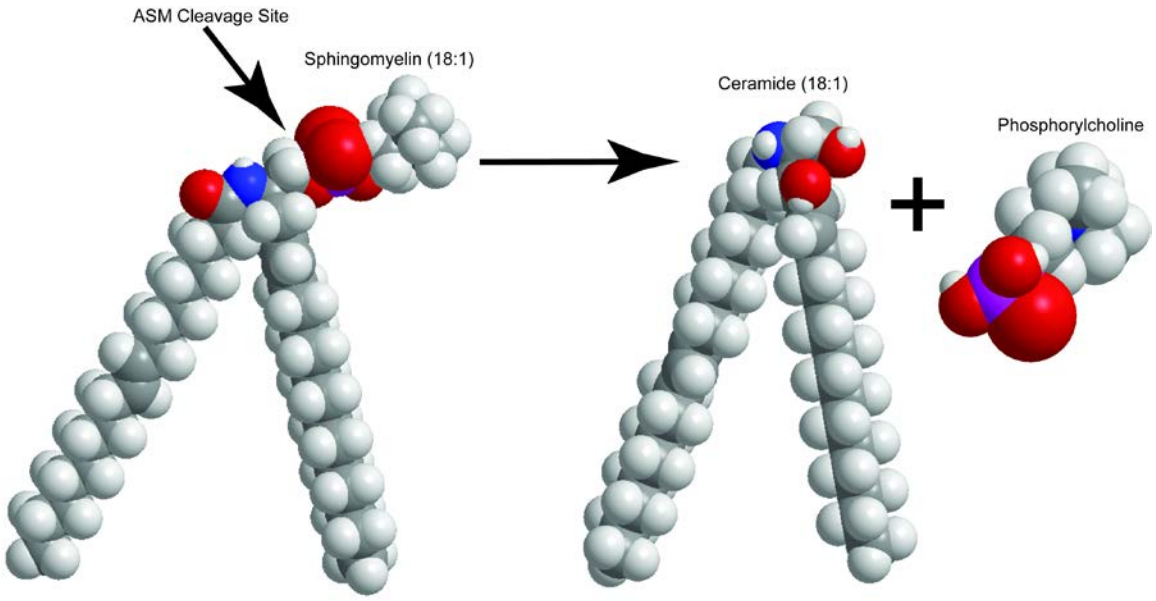

Substrate and products of ASM.

ASM is a phosphodiesterase that utilizes a water molecule to effectively cleave the ester bond of sphingomyelin, producing ceramide (ceramide 18:1 shown) and phosphorylcholine. A space filling model (the size of the sphere is representative of the atomic radius of the atom) of the molecules is shown. Carbons are in gray, hydrogens in white, nitrogens in blue, oxygens in red, and phosphori in fuchsia.

parameter partially controlled by lipid content of the lysosomal membrane bilayer, ASM may be important in the baseline control of this process.[5, 9, 10]

The work contained herein investigates how acid sphingomyelinase acts to regulate autophagy. We will demonstrate that ASM is required for signaling by mammalian target of rapamycin (mTOR), an endogenous inhibitor of autophagy, and, thus, plays a major role in the induction of autophagy. The exact mechanism for this regulation was not elucidated, but may be related to the lysosomal membrane permeable metabolite of ceramide, sphingosine.

1.2 Autophagy

"Self-eating" is the literal Latin-to-English translation of the term autophagy, which was coined by Christian de Duve at the 1963 Ciba Foundation Symposium on Lysosomes, during which he proposed the renaming of Alex Novikoff's cytolysomes to autophagic vacuoles.[11] In times of nutrient and energy deprivation during the life of a cell, autophagy is the process that allows the cell to continue to function by digesting and reallocating a portion of its cytoplasmic contents in an effort to return to an overall replete state (Figures 2 and 3).[3] The autophagic process involves several proteins that work in concert, both spatially and temporally, to produce an intracellular store of accessible nutrients when none are available.[12] There are three modes of autophagy: micro-autophagy, chaperone-mediated autophagy, and macro-autophagy. All three modes involve sequestration of cytoplasmic contents, fusion with a lysosome, and degradation within the newly generated compartment.[13]

Figure 2.

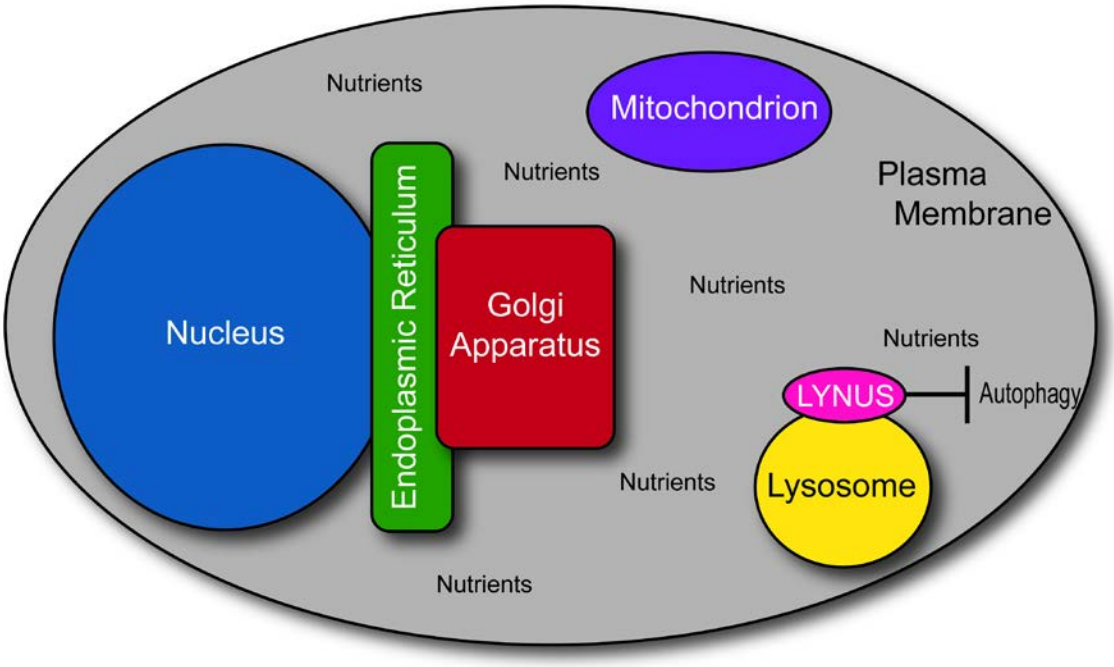

Nutrient Replete State.

During times of nutrient plentitude, protein synthesis occurs and autophagy is not necessary for the cell to survive. Graphic representation of a cell and its organelles, which are indicated with text, color, and shape.

Figure 3.

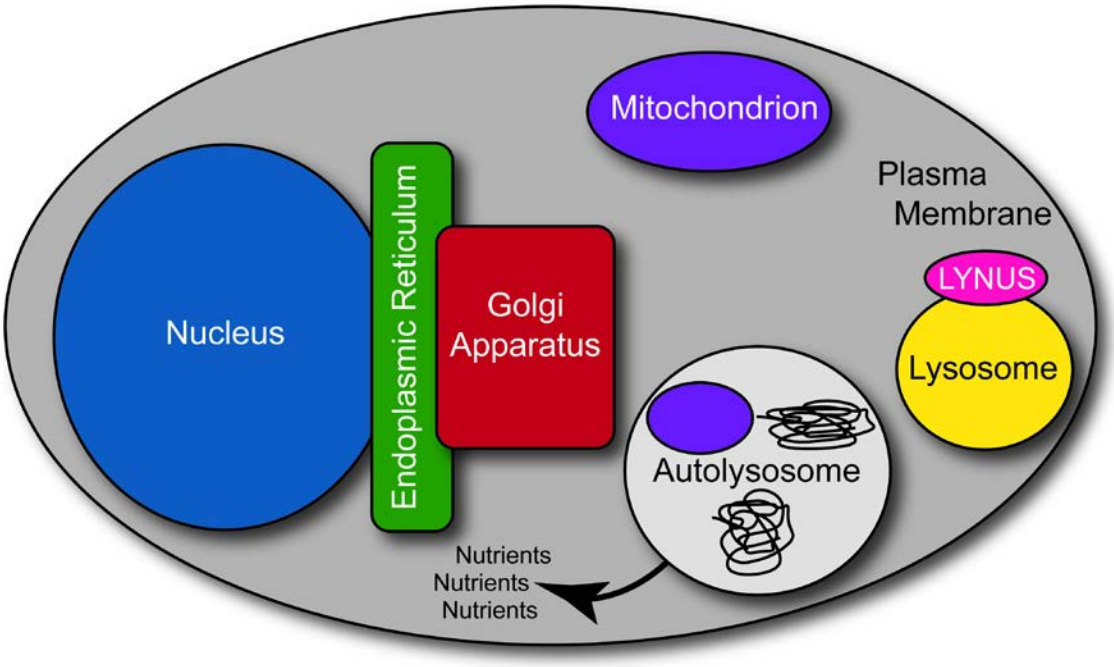

Nutrient deplete state.

During times of starvation, the autophagic process is induced and autolysosomes are formed. Digestion of autolysosomal contents produces nutrients that are distributed back to the cell for survival. Graphic representation of a cell and its organelles, which are indicated with text, color, and shape.

Micro-autophagy refers to an autophagic process in which cytoplasmic contents fuse directly with the lysosome in order to be degraded (Figure 4). In the lysosomal membrane, regions of high lipid content and low protein content allow segments of the membrane to lend themselves to invagination.[14] These microdomains are the sites of micro-autophagic tubule formation, an ATP-dependent process.[15] The tubule elongates, protruding into the lysosomal lumen and drawing the cytoplasmic contents inward. Scission then occurs, trapping the tubule inside the lysosome, where it is degraded by lysosomal hydrolases. Once the contents are degraded, permeases release the energy and nutrients back into the cytosol. This process can engulf both nonspecific and specific substrates, with the latter being the case for the sub-classifications of micro-autophagy of peroxisomes (micropexophagy), micro-autophagy of mitochondria (micromitophagy), micro-autophagy of the ER (ER-phagy), and micro-autophagy of nuclei (piecemeal micro-autophagy of the nucleus).[16]

Chaperone-mediated autophagy is an autophagic process in which specific proteins that contain a particular recognition motif are targeted for degradation and are delivered to lysosomes in, as the name implies, a chaperone-mediated fashion (Figure 5).[17] The recognition motif of a protein to be degraded is a prerequisite for this type of autophagy and can be formed or exposed by either posttranslational modifications or disassembly of complexes. Heat shock protein 70, along with other co-chaperones, recognize and transport the cargo to the lysosomal membrane. At the lysosomal membrane, lysosome-associated membrane protein 2A (LAMP2A) accumulates and facilitates the unfolding of the

Figure 4.

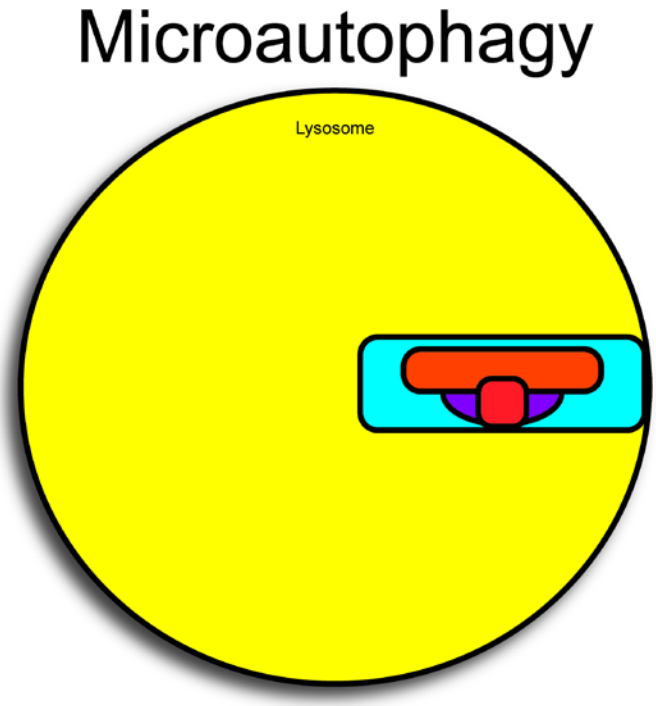

Microautophagy.

Cytosolic contents directly enter the lysosome through invaginations that are caused by differing local lipid/protein contents. After elongation of the tubule, scission occurs, segregating the tubule from the cytosol. The contents of the tubule are then digested for purposes of reallocation. Graphic representation of a lysosome digesting organelles, which are indicated with color and shape (inside of tubule which is indicated with blue).

Figure 5.

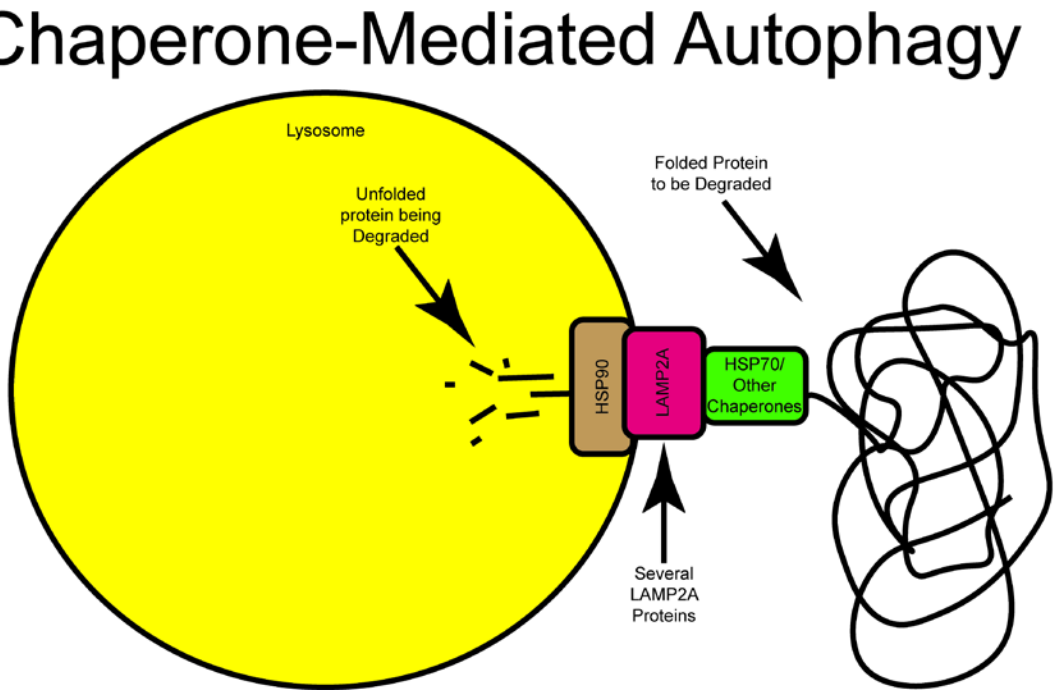

Chaperone-mediated autophagy.

Proteins with certain recognition motifs are recognized by chaperone proteins, which traffic them to lysosome, where other chaperones and lysosome-associated proteins facilitate the unfolding of the protein as well as the crossing of the lysosomal membrane bilayer. Graphic depiction of a protein being unfolded, crossing the lysosomal membrane, and subsequently being degraded.

cargo protein for transit across the lysosomal membrane. Heat shock protein 90, on the luminal side of the lysosome, stabilizes the multiple copies of LAMP2A that are required for passage. Once in the lysosome, degradation happens as described previously.

Macro-autophagy, referred to as simply autophagy hereafter, is the most studied of the different types of autophagy and will be the only type considered in this dissertation. The act of digesting a portion of a cell for the survival of that cell may seem rather trivial, but the molecular mechanisms involved in this “simple” process are quite intricate. When autophagy is induced, an autophagosome forms around the contents to be degraded. An autophagosome must be initiated, elongated, and closed before the autophagosome can be delivered to a lysosome, where it will then fuse with the lysosome, creating an autolysosome [3]. Once the outer bilayer of the autophagosome fuses with the bilayer of the lysosome, degadative enzymes are released into the autolysosome. This is the degradative compartment in which autophagic substrates are broken down for release into the cytosol. Several proteins must act in an orchestrated manner for this process to occur.[12]

Autophagosome formation—specifically, the site(s) where an autophagosome forms and the origins of autophagosomal membranes—is the least understood aspect of autophagy.[12] Several autophagy-related (ATG) proteins take part in the initiation of the autophagosome, but only one kinase, Unc-51-like kinase (ULK), plays a role in initiation; furthermore, the activity of this kinase is currently known to be involved in initiation.[12] The pre-autophagosomal structure that will give rise

to an autophagosome is called the phagophore, or isolation membrane. The phagophore has been thought of as a liposome that has been flattened, having little or no interior region, thus giving rise to two membrane bilayers that can be likened to two pancakes sitting one on top of the other, connected at the edges– much like the folds of the endoplasmic reticulum (ER). Reports in the literature suggest this membrane does originate from ER; however, many different membrane sources, such as mitochondria and molecular mechanisms distal to the ER, are involved and are necessary for autophagosome formation and maturation.[18, 19]

The elongation or expansion of the double-bound autophagosomal membrane requires two ubiquitin-like conjugation systems: the ATG12-ATG5 system and the microtubule-associated protein light chain 3 beta-phosphatidylethanolamine system (LC3B-PE).[12] Just like the attachment of ubiquitin to a protein requires several steps, ATG12 attachment to ATG5 and LC3B attachment to PE—both ubiquitin-like conjugations—do as well. The first step in ubiquitin conjugation is when an E1 activating enzyme, in an ATP-dependent manner, binds ubiquitin. Secondly, the ubiquitin is transferred from the E1 activating enzyme to an E2 conjugating enzyme. Lastly, the E2 conjugating enzyme binds an E3 ligase, which binds the substrate to be ubiquitinated, and the ubiquitin is then transferred to the substrate. The ATG12-ATG5 system is required for elongation of the autophagosomal membrane and is the E3 ligase-like component of the LC3B-PE system. Both systems utilize ATG7 as the E1-like activating enzyme. For the ATG12-ATG5 complex, the terminal

glycine of ATG12 is attached to a cysteine on ATG7 in an E1-like manner. Then ATG7 is switched out for ATG10 in an E2-like manner. ATG12 is then bound to ATG5, which binds ATG16 in an E3-like manner, forming the ATG12-ATG5-ATG16 complex, which serves as the E3 ligase-like component for the phosphoethanolamine lipidation of LC3B. The LC3B protein is produced in a pro-form that has a terminal arginine, which can be cleaved by ATG4, leaving a terminal glycine that can be lipidated in an ubiquitin-like manner. This form of LC3B is referred to as LC3B-I. When autophagy is signaled, the ATG7 enzyme then activates LC3B-I; subsequently ATG3, the E2-like enzyme for this system, switches out with ATG7. Then ATG3 interacts with the E3-like ATG12-ATG5-ATG16 complex, which covalently links LC3B-I to phosphoethanolamine in the membrane of the phagophore. LC3B-I bound to phosphoethanolamine is known as LC3B-II, the most widely accepted marker of autophagosomes. Once the autophagosome is closed, the ATG12-ATG5 machinery dissociates from the autophagosome.

When the autophagosome is formed, it has to be trafficked to a lysosome. The largely accepted mode of transport is *via* the dynein/dynactin system of movement upon microtubules.[20] When the autophagosome arrives at the lysosome, fusion of the outer membrane of the autophagosome with the lysosome must occur in order to make an autolysosome. The transport of autophagosomes to lysosomes is thought to be a calcium-dependent process.[4] Exactly how this process works is largely unknown, but it does not depend on lysosomal acidification.[21] Once an autolysosome is formed, the contents are

degraded in a normal fashion by lysosomal hydrolases and proteinases. These resultant, fundamental building blocks are distributed back to the cytosol *via* permeases in the lysosomal membrane. Upon degradation of the autolysosome, LC3B-II encounters ATG4, which removes the phosphoethanolamine moiety from LC3B-II, thus returning it to LC3B-I and dissociating it from the autolysosomal membrane. The process *in toto*, from initiation to distribution of reallocated essentials, is known as fluxing autophagy–a truly dynamic event.[22]

1.3 LYNUS Complex/mTOR Signaling

There are two distinct complexes, with different functions, in which mTOR is present, mTOR complex 1 (mTORC1) and mTOR complex 2 (mTORC2).[23] The substrate specificity of the complexes are determined by regulatory-associated protein of mTOR (RAPTOR), which is specific to mTORC1, and rapamycin-insensitive companion to mTOR (RICTOR), which is specific to mTORC2. While mTORC2 has role in the regulation of Akt signaling, an upstream mediator of mTORC1, only mTORC1 plays a role in inhibiting autophagy. Henceforth, mTOR will refer to that which resides in mTORC1 and not that of mTORC2.The ULK1 complex was mentioned earlier as the most upstream step in the initiation of autophagosome formation. The ULK1 complex consists of ULK1, ATG13, and FIP200.[24] ULK1 has several phosphorylation sites that determine its kinase activity. Some of these sites, such as the ones phosphorylated by the serine/threonine kinase mTOR, inhibit the kinase ability of ULK1.[25] When the inhibitory sites are not phosphorylated, ULK1 can auto-phosphorylate different sites, greatly increasing its kinase ability. When this happens, ULK1

phosphorylates both ATG13 and FIP200, causing translocation of the ULK1 complex from the LYNUS to ER, initiating autophagy.

The LYNUS is docked at the lysosomal membrane and serves as the metabolic sensor for the cell (Figure 6 and 7).[9] It senses the nutrient status of the cell and promotes protein synthesis during nutrient plentitude and increases autophagy during times of nutrient deprivation. This complex is capable of sensing the availability of amino acids to the cell, the ATP levels in the cell, and whether or not growth factors are present outside of the cell. If glutamine, arginine, and/or leucine as well as ATP and growth factor signaling are present, and the LYNUS is docked at the lysosome, the LYNUS favors mTOR activation.[26] If any one of these conditions is not met, the LYNUS deactivates mTOR and autophagy increases.

In order to accurately incorporate growth cues and survey the energy and nutrient status of the cell, the LYNUS transduces signals from several different proteins, both within the complex as well as externally.[27] The Ragulator, upon sensing amino acids, translocates and helps anchor mTOR from its cytosolic location to the LYNUS.[9] The Ras homolog enriched in brain (RHEB) is a guanine triphosphate phosphatase (GTPase) that localizes to the lysosome where it binds and enhances mTOR activity.[28] RHEB is inhibited by the TSC1/2 complex which receives growth cues from external growth factors *via* the Akt pathway and is necessary for mTOR activity. [9, 29] RHEB also helps to anchor the LYNUS complex to the lysosomal membrane through farnesylation, which involves protrusion of a carbon chain moiety into membrane bilayers.[28, 30] Deciphering of

Figure 6.

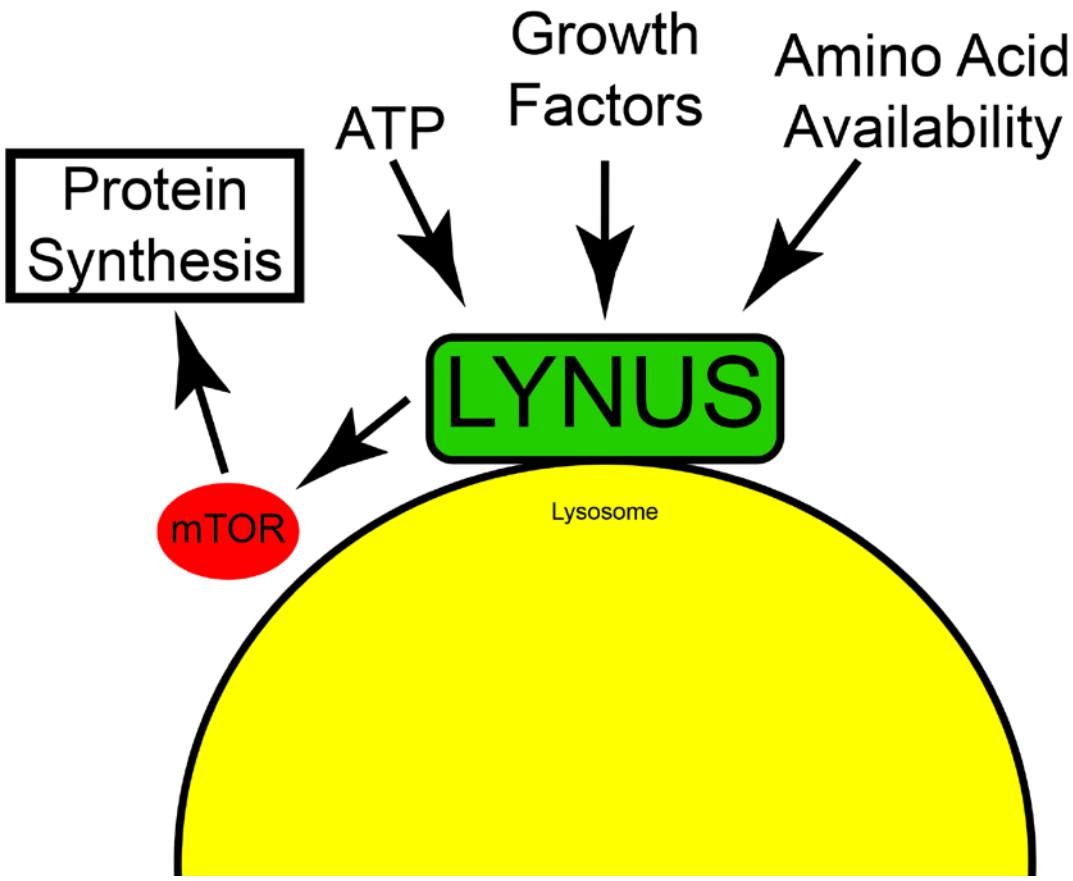

LYNUS signaling in nutrient replete conditions.

If adequate amounts of ATP and amino acids are available and growth factors are present, mTOR phosphorylates its downstream substrates, and protein synthesis occurs. Graphic depiction of the LYNUS machinery, its proximity to the lysosome, and signaling during plentitude of nutrients.

Figure 7.

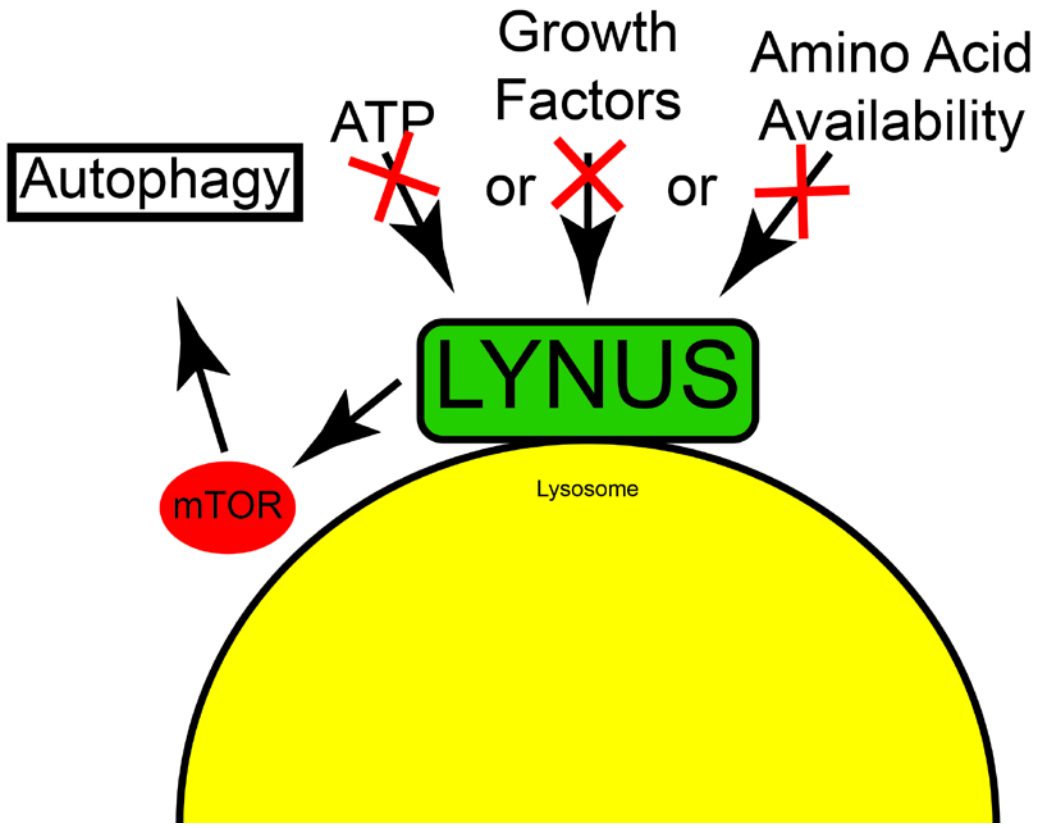

LYNUS signaling in nutrient deplete conditions.

If ATP or amino acids are not available or growth factors are not present, protein synthesis will not occur, and autophagy will ensue. Graphic depiction of the LYNUS machinery, its proximity to the lysosome, and signaling during absence of nutrients.

growth factor signaling and the energy status of the cell happens *via* LYNUS. Together, these proteins sense the needs of the cell and activate signaling complexes accordingly.

The Ragulator consists of five proteins, p18, p14, MP1, HBXIP, and C7orf59, which effectively function as a guanine nucleotide exchange factor (GEF) for the Rag GTPases, Rag A, Rag B, Rag C, and Rag D.[31] A GTPase is able to hydrolyze guanine triphosphate (GTP) to guanine diphosphate (GDP), which switches cascade signaling from on to off. To switch signaling cascades from off to on, GEFs exchange GDP for GTP. Upon sensing amino acids, the Ragulator activates heterodimers of the Rag GTPases, thus recruiting mTOR from a cytosolic location to the lysosome, where it can interact with RHEB, which is necessary for mTOR activity.[32]

When RHEB is located at the lysosome and is in the GTP-bound state, mTOR is active. When RHEB-GTP is hydrolyzed by the tuberous sclerosis 1/2 (TSC1/2) complex to RHEB-GDP, mTOR is no longer active. The TSC1/2 complex effectively inactivates RHEB by acting as a GTPase-accelerating protein (GAP) that constantly associates with RHEB, promoting the hydrolysis of RHEB-GTP to RHEB-GDP.[29] In this way, it acts as an inhibitor to mTOR. The TSC1/2 complex can incorporate exogenous growth factor signals through transduction cascades. For example, when insulin-like growth factor attaches to its receptor, the receptor will change conformation and thereby auto-phosphorylate. The receptor spans the plasma membrane with the ligand site on the extracellular side and the auto-phosphorylation sites on the intracellular side. Phosphorylation

stimulates phosphoinositide 3 kinase (PI3k), catalyzing the production of phosphatidylinositol 3,4,5 trisphosphate (PIP3) from phosphatidylinositol 3,4 bisphosphate (PI(4,5)P2). This newly modified lipid activates PDK1, a master kinase that phosphorylates protein kinase B (PKB/Akt). PKB can phosphorylate TSC2, thus dissociating the TSC1/2 complex and making mTOR active (Figure 8).[23]

Sensing of the cell's energy status, or adenosine triphosphate (ATP) to adenosine diphosphate (ADP) ratio, is an important input to the LYNUS as well. When the intracellular ATP:ADP ratio is low, adenosine monophosphate-activated protein kinase (AMPk) phosphorylates the downstream targets TSC2 and RPTOR, an mTOR binding protein that also dictates mTOR activity. AMPk phosphorylation of RPTOR promotes 14-3-3 binding and suppression of mTOR signaling in energy-deprived states.[24]

As mentioned previously, mTOR inhibits autophagy *via* the phosphorylation of ULK1 inhibitory sites. When active, mTOR directly phosphorylates transcription factor EB (TFEB), a master regulator of lysosomal biogenesis and *ATG* genes, which keeps TFEB sequestered in the LYNUS, rendering it unable to up-regulate genes involved in autophagy and lysosomal biogenesis. When mTOR is inactive, TFEB is dephosphorylated and autophagy is initiated through ULK1. When TFEB is dephosphorylated, it leaves the LYNUS and translocates to the nucleus.[27, 33] When this transcription factor translocates to the nucleus, it up-regulates the production of more than a dozen genes. It is responsible for the up-regulation of itself, genes involved in autophagy, and genes involved in lysosomal biogenesis.

Figure 8.

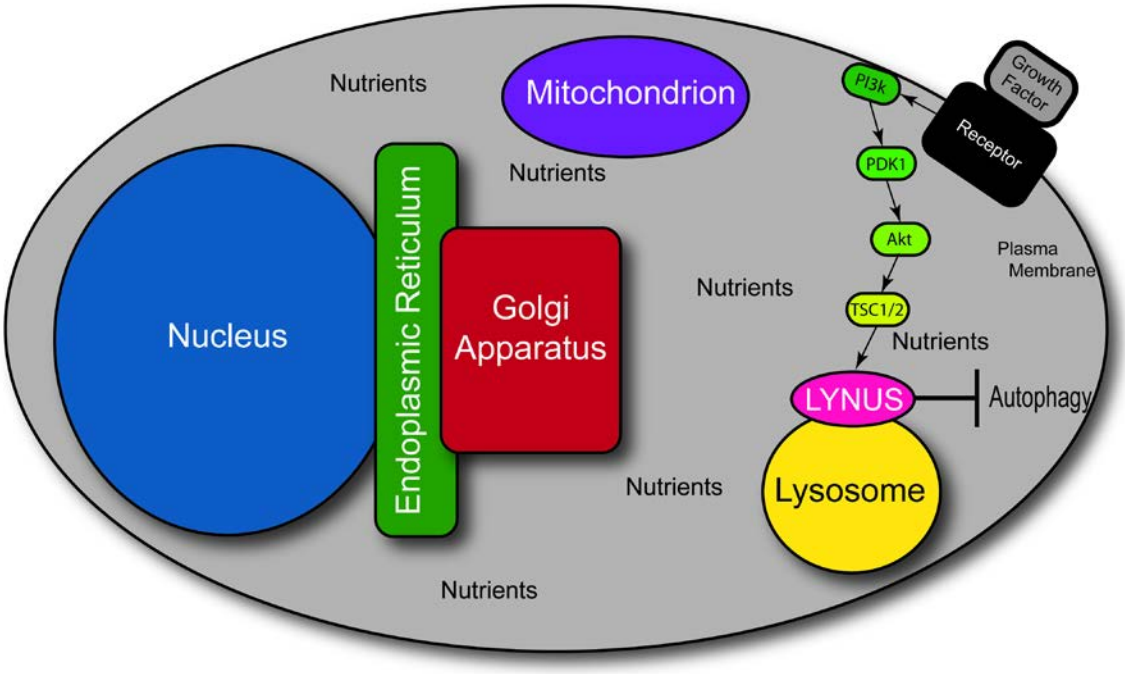

External growth factor signaling cascade.

Extracellular growth factor signal transduction occurs *via* an intricate mechanism that involves many steps, which culminate in the LYNUS's decision to synthesize proteins or break them down to extract their energy. Graphic representation of a cell and its organelles.

The switch from nutrient-generating processes to nutrient-depleting processes occurs when mTOR is switched from off to on by the mechanisms previously described. When active, mTOR phosphorylates P70S6k which subsequently phosphorylates ribosomal protein S6 and thus has implications for enhancing protein synthesis.

Another target of mTOR involved in protein synthesis is eukaryotic initiation factor 4E binding protein (4E-BP).[34, 35] When phosphorylated, 4E-BP dissociates from eukaryotic initiation factor 4E (eIF4E) and allows interaction between eIF4E and the rest of the eukaryotic initiation factor 4F (eIF4F) complex. The 7-methyl guanosine cap of messenger RNA (mRNA) binds to eIF4E, which binds to eukaryotic initiation factor 4G (eIF4G), which is a scaffold that connects to poly A binding protein (PABP) to bind the poly A tail, promoting circularization and translation of mRNA. The LYNUS incorporates the nutrient status of the cell and, through mTOR, induces autophagy when nutrients are low.

1.4 Diagnostic Principles

To assess the autophagic state of a cell, a set of complementary methods need to be employed.[22, 36] Although autophagy is highly dynamic, most available tools only assess snapshots of this process. Even live microscopy has limitations due to decreased resolution and, unfortunately, no live electron microscopy techniques exist at this time. It is possible, however, to label proteins with molecules that fluoresce and to follow the fluorescent labels over time, inferring the underlying actions of the proteins. A combination of endpoints such as autophagic protein levels, light images, fluorescent images, electron microscopic

images, and mRNA levels are available to assess the autophagic state of a given population of cells.[22] To rigorously assess autophagy, at least two complementary methods and proper controls should be used when assessing autophagy. Also, the proper controls to assess autophagic induction versus autophagic flux must be incorporated into autophagy experiments.

As stated previously, the most widely accepted marker of autophagosomes is the identification and quantification of lipidated LC3B-II. Often, Western blotting is used to probe protein levels of tissue or cells for LC3B-II. Accumulation of LC3B-II represents increased autophagosome abundance (Figure 9).[22, 37] To help determine if autophagy is being induced or if autophagic degradation is being decreased when an LC3B-II-increasing stimulus is applied, the autophagic flux must be assessed. Chloroquine (an anti-malarial agent) is a useful tool to assess autophagic flux; this weak base allows assessment by raising lysosomal pH through ion-trapping in the lysosome. Another way to raise lysosomal pH without utilizing lysosomotropic properties is by inhibiting vacuolar ATPases, such as with bafilomycin. Since lysosomal enzymes are pH-dependent, raising the pH of the lysosome will inhibit the activity of these enzymes, prevent autophagic cargo breakdown, and decrease LC3B-II turnover—known as blockage of the autophagic flux (Figure 10).[22] The increase of LC3B-II levels when chloroquine and stimulus are applied together, above that of stimulus alone, indicate that autophagy is being induced.[22] If the levels of LC3B-II are the same with stimulus in the presence and absence of chloroquine, the autophagic flux is thought to be blocked by the stimulus.

Figure 9.

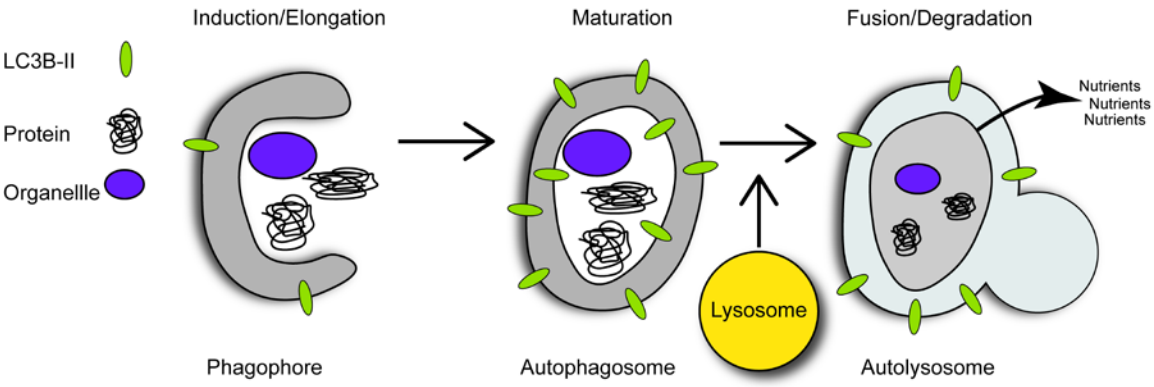

LC3B-II accumulation in relation to autophagosome formation and degradation.

When autophagy is induced, the autophagosomal marker LC3B-II is incorporated into the phagophore. Increased levels of LC3B-II are present in a fully formed autophagosome. Since LC3B-II is turned over in the degradation process, decreased levels of LC3B-II are associated with autolysosomes.

Figure 10.

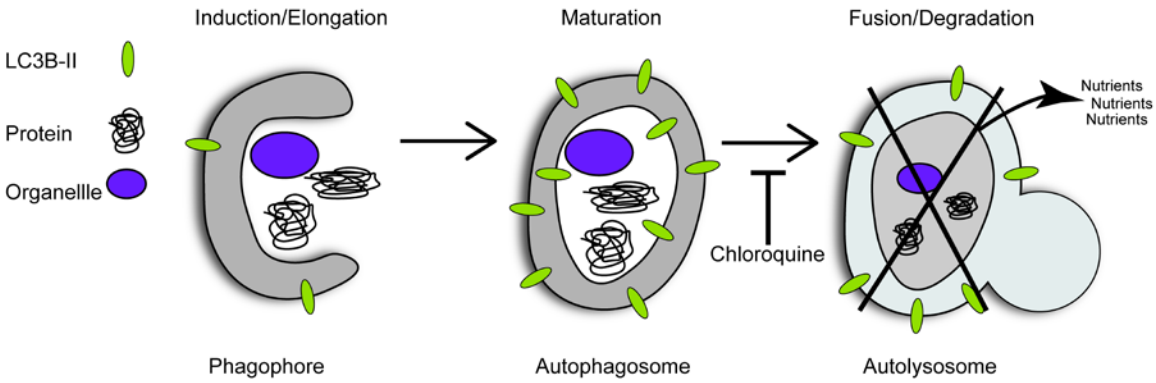

Blocked autophagic flux increases LC3B-II levels.

Autophagosomal marker LC3B-II can be increased in a cell due to either increased autophagic induction or decreased autolysosomal degradation. Color representation of autophagosome-lysosome fusion.

1.5 The Ceramide Pathway

Ceramide is a bioactive sphingolipid that acts as both a second messenger and as an architectural lipid.[38, 39] The cell can synthesize ceramide from the *de novo* pathway, the recycling pathway, and the hydrolysis pathway (Figure 11).[40] Downstream metabolites of ceramide, such as sphingosine and sphingosine-1-phosphate, have crucial signaling roles in the cell as well.[41] The generation of specific chain length ceramides is also possible.[42]

Ceramide is a general term that signifies a class of sphingolipids due to the "R" group that exists on this molecule. The "R" group refers to an acyl chain that can be of varying length and can contain double bonds. Each ceramide molecule contains a carbon chain of 18 carbons with a double bond between carbons four and five. The number two carbon has an amide linkage, while the first and third carbons have hydroxyl groups. The length of the acyl chain that emanates from the amide group determines the exact ceramide species. Acyl chains up to 20 carbons in length are considered long chain ceramides, while acyl chains of greater than 20 carbons are considered very-long chain ceramides.

The *de novo* pathway of ceramide generation, which happens in the endoplasmic reticulum, utilizes the substrates palmitoyl coenzyme A and an amino acid (usually serine), along with the serine palmitoyltransferase enzyme, to produce 3-ketosphinganine (Figure 12). This is the rate-limiting step of the reaction, i.e., it controls the rate at which ceramide can be made *via* the *de novo* pathway. The enzyme 3-ketosphinganine reductase acts on 3-ketosphinganine to form sphinganine, also known as dihydrosphingosine. Once dihydrosphingosine

Figure 11.

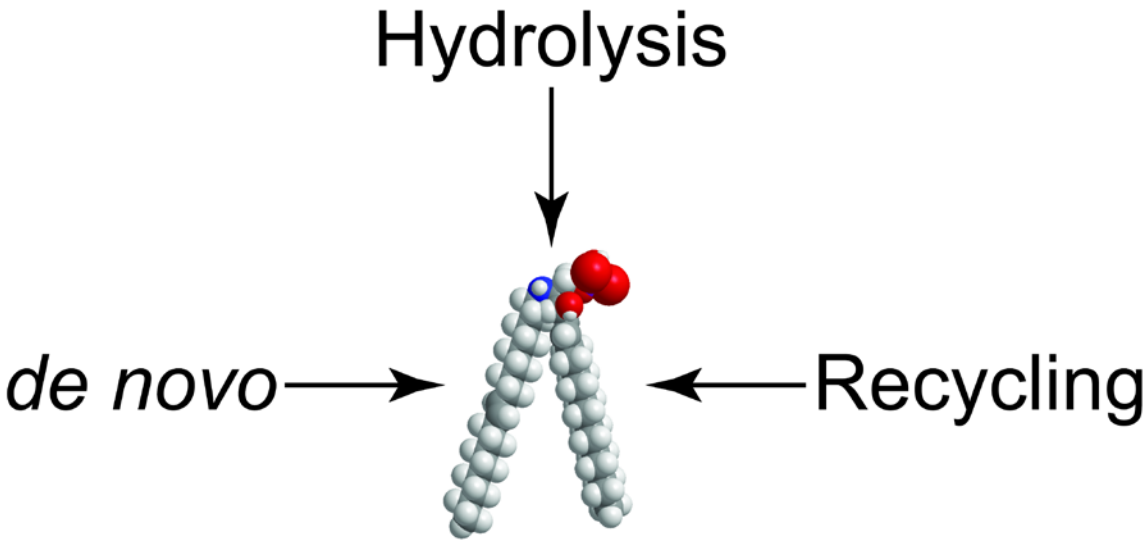

Ceramide synthesis.

Ceramides can be synthesized in the endoplasmic reticulum *via* the *de novo* pathway; they can be synthesized from downstream metabolites (recycling); or they can be produced rapidly by the hydrolysis of sphingomyelin. Carbons are in gray, hydrogens in white, nitrogens in blue, and oxygens in red.

Figure 12.

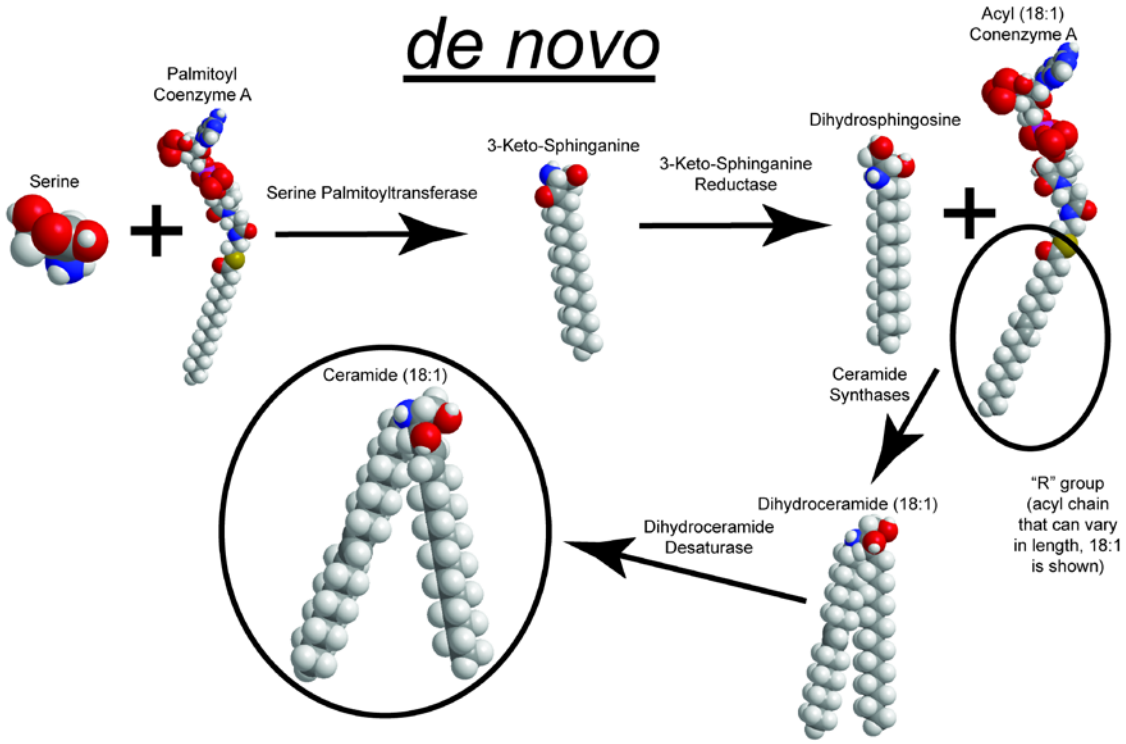

The *de novo* generation of ceramide.

Generation of 3-keto-sphinganine occurs when serine and palmitoyl coenzyme A are utilized as substrates by serine palmitoyltransferase. This if the first step in the synthesis of ceramide and also the rate-limiting step. After dihydrosphingosine is synthesized, ceramide synthases, that utilize acyl coenzyme A, generate dihydroceramide. The acyl chain length can vary and is depicted by an "R" group. Ceramide desaturases insert a double bond to generate ceramide. Carbons are in gray, hydrogens in white, nitrogens in blue, and oxygens in red.

is formed, ceramide synthase acts on this substrate, producing dihydroceramide. Dihydroceramide desaturase utilizes dihydroceramide to produce ceramide. Once ceramide is formed, ceramidases are able to convert this molecule into sphingosine. Finally, sphingosine kinases can act upon sphingosine to form the molecule sphingosine-1-phosphate. This is the most downstream metabolite in the ceramide pathway and can be acted upon by sphingosine-1-phosphate lyase (S1PL) to form hexadecenal and phosphoethanolamine. The last reaction by S1PL is a terminal reaction, as its products permanently exit the ceramide pathway.

The recycling/salvage pathway consists of any route back to ceramide from either a ceramide precursor or ceramide metabolite. Most metabolites in the ceramide pathway can be converted back to ceramide, including sphingosine, ceramide-1-phosphate, glucosyl ceramides, and galactosyl ceramides (Figure 13). The other route to ceramide production is via the hydrolysis of sphingomyelin (Figure 14).

The enzymes responsible for ceramide generation *via* the hydrolysis pathway are sphingomyelinases, which fall under either category of neutral sphingomyelinases (NSMs) or acid sphingomyelinases (ASMs). The different groups of sphingomyelinases have different pH optima, spatial distributions throughout the cell, and divalent ion dependence. Five mammalian sphingomyelin phosphodiesterases (SMPDs) have been characterized to date.[43] SMPD1 is an acidic acid sphingomyelinase and is the focus of this work.[44] SMPD2-4 are neutral sphingomyelinases and correspond to NSM (MA-NSM).[45]

Figure 13.

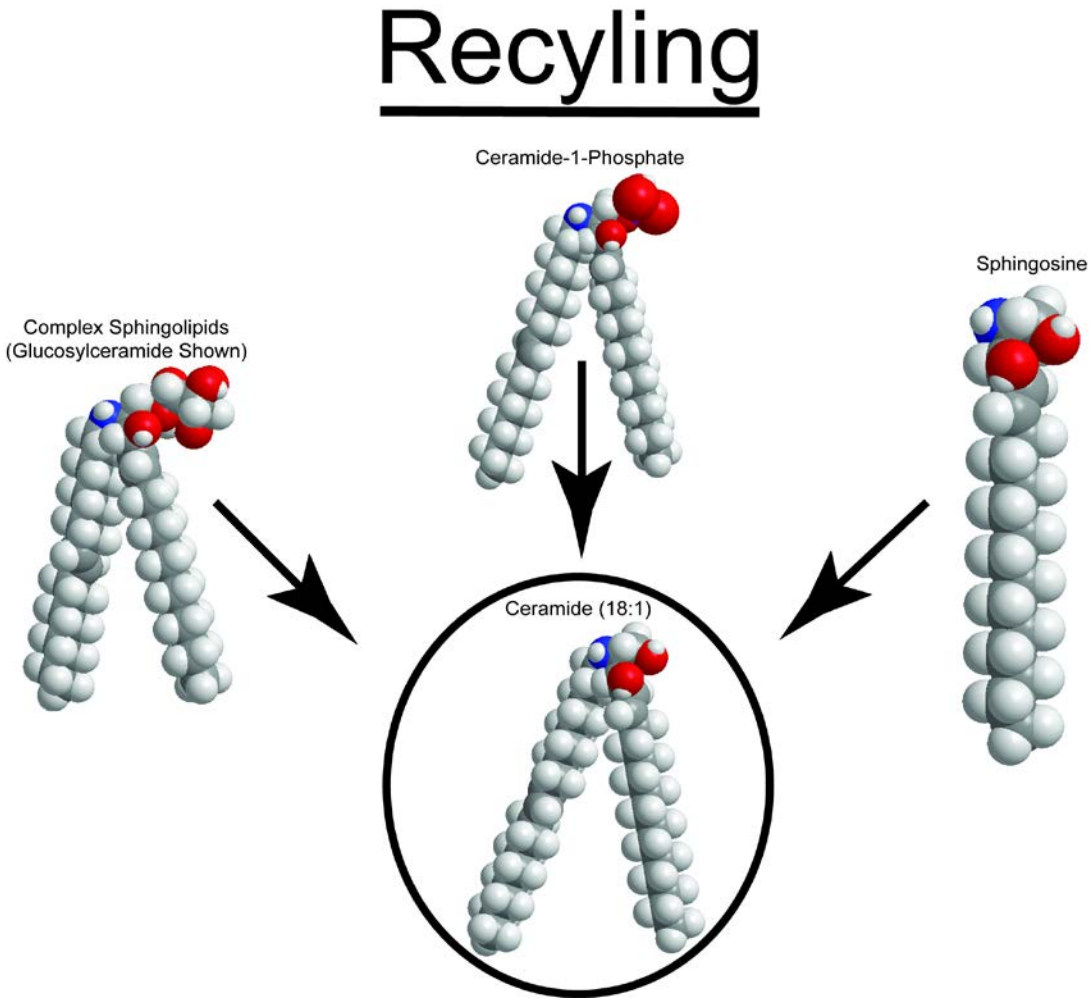

The recycling pathway.

Ceramide is modified by addition or subtraction of certain moieties that can be modified in the opposite manner to generate ceramide. Carbons are in gray, hydrogens in white, nitrogens in blue, and oxygens in red.

Figure 14.

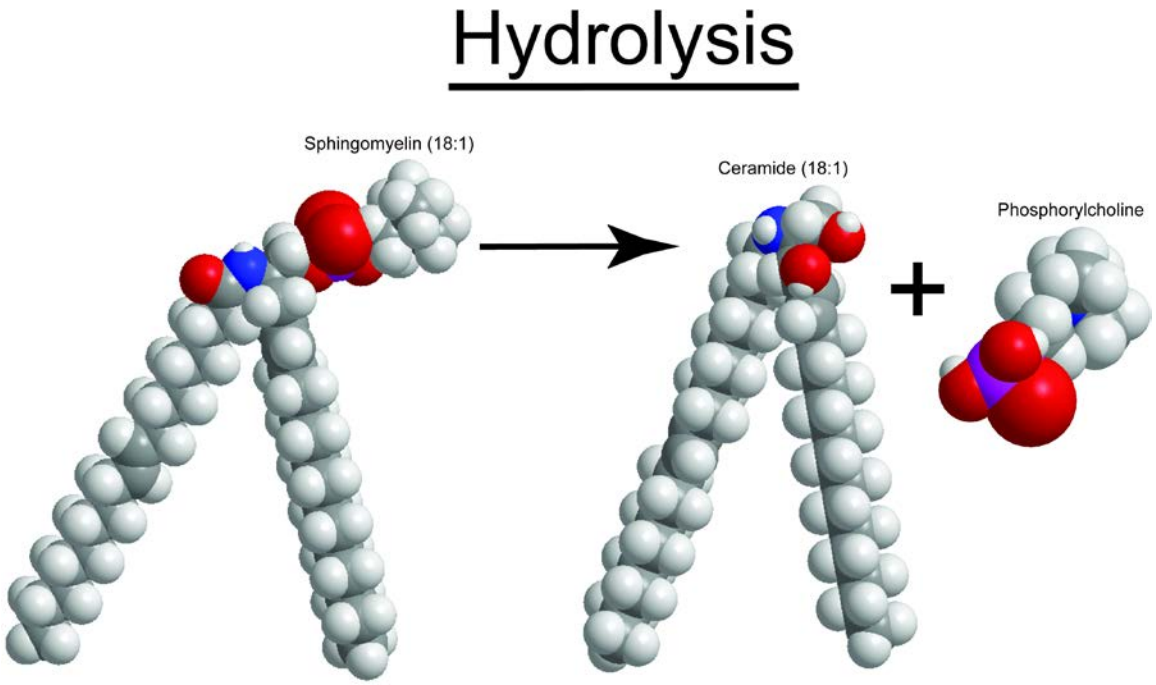

The hydrolysis pathway.

Sphingomyelin, part of the lysosomal membrane bilayer, can be rapidly hydrolyzed to produce ceramide. Carbons are in gray, hydrogens in white, nitrogens in blue, oxygens in red, and phosphori in fuchsia.

These enzymes work optimally at a pH of around 7. All of the NSMs share the characteristic of divalent cation dependence, which Mg^{2+} or Mn^{2+} usually satisfies. SMPD2 (corresponding to NSM1) is localized and performs its function at the endoplasmic reticulum. Little is known about this enzyme, as overexpression did not lead to changes in sphingolipid abundance or metabolites and SMPD2 knockout mice did not exhibit any phenotypical changes. SMPD3 (corresponding to NSM2) is a brain-specific enzyme and may preferentially produce very-long chain ceramides from very-long chain sphingomyelins.[46] The location of this enzyme is primarily at the inner leaflet of the plasma membrane, but it has been reported to be located at the Golgi apparatus. SMPD4 (corresponding to NSM3), unlike SMPD2 and SMPD3, does not have transmembrane domains but is a C-tail anchored protein.[47] The sequence identity of SMPD4 has very little in common with SMPD2 or SMPD3 but is highly conserved across species. Although SMPD4 is not homologous to SMPD2 or SMPD3, it does share functional similarities in that it is able to hydrolyze sphingomyelin to produce ceramide and phosphorylcholine.[48] There are reports in the literature that this enzyme has been found at the mitochondrial outer membrane, the endoplasmic reticulum, and the Golgi apparatus. SMPD5, a MA-NSM, is the most recently characterized NSM and shares sequence identity with SMPD3.[45] SMPD5 can be found at the mitochondria and endoplasmic reticulum.

1.6 Ceramides Stiffen Membranes

The structure and function of a lipid bilayer is dependent upon the lipids in that bilayer. How likely the outer membrane of an autophagosome is to fuse with

the lysosomal membrane is partially dependent upon the lipid constituents of the two membranes. Whether or not microdomains needed for signaling coalesce are determined by the biophysical properties of the membrane as well. Since ASM produces ceramides, and ceramides tend to incorporate into lipid membrane bilayers, it is essential to understand how such a perturbation affects membrane bilayers.

In the late 1700s, Benjamin Franklin observed that a teaspoon of oil, when poured into a pond, spread out on top of the water, covering an area of about one-half acre. Oil behaves in this manner due to interactions between the water and the oil, more specifically, between the hydrophilic portions of the fatty acids that constitute the oil and the polar water molecules. Fatty acids contain a polar carboxylic acid attached to a hydrophobic carbon chain. The lowest energy state for this system is when the hydrophilic or polar portion of the fatty acid molecule is in contact with the water. When this happens, the hydrophobic carbon chains are exposed to the air, and the oil molecules will spread out side by side, creating an area of oil that is only one oil molecule thick. The very same forces are at work in membrane bilayers.

In 1925 Grendel and Gorter solidified the idea that a fatty layer, two molecules thick, covers chromocytes of the blood.[49] Around 1960, it was proven by electron microscopy that a membrane bilayer, the plasma membrane, enveloped cells, allowing for semipermeable diffusion.[50] In the early 1970s, the fluid mosaic model of the plasma membrane was proposed and is now widely accepted.[51] This model of the plasma membrane consists of a membrane bilayer

with proteins protruding halfway or all the way through the membrane. In the fluid mosaic model, lateral lipid diffusion occurs, allowing lipids in an individual bilayer to move laterally within that bilayer. Today we know that organelles and other structures, such as vesicles or autophagosomes, are enveloped by one or more membrane bilayers.[52] For example, lysosomes are walled off by a single-membrane bilayer, and autophagosomes enclose cytoplasmic contents with a double-membrane bilayer.

In full cognizance of other organizing principles, such as van der Waals forces, Haamaker constants, and inter- and intramolecular forces, it suffices for this work to state that the hydrophobic portions of a lipid-water system will aggregate in such a manner as to attain the system's lowest possible energy state. [53] When hydrated, lipids, the primary constituent of membrane bilayers, will arrange themselves into lipid bilayers with the hydrophobic regions segregated from the hydrophilic regions (Figure 15).[54] The hydrophobic fatty acid portion of lipids will always be in very close proximity with the fatty acids of the other lipids in the system, so the membrane bilayer will always remain intact. As mentioned earlier, lipids can move laterally within this "intact" bilayer—a fluid sheet (Figure 16). These properties allow for the semi-permeability, which is crucial for biological processes. Lipids also have many other available motions or degrees of freedom within the membrane bilayer. The system of a bilayer is not totally ordered, as is a crystal, yet it is not totally disordered, as is a liquid. It is, rather, somewhere in between these two extremes and can be described as a liquid-crystalline system. Whole lipids have the ability to move quickly in two

Figure 15.

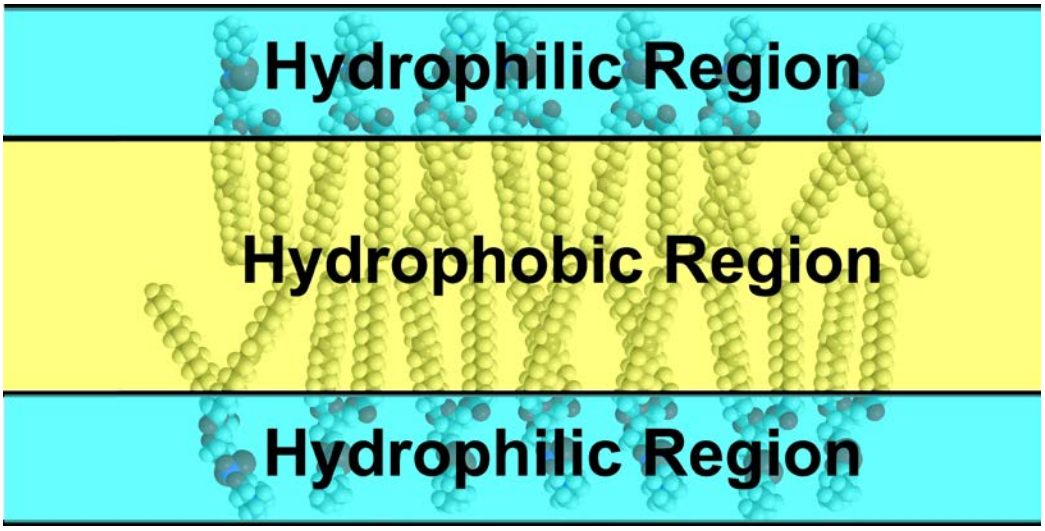

Amphiphilic nature of membrane bilayers.

When hydrated, lipids will form membrane bilayers with hydrophobic fatty acyl chains comprising the “middle” portion of the bilayer, leaving the polar head groups to face away from the hydrophobic region.

Figure 16.

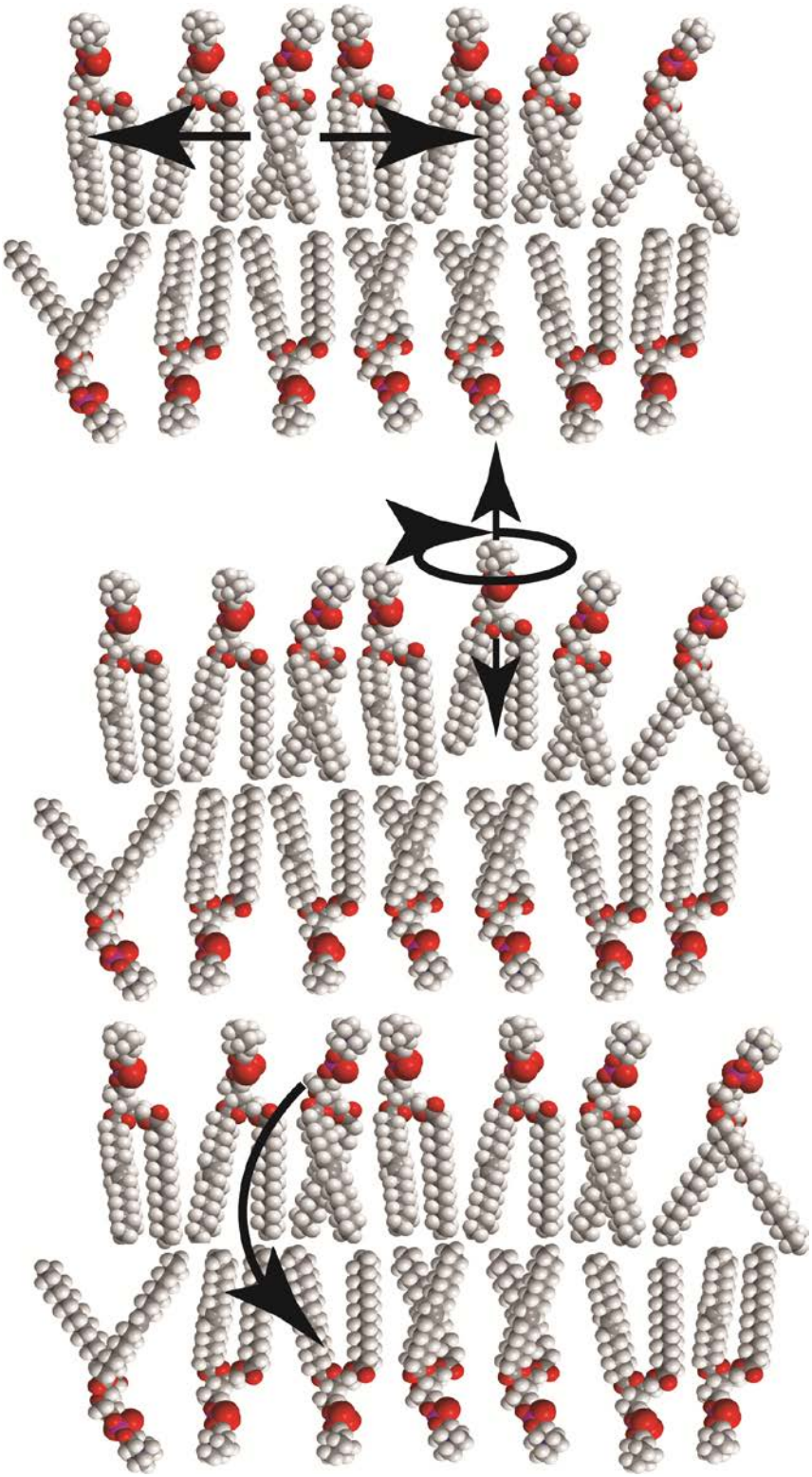

Movements of lipids within bilayers.

Lipids in a bilayer are free to move laterally in the bilayer, but the hydrophobic region remains associated with the interior of the membrane during these translations (top). Lipids are free to rotate in the bilayer and may move up and down with respect to the bilayer normal as well (middle). Lipids have the ability to cross the hydrophobic barrier to the opposite leaflet of the membrane (bottom).

dimensions inside the lipid bilayer and, depending upon the lipid constituents of the rest of the bilayer, may or may not readily coalesce with other freely mobile lipids inside the same sheet. Therefore, it is possible to have a “lipid raft” inside the sheet, enabling lipid composition of the bilayer to influence signaling domains required for transduction of extracellular stimuli. Lipids can move in an up and down direction perpendicular to the sheet and are able to rotate about this same axis (Figure 16). “Flip-flop transition,” or movement of a lipid across the bilayer, is possible but is energetically unfavorable (Figure 16).[55] Proteins called "flippases” transport lipids across the hydrophobic region in response to signaling cues or at basal rates.[56] Lipids are also free to rotate and traverse the lipid bilayer. Lipids are amphiphilic molecules, whereby, the polar head group of a lipid is the hydrophilic portion, and the fatty acyl chain is the hydrophobic portion rendering the membrane bilayer two lipid molecules thick (Figure 15).

The composition of lipids that make up the bilayer is a partial determinant of membrane function. For example, if all of the lipids in a membrane bilayer were stiff, the membrane as a whole would be rigid and have a higher energy barrier for fusion—such as an autophagosome fusing with a lysosome. If the lipids in the bilayer were less stiff, the membrane as a whole would be more undulating, creating a lower energy barrier for fusion. Membrane composition determines the stiffness of the bilayer partially *via* acyl chain order parameters.[57] A fatty acyl chain is a series of carbons with a carboxylic acid at the end that is able to be esterified, thus linking it to a lipid head group. A lipid can be thought of as a head group with fatty acyl tails. If the head is held still, then the first carbon in the tail,

adjacent to the head group, is “anchored.” The second carbon, attached to the first and third carbon, is able to swing through a certain arc of motion. The third carbon, attached to the second and fourth carbons, is also able to swing with more motion than the second but less than the fourth. Because it is farther down the chain and a greater distance from the head, the third carbon has a wider range of motion than the second. The same principle transmits all the way down the chain through the terminal methyl group (Figure 17). The terminal group has the greatest motion, or the least order. An apt analogy is what happens when someone holds a chain that is 20 chain links long by their thumb and forefinger. If the person’s hand is still, the chain is still and hangs in a straight line. If the person moves his or her hand slightly back and forth, the chain will move. The chain link that is being held by the thumb and forefinger has no motion other than that of the collective thumb-chain-forefinger system movement. The second chain link is free to move, but only within the parameters that are set by the physical aspects of the chain link, such as its length. The third link will have greater motion than the second, and the fourth greater than the third, until the final chain link, which will have the greatest motion.

The motion potential of a unit within a chained structure can alternatively be described it in terms of how ordered it is. For example, the last, or greatest motion, chain link from the preceding example can be described as being the least ordered, the first chain link the most ordered. In liquid-crystalline systems the scalar, which is averaged both in space and in time, used to represent order parameter of carbons is denoted as S_{CD}.[58] This parameter can range from zero to

Figure 17.

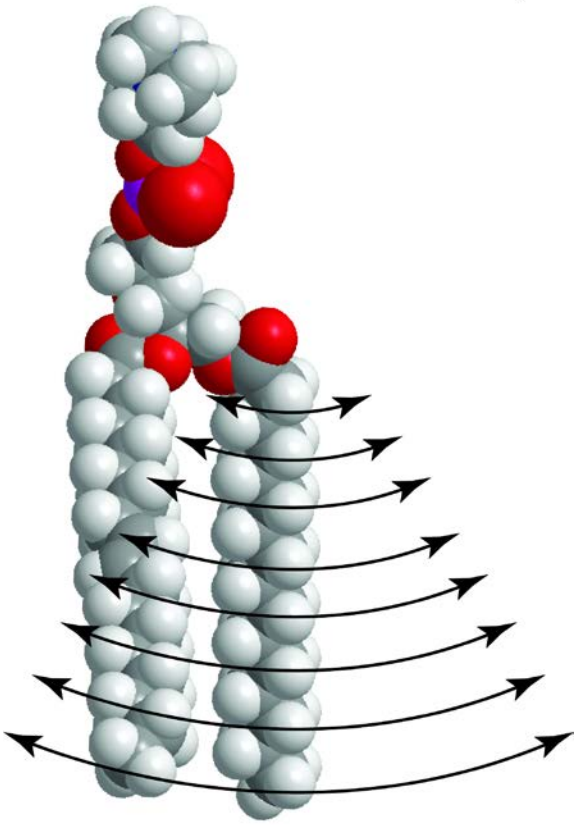

Acyl chain motions within the bilayer.

The acyl chains of a lipid constantly move in the hydrophobic region of the membrane, with the carbon closest to the head group having the least movement and the terminal methyl having the most. Alternatively, the carbon closest to the head group has the most order and the terminal methyl the least. Double-headed arrows represent possible motions of respective carbons.

one-half, with zero representing no order and one-half representing the most order. The motion of individual carbons in the fatty acyl tail of a lipid can be determined using several different methods, one of which is by solid state deuterium nuclear magnetic resonance (NMR).[59] Order parameters are measured by effectively looking at the orientation of carbon-deuterium bonds in a perdeuterated lipid.

A perdeuterated lipid is one that has had all of the hydrogens removed from one of the fatty acyl tails and replaced with deuterium atoms (Figure 18). The van der Waals forces are virtually unchanged by the substitution. A signal from the deuterium is obtainable *via* NMR, which allows for the calculation of the order parameter of the carbon-deuterium bond for each carbon in the chain, starting with the second carbon since the first one is “anchored.” The forces that govern intramembrane properties are much greater than intermembrane forces; therefore, a small change in order parameter can cause a large change in the behavior of the membrane bilayer and how it interacts with other bilayers. Intermembrane forces may be much smaller in magnitude, but they are just as important. The most abundant lipids in human cells are those of the phosphorylcholine (PC) class.[38] The majority of lipid components of the outer leaflet of plasma membranes that encapsulate cells are of this class. PCs comprise a large portion of most intracellular organelle-encapsulating membrane bilayers as well. When trying to study the complexly functioning membrane bilayer of a mammalian cell, it can be advantageous to model the membrane with only lipids to eliminate the confounding factors that exist in cells. Membrane

Figure 18.

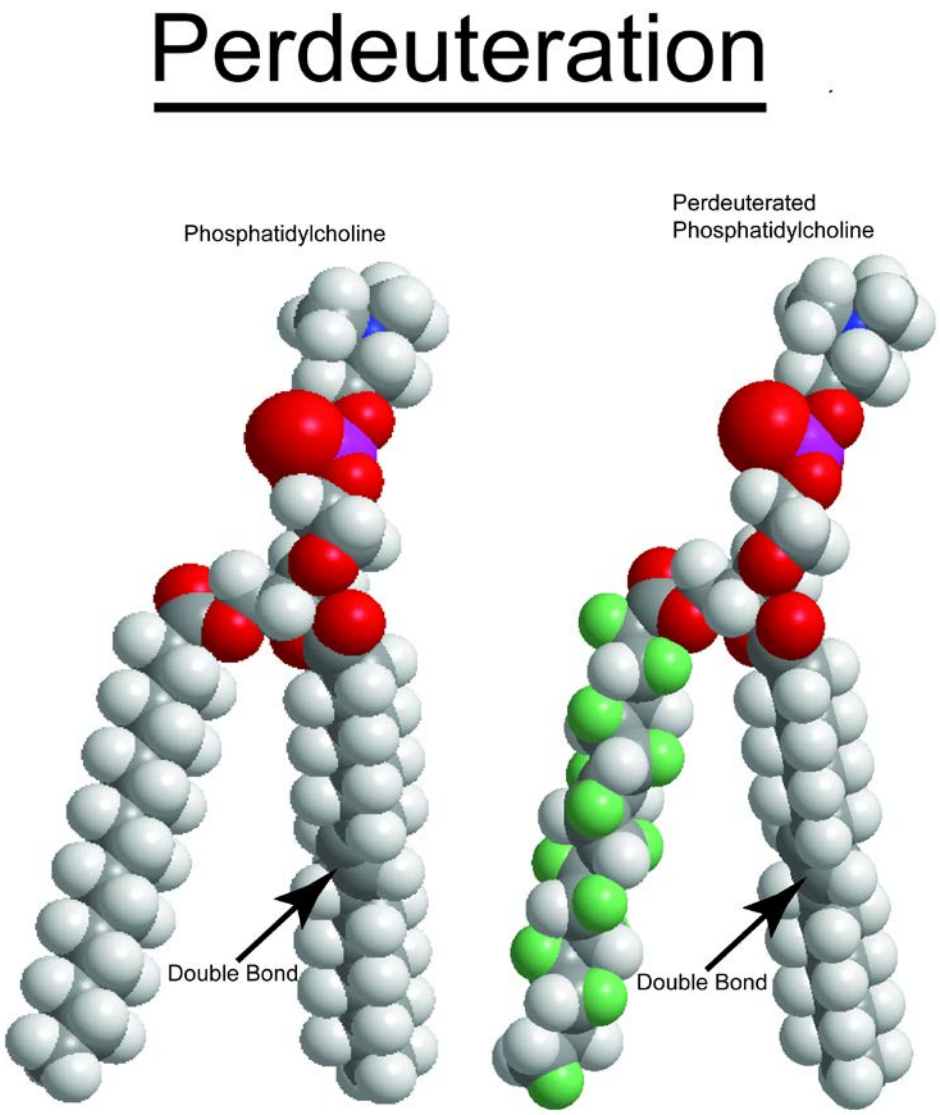

Perdeuteration.

A perdeuterated lipid has deuteriums instead of hydrogens on one of the fatty acyl chains. This is a very small perturbation to the system that allows the motion of the fatty acyl chain to be studied. Deuteriums are in green, carbons are in gray, hydrogens in white, nitrogens in blue, oxygens in red, and phosphori in fuchsia.

bilayers that are created with only purified or synthesized lipids are called "model membranes." The PC class refers only to the head group of the lipid and ignores the fatty acyl chains. 1-palmitoyl-2-oleoyl-*sn*-glycero-3-phosphocholine (POPC), the most abundant, naturally occurring phospholipid lipid, has one fatty acyl tail that is 18 carbons long with one double bond between the ninth and tenth carbons and another that is 16 carbons long with no double bonds (Figure 18). Since this is the main lipid in most bilayers, it makes sense to use this as the main building block for modeling a membrane bilayer. Justice *et al*. showed how ceramide incorporation into POPC membranes raised the order parameter of the POPC lipids with two different ceramides, ceramide 18:1 and ceramide 6:0 (Figure 19).[57]

1.7 ASM Maturation and Subcellular Location

The first sphingomyelin phosphodiesterase purified was found to hydrolyze sphingomyelin into ceramide and phosphorylcholine at an acidic pH and was designated SMPD1.[44] The corresponding gene, *SMPD1*, gives rise to two different enzymes that perform the same function at two distinct subcellular locations.[60] The enzyme SMPD1 is post-translationally modified several times, ultimately determining where and on which substrates it acts. Although the processing of ASM has been extensively studied, it is unclear exactly how this enzyme matures into its secreted and lysosomal forms (Figure 20).[61]

SMPD1 has an N-terminal endoplasmic reticulum signal sequence, which allows for co-translation to occur.[61] The endoplasmic reticulum is where the folding process of prepro-ASM begins. Further processing of ASM is thought to happen

FIGURE 19.

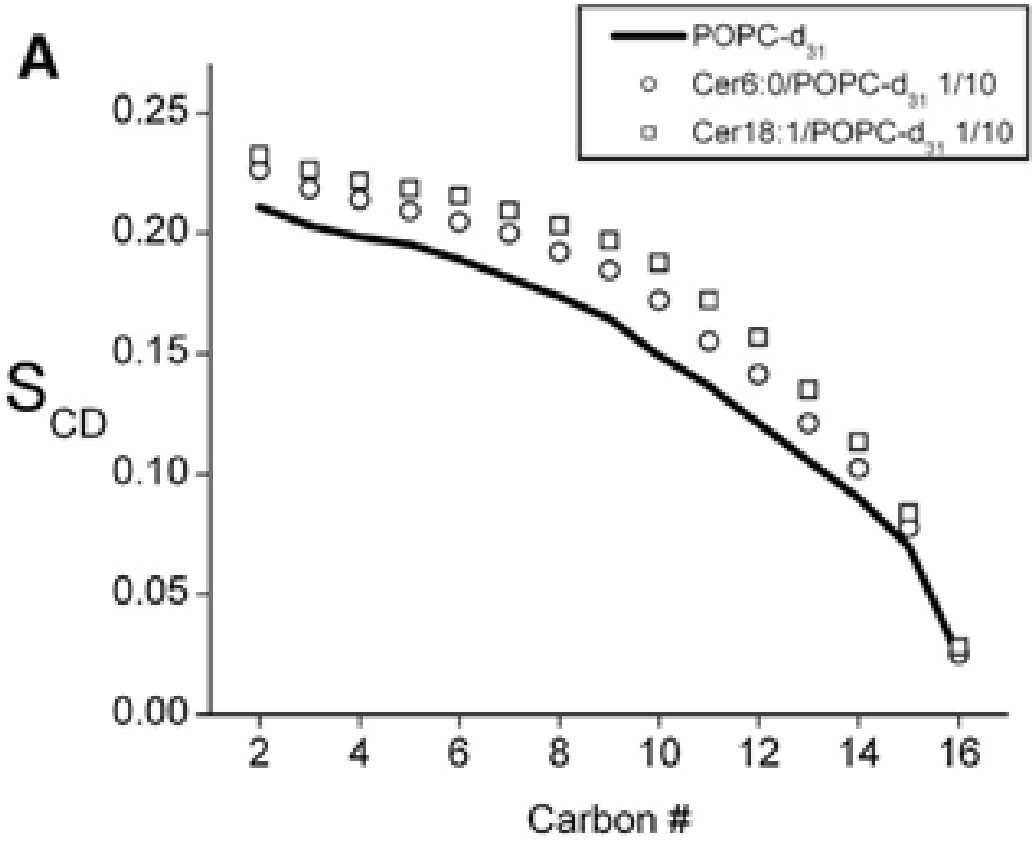

Ceramide incorporation increases order parameters of neighboring lipids.

From Justice *et al*. 2014 *Biophysical* Journal, with permission.[57] Smoothed profile of order parameter S_{CD} versus position along the *sn*-1 chain at 30°C for (A) POPC-d_{31} in POPC (solid line), Cer6:0/ POPC (1:10 mol% ceramide:POPC) (open circles), and Cer18:1/POPC (1:10 mol% ceramide:POPC) (open squares).

Figure 20.

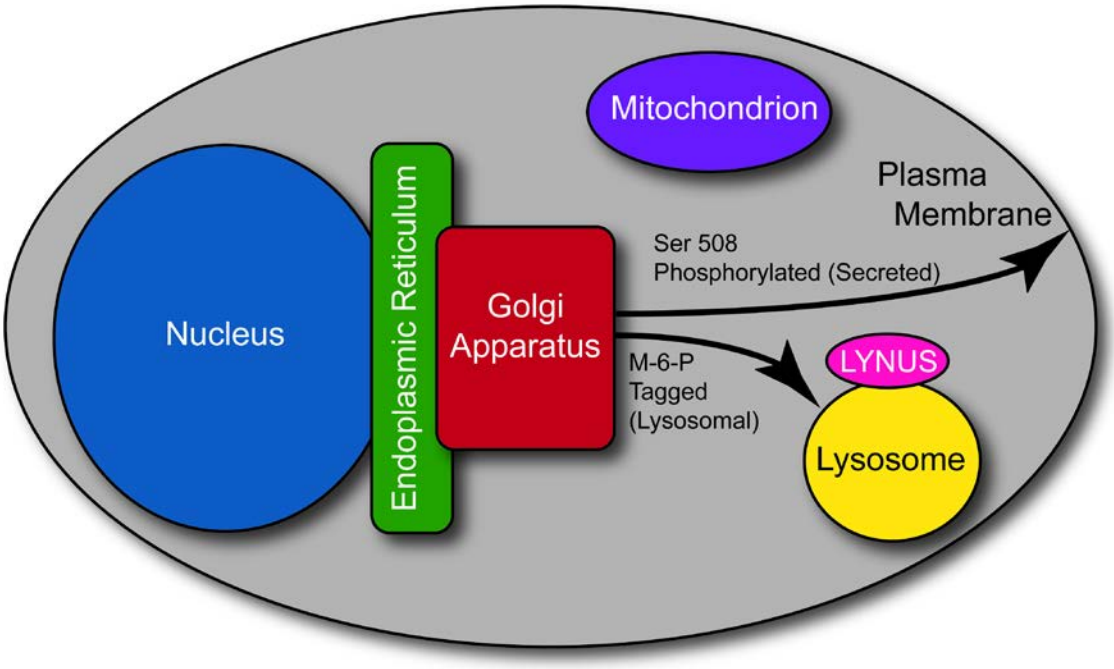

ASM subcellular location.

ASM is either shuttled to the plasma membrane or to the lysosome. Graphic representation of a cell and its organelles.

in acidic compartments after the protein has been folded and glycosylated.[60] When ASM is properly folded, there are 16 cysteine residues that are utilized for disulfide bonds, making this enzyme susceptible to reducing agents. Interestingly, ASM contains one more cysteine that does not make a disulfide bridge, and, if this residue is oxidized or deleted, the enzyme has much greater activity. As with most secretory proteins, after the stop codon is recognized, the endoplasmic reticulum signal sequence is removed and the glycosylation process begins. The glycosylation process occurs in the endoplasmic reticulum and then may be modified to incorporate the lysosome-targeting mannose-6-phosphate (M-6-P) tag, a process that happens in the Golgi apparatus before the enzyme is shuttled to its final destination. ASM does not always receive an M-6-P tag and after glycosylation, ASM will be shuttled and processed (amino acids cleaved) outside of the Golgi. Serine 508 phosphorylation and M-6-P tagging partially determine the subcellular localization of this protein. If serine 508 is phosphorylated, SMPD1 will be secreted in acidic vesicles and is known as soluble ASM (Figure 20).[62] M-6-P tagging shuttles SMPD1 to the lysosome if serine 508 is not phosphorylated and is known as lysosomal ASM. Exactly how ASM is transported and processed in unclear. Some groups believe the sortilin pathway of sorting saposins might be a shuttling method utilized to transport ASM to the lysosome; however, it is believed that the M-6-P pathway is the predominant pathway.[63] ASM has five out of six possible glycosylation sites glycosylated, and these are believed to help ASM endure the harsh acidic environment of endolysosomal compartments and may be important to its

activity, as ASM activity has been shown to be reduced after treatment with a glycosidase.

While similar in structure and function, soluble and lysosomal ASM have some differences other than their subcellular locations. Both require zinc as a cofactor; while the activity of soluble ASM can be greatly increased with the addition of zinc, lysosomal ASM is slightly sub-saturated with zinc and is thought to acquire it during trafficking to the lysosome in early endosomes, late endosomes, or possibly in pre-lysosomes.[64] Soluble ASM is thought to hydrolyze long chain sphingomyelins to produce long chain ceramides; lysosomal ASM is thought to produce very-long chain ceramides.[60] The first amino acid in the mature soluble ASM is histidine 60, while the first amino acid in the mature lysosomal form is glycine 66. Although both forms of ASM arise from the same gene precursor and both hydrolyze sphingomyelin into ceramide and phosphorylcholine, they may have very different signaling effects when activated.

The molecular weight of full-length prepro-ASM is 75 kDa. This enzyme is soon processed, within three hours, to pro-ASM that is 72 kDa and further processed to a 65 kDa, mature form after four hours. This processing was inhibited when cells were treated with brefeldin A (inhibits transport from ER to Golgi), suggesting that processing of ASM occurs after efflux from the endoplasmic reticulum. A C-terminally tagged ASM was found to localize with the Golgi apparatus rather than with lysosomes, suggesting the mature lysosomal form was processed at the C-terminus after exiting the Golgi.[61] The processing from 72 kDa to 65 kDa is believed to occur in or near an endolysosomal

compartment. When ASM is inhibited with a tricyclic amine, the 65 kDa mature form is lost and a 52 kDa form appears. Jenkins *et al*. reported the loss of lysosomal ASM activity after pharmacological inhibition of ASM with a concomitant reduction of 65 kDa ASM, suggesting that this is the mature lysosomal form of ASM. The work contained herein only investigates the mature lysosomal form of ASM, which will hereafter be referred to simply as ASM.

1.8 Functional Inhibitors of ASM

Imipramine, a tricyclic antidepressant (TCA), has been administered to treat depressive conditions for more than half a century.[65] It has a different mechanism of action as compared to most enzymatic inhibitors.[66] Most small molecule enzyme inhibitors work through a direct mechanism that reduces the catalytic ability of the enzyme. This usually occurs by binding of the small molecule to either the catalytic pocket or an allosteric regulatory site of the enzyme. When small molecules bind in the catalytic pocket, other entities, such as the substrate or cofactors needed for the reaction, cannot bind, thus reducing the catalytic activity of the enzyme. Allosteric regulation is when a molecule binds to a non-catalytic site, which usually changes the conformation of the protein and either promotes or decreases activity of the enzyme. Imipramine, on the other hand, acts through an indirect mechanism termed “functional inhibition.”[67]

Imipramine, a weak base, was used to treat depression as early as 1958. In 1981 it was determined that a weak base had to have a side chain in order to be effective as an ASM inhibitor because weak bases without a side chain had no inhibitory effects on ASM.[68] In 1994 it was determined that proteolytic

degradation was responsible for loss of ASM activity.[66] In 2008, steric hindrance of the most basic nitrogen was found to determine the effectiveness of the drug.[67] As such, several new functional inhibitors of ASM (FIASMAs) have been documented. Since weak bases are not fully ionized when in solution, some of their molecules are able to pass through membrane bilayers. If one of these molecules passes through the lysosomal membrane, which has a low pH, it will become protonated. Once this happens, the molecule can no longer diffuse through membrane and, therefore, becomes trapped inside the lysosome—a process known as “ion-trapping.” This will interfere with the bonds that adhere ASM to the intraluminal side of the lysosomal membrane, and ASM will dissociate from the membrane. Once this happens, lysosomal proteases will digest ASM, whereby ASM activity is diminished. This is the crux of functional inhibition.

In this research, ASM will also be specifically inhibited with small interfering RNA (siRNA) against *SMPD1*, the gene precursor to ASM. Through binding of siRNA to both the five prime and three prime ends of mRNA, the siRNA can facilitate degradation of mRNA as well as block translation of mRNA.[69] Both pharmacological and RNA interference to inhibit ASM, reduce the level of ASM protein in the cell, thereby reducing ASM activity. When inhibiting ASM, the distinction between ASM activity and the presence of ASM will not be made.

1.9 ASM and Autophagy in Disease

Several diseases that have aberrant autophagic induction and/or autophagic flux as part of their pathogenesis have been identified: acute ischemia, acute lung injury, aging, Alzheimer's disease, amyotrophic lateral sclerosis, asthma, Barth syndrome, several cancers, cardiovascular diseases, chronic kidney diseases, COPD, Crohn's disease, cystinosis, diabetes, esophageal diseases, glomerulosclerosis, hepatic steatosis, Huntington's disease, idiopathic pulmonary fibrosis, myocardial ischemia/reperfusion injury, kidney fibrosis, lysosomal storage diseases, mitochondrial diseases, multiple sclerosis, myocardial infarction, obesity, Paget's disease of bone, Parkinson's disease, polycystic kidney disease, pulmonary arterial hypertension, pulmonary hypertension, rheumatic diseases, sarcopenia, sepsis, skin diseases, spastic paraparesis, pulmonary tuberculosis, ulcerative colitis, ventricular hypertrophy, Vici syndrome, viral replication, and viral transmission.[70-83] It is unknown whether these diseases have dysregulated ASM as well. As mentioned earlier, outside of the devastating effects of having little to no ASM activity, not much is known about small, chronic variations in the activity of this enzyme. Most studies involving ASM in disease have been focused on Niemann-Pick disease or the induction of apoptosis in cancer.[84, 85] Recently, several publications have linked ASM and abnormal autophagic states with somewhat discrepant results.[5] "The emerging role of acid sphingomyelinase in autophagy," by Perotta *et al*. highlights different diseases and correlates their ASM expression/activity with autophagic status. It also points

out the conundrum of increased as well as decreased ASM activity leading to increased levels of LC3B-II.

Degradative autophagy is thought to play a role in clearing atherosclerotic plaques; however, the plaques are rich with 7-ketocholesterol, which decreases ASM activity in the lysosome, leading to poor calcium release from the organelle.[4] Calcium release from the lysosome is required to activate dynein in order to move autophagosomes closer to lysosomes, a key step in the degradative autophagic process. Alzheimer's disease (AD) is characterized by buildup of plaques in the brain, leading to apoptosis of neurons, memory loss, and eventual death.[86] Neurons and fibroblasts of AD patients have increased ASM activity and a dysregulated degradation mechanism affecting the autophagy-lysosome pathway, namely blocked autophagic flux, which causes plaques to accumulate and leads to the symptoms described previously.[7] Symptoms of AD in a murine model, characterized by increased ASM activity and decreased autophagic flux, were attenuated by a pharmacological ASM inhibitor that induced autophagy and restored cognitive function. Emphysema is yet another disease that has as part of its pathogenesis hyperactive ASM coupled with increased abundance of autophagosomes due to decreased autophagic flux that eventually leads to apoptosis and irreversible loss of tissue.[87-89] A disease with uncontrollable cell proliferation, cancer, is known to have decreased ASM, increased autophagy, and apoptosis evasion as part of the pathogenesis.[90-92] In melanomas, progression stage can be determined by ASM abundance.[90] In general, it can be postulated that increased ASM activity may eventually lead to

blocked autophagic flux, culminating in excessive apoptosis, whereas lack of ASM activity may engage pro-survival autophagy.

1.10 Hypothesis

ASM contributes to ceramide content of the lysosome, and lysosomally produced ceramides are not shuttled to other locations and should exert their effects within or around this organelle.[93, 94] Downstream metabolite sphingosine is able to leave the lysosome and can modulate TFEB signaling through calcineurin and modify autophagic signaling. Sphingosine can be further metabolized to S-1-P which can change mTOR signaling through S-1-P receptor three. Even brief changes in ceramide may alter the biophysical properties of the lysosomal membrane, which would have implications in the docking of complexes as well as fusion of autophagosomes with lysosomes.

Since the LYNUS is anchored in the lysosomal membrane, where ASM contributes to the ceramide content, and mTOR is a member of the LYNUS, we hypothesize **that ASM function is required for mTOR signaling and inhibition of autophagy during homeostasis**. As a corollary, reduced ASM activity is sufficient to induce autophagy while concomitantly changing lysosomal membrane lipid composition to favor autophagosome-lysosome fusion.

Since emphysema is a disease with no known cure, exhibits aberrant autophagy, has hyperactive ASM as part of its pathogenesis, and eventually leads to excessive apoptosis of pulmonary cells, we chose to perform our work mainly in ASM-rich primary human pulmonary artery endothelial cells

(HPAEC).[82, 88] Some data were acquired from other human cell types as well as a murine model.

Here, we report that homeostatic ASM inhibition is required for the proper function of LYNUS and to inhibit excessive autophagy. Also, ASM activity is required to maintain proper sphingosine levels, which may play a role in the LYNUS activation status.

Chapter 2. Methods

2.1 Reagents

Unless otherwise stated, all reagents were purchased from Sigma-Aldrich.

2.2 Cell Culture

All experiments were performed in full media unless otherwise stated. HPAEC (Invitrogen, C0085C) were cultured in Medium 200 (Invitrogen, M200500), supplemented with low serum growth supplement (Invitrogen, S00310). HLMVEC (Invitrogen, CC2527) were cultured in an EGM-2MV BulletKit (Invitrogen, CC3202). HUVEC, a kind gift from Dr. Mathias Clauss (Indiana University), were cultured in VasculLife VEGF Medium Complete Kit (LifeLine, LL0003). THP-1 monocytes (ATCC, TIB202) were cultured in RPMI (Invitrogen, 11875119), supplemented with 10% fetal bovine serum (FBS) (ThermoFisher Scientific, sh30910-03HI). Bronchial epithelial cells (BEAS2b) were cultured in Dulbecco's modified Eagle's medium (DMEM) with high glucose and pyruvate (Invitrogen, 11995-073), supplemented with 10% FBS (ThermoFisher Scientific, sh30910-03HI) and 1% penicillin/streptomycin (Sigma, P4333-100ML). All cells were incubated at 37ºC with 5% CO2 and 100% humidity. Experiments were performed between 50 and 90% confluency.

2.3 ASM activity

Lysosomal ASM activity was measured with an Amplex Red Sphingomyelinase Activity kit (Invitrogen, A12220) or radioactivity. Briefly, the kit utilizes an indirect two-step reaction that produces a fluorescent readout of ASM activity. Cells were washed in ice-cold phosphate buffered saline (PBS) at end of

treatment, scraped in ice-cold PBS and centrifuged at 16,000 x g for 10 min. Supernatant was removed, and the remaining cell pellet was snap frozen in liquid nitrogen. At time of assay, pellets were hydrated with a reaction buffer for lysosomal sphingomyelinase activity, incubated with 5 mM sphingomyelin, 2 U/mL horseradish peroxidase, and 8 U/mL alkaline phosphatase. Kinetic fluorescence measurements were read using a wavelength of 590 nm over a period of two hours at 37ºC in a SpectraMax m2e microplate reader using SoftMax Pro software.

For the radioactive assay, cells pellets were lysed in 75 µL of a buffer containing 25 mM TRIS (pH = 7.6), 5 mM EDTA, 0.2% Triton-x, phosphatase inhibitors, and protease inhibitors. To 4 mL of the same buffer used to lyse cells, 3 µL of ^{14}C-choline methyl sphingomyelin @ 55 mCi/mmol and 0.1 mCi/mL was added to create a substrate buffer (1.4 pmol/µL). To 103 µL of the reaction buffer, 35 µL of lysate, 12 µL of 0.2 M acetic acid, and 50 µL of substrate buffer was added, mixed by vortex and allowed to react at 37ºC for 2.3 hours. To stop the reaction, 250 µL of a 2:1 (chloroform:methanol) solution was added and vortexed. To this, 800 µL of a 2:1 (chloroform:methanol) plus 250 µL of water was added and vortexed. From the aqueous phase, 200 µL was extracted and added to 800 µL of MicroScint PS (Perkin-Elmer, 6013631) and radioactivity quantified on a Topcount scintillation counter.

2.4 Western Blotting

Cells were washed with ice-cold PBS, gently scraped in ice-cold PBS, centrifuged at 16,000 x g for 10 min., supernatant removed and pellets snap frozen in liquid nitrogen. Cell pellets were thawed at 4ºC in cell lysis buffer containing 1% triton-x (EMD, 9002931), 150 mM NaCl (ThermoFisher, BP3581), and 50 mM Tris (pH 7.6) (Invitrogen, 15504020). Cells, at 4ºC, were vigorously vortexed five times during a 1 hour period and were centrifuged at 4ºC at high speed for 10 min. Supernatant was kept as whole cell lysate.

Protein concentration was determined using a bicinchoninic assay (BCA) (Pierce, 23227). Equal amounts of protein (2-20 µg) were diluted in Laemmli 4X buffer (reducing) (Boston Bioproducts, NC9099736) and resolved in Criterion 12+2 well 4-20% TGX gels (Bio-Rad, 5671093). A semi-dry transfer apparatus (Bio-Rad, 1703848) was employed to transfer proteins to a polyvinylidene fluoride membrane (EMD, IPVH00010). Membranes were probed with the following antibodies: anti-β-actin (A5441), anti-LC3B (Sigma, L7543), anti-vinculin (Abcam, ab10858), anti-GAPDH (Abcam, ab9485), anti-phospho P70S6k (Thr 389) (Cell Signaling Technologies, 9205) and anti-phospho mTOR (Ser 2448) (p-mTOR) (Cell Signaling Technologies, 5536). Appropriate secondary antibodies (goat anti-rabbit/mouse, HRP conjugate) (GE Healthcare, 45001175 /45001187) were used in conjunction with ECL prime or Luminata Forte (ThermoFisher, RPN2232/EMDMillipore, WBLUF0500) for chemiluminescent reaction. Images were taken with a ChemiDoc (Bio-Rad) XRS system with ImageLab software.

2.5 Densitometry

Density quantification of protein bands in Western blots was performed with ImageJ software (Rasband, W.S., ImageJ, U. S. National Institutes of Health, http://imagej.nih.gov/ij/, 1997-2012).

2.6 Transfection

Nucleofector Kits for Primary Endothelial Cells (Lonza, VVPI-1001) in conjunction with Amaxa Nucleofector to transfect HPAEC with siGenome siRNA (Dharmacon, siGlo/non-targeting pool 1/non-targeting pool 2/*SMPD1*, D0016300205/D-001206-13/D-001206-14/M-006676-01-0020) using program U-017 per manufacturer's protocol (1-1.5 million cells per transfection were used). Concentration of siRNA ranged from 1-3 µM in up to a volume of 150 µL (inside cuvette) just prior to electroporation. After electroporation, cells were added to 10 mL of full media. Media was changed 18 to 24 hours after electroporation.

2.7 Quantitative Polymerase Chain Reaction (qPCR)

Cells were washed with ice-cold PBS, gently scraped in ice-cold PBS, centrifuged at high speed for 10 min., supernatant removed and pellet snap frozen in liquid nitrogen. RNA was extracted with a GenElute mammalian total RNA minikit (Sigma, RTN70-1KT) per manufacturer's protocol, and cDNA was reverse transcribed with a high capacity cDNA reverse transcription kit with RNase inhibitor (Applied Biosystems, 4374966). Using SYBR select master mix (Applied Biosystems, 4472908) and *SMPD1*/*PGK1* primers (Qiagen, PPH02494A/PPH02049A), 25 ng of cDNA was amplified on an ABI 7500 real-time PCR System (Applied Biosystems). Using Taqman Universal PCR Master

Mix (ThermoFisher, 4364340) and *TFEB/PGK1* primers (Hs00292981_m1/ Hs00943178_g1), 25 ng of cDNA was amplified on an ABI StepOne Real-Time PCR System (Applied Biosystems).

2.8 Immunofluorescence

HPAEC cells were cultured (125,000 cells per well) on 18 mm glass cover slips (VWR, 48380046) residing in 12-well dishes (Costar, 3513) coated with a gelatin-based coating solution (Cell Biologics, 6950). After treatment, media was removed and formaldehyde (4%) was added to wells at room temperature for 10 minutes. Cells were rinsed once with PBS (quickly) and washed 3 times with PBS (5 minutes) and placed at 4ºC until time of immunostaining. Cells were blocked for one hour with PBS containing 5% normal goat serum and 0.3% triton-x, rinsed once with PBS (quickly) and washed 3 times with PBS (5 minutes), exposed to rabbit anti-TFEB polyclonal antibody, Alexa Fluor 555 conjugated (Bioss, bs-5137R-A555) in a PBS buffer containing 1% bovine serum albumin and 0.3% triton-x, rinsed once with PBS (quickly) and washed 3 times with PBS (5 minutes), and mounted with SlowFade Gold Antifade reagent with DAPI (Invitrogen, S36939) to microscope slides (ThermoFisher, 12-544-3). Images were taken on a Nikon Eclipse 80i microscope.

BEAS2b that stably express eGFP-LC3B were cultured in 4 well Lab-Tek (ThermoFisher Scientific, 154526) slides (50,000 cells per well). After treatment, media was removed and formaldehyde (4%) was added to wells at room temperature for 10 minutes. Cells were rinsed once with PBS (quickly) and washed 3 times with PBS (5 minutes) and placed at 4ºC until time of

immunostaining. Cells were blocked for one hour with 10% normal goat serum in PBS that contained 0.1% triton-x, they were exposed to rabbit anti-LAMP1 (Cell Signaling Technology, 9091; 1:200) in the same buffer, rinsed and washed in the same manner as stated above, incubated with Alexa Fluor 594 (ThermoFisher, A20185; 1:2,000) in the same buffer, and mounted with SlowFade Gold Antifade reagent with DAPI (Invitrogen, S36939) to cover slips (ThermoFisher,12-544-14) and imaged on a Nikon Eclipse 80i microscope.

2.9 Electron Microscopy

After washing with ice-cold PBS (Fisher, 21-040-CV), cells were fixed with glutaraldehyde (Sigma, G7776) and formaldehyde (ThermoFisher, 28908), both at 2% in 0.1 M phosphate buffer for 30 min. at room temperature. Cells were gently scraped in PBS after two rounds of washing with PBS, centrifuged at high speed for 10 min. and given to the Electron Microscopy Core Facility at IU School of Medicine for post fixing, embedding, cutting and mounting on slides. Images were taken with a Tecnai G2 12 Bio Twin (FEI, Hillsboro) equipped with an AMR CCD (Advanced Microscopy Techniques).

2.10 Differential Centrifugation

Cells were cultured as above in five 15 cm dishes until 80% to 90% confluent. Growth media was exchanged for media warmed to 37ºC containing vehicle or treatment. After 30 min., media was aspirated and ice-cold Accutase (10 mL) was added to dishes. All reagents and centrifuges were kept at 4ºC from this point until storage in methanol. Cells were collected by pipette and spun at 500 x g for 5 min. After the supernatants were aspirated, the pellets were suspended in

1 mL of PBS and spun at 500 x g for 5 min. After aspirating the PBS, the pellets were suspended in solution “B” from Axis-Shield Application S53 plus phosphatase and protease inhibitors. An aliquot of these suspensions was immediately taken and spun at 500 x g for 5 min. to prepare whole cell samples for analysis. After 25 min., each of the 10 samples was homogenized separately (30 strokes) in a 1 mL Dounce homogenizer with pestle “B.” Samples were then spun at 16,000 x g for 5 min. The supernatant was considered the cytosolic fraction, with the remaining pellet being the organelle fraction. The organelle fraction was then suspended in 10% v/v with solution “C” as per S53. A 14 mL gradient with 2 mL discontinuous steps was made with v/v dilutions of OptiPrep as follows: 10% (sample), 12%, 14%, 16%, 18%, 20%, 25% and spun at 150,000 x g for 20 h. Fractions were collected from the bottom using a 3 mL syringe with a 4-inch, 16 gauge blunt needle attached until the 2 mL mark on the syringe was reached. Six fractions were able to be collected in this manner with fraction six being the first collected. An aliquot of 150 µL from each fraction was removed and added to 4X Laemmli (Boston Bioproducts, NC9099736) for Western blotting purposes. These fractions were diluted with 10 mL of PBS and spun at 150,000 x g for 10 min. The supernatant was decanted and 1 mL of methanol was used to prepare the pellet for lipid extraction. The samples were then stored at -20ºC until the extraction process.

2.11 Lipid extraction and Sphingolipid quantification by LC-MS/MS

Methanol, water and acetonitrile (HPLC grade) were purchased from Burdick and Jackson (Muskegon, MI). Sphingosine (Sph), dihydrosphingosine (DHSph), a 17-carbon analog of sphingosine (C17-Sph), sphingosine-1-phosphate (S1P), dihydrosphingosine-1-phosphate (DHS1P), a 17-carbon analog of S1P (C17-S1P), N-acylated (C14:0-, C16:0-, C18:1-, C18:0-, C20:0-, C24:1-, C24:0-) sphingosines (Ceramides, Cer), N-heptadecanoyl-sphingosine (C17:0-Cer), N-acylated sphingosylphosphorylcholines (sphingomyelins, N-12:0-, N-16:0-, N-18:0-, N-24:1-, and N-24:0-), and glucosylceramides (N-16:0-, N-24:1-, N-24:0-) were obtained from Avanti Polar Lipids (Alabaster, AL). N-D3-16:0-glucosylceramide and N-D3-16:0-lactosylceramide were purchased from Matreya LLC (State College, PA). The standards were dissolved in methanol (sphingoid base phosphates were dissolved with the addition of a trace amount of concentrated hydrochloric acid) and stored at -20°C. L-[U-13C(98%),15N(98%)]-serine was from Cambridge Isotope Laboratories, Inc (Andover, MA). Pyridine (acetylation grade) and acetic anhydride were products of Alltech Associates (Deerfield, IL).

Cellular lipids were extracted with a modified Bligh and Dyer procedure with the use of 0.1N HCl for phase separation.[95, 96] C17-S1P (30 pmols), C17-Sph (30 pmols), N-C17:0-Cer (30 pmols), N-12:0-sphingosylphosphorylcholine (12:0-SM, 100 pmols), N-D3-16:0-glucosylceramide (25 pmol) and N-D3-16:0-lactosylceramide (25 pmol) employed as internal standards, were added during the initial step of lipid extraction. The extracted lipids were dissolved in ethanol

and aliquots were taken out to determine total phospholipid content as described by Vaskovsky *et al*.[97] Samples were concentrated under a stream of nitrogen, transferred to autosampler vials, and subjected to consecutive LC-MS/MS analysis of sphingoid bases, ceramides, glycosyl/lactosyl ceramides, and sphingoid base-1-phosphates.

2.12 Analysis of sphingoid base-1-phosphates, ceramides, sphingoid bases, and sphingomyelins

Analyses of sphingoid base-1-phosphates, ceramides, sphingoid bases, sphingomyelins, glycosylceramides and lactosylceramides were performed by electrospray ionization tandem mass spectrometry (ESI-LC/MS/MS). The instrumentation employed was Sciex 6500 QTRAP hybrid triple quadrupole linear ion-trap mass spectrometer (AB Sciex, Redwood City, CA) equipped with an Ion Drive Turbo V ionspray ionization source interfaced with a Shimadzu Nexera X2 UHPLC system. All lipid molecules and their derivatives were separated using Ascentis Express RP-Amide 2.7 µm, 2.1 x 50 mm column and gradient elution from methanol:water:formic acid (65:35:0.5, 5 mM ammonium formate) to methanol:chloroform:water:formic acid (90:10:0.5:0.5, 5 mM ammonium formate). S1P and DHS1P were analyzed as bis-acetylated derivatives with C17-S1P as the internal standard employing negative ion ESI and MRM analysis as described in Berdyshev *et al*.[98] Ceramides and sphingoid bases were analyzed with C17-ceramide and C17-Sph as internal standards using positive ion ESI and multiple reaction monitoring (MRM) analysis as described in Berdyshev *et al*.[96] To facilitate sphingomyelin analysis and to avoid stable isotope overlap between

phosphatidylcholines and sphingomyelins, lipids were hydrolyzed using a methylamine reagent for 2 hours at 55ºC.[99] Reagents were evaporated with a nitrogen stream. The residual non-saponified lipids were then dissolved in 0.2 ml of methanol and subjected to LC-MS/MS analysis of sphingomyelins. Sphingomyelins were detected as positive ions in MRM mode by a transition from the corresponding molecular ion to the m/z of 184 (phosphocholine). Sphingomyelin quantification was achieved by creating standard curves of variable amounts of sphingomyelin standards (N-16:0-, 18:0-, 24:1, and 24:0-sphingomyelins) versus a fixed amount of N-12:0-sphingomyelin (internal standard). Glycosylceramides and lactosylceramides were detected as positive ions in MRM mode by a transition from the corresponding molecular ion to the m/z of 264 (ceramide ionization). Glycosphingolipid quantification was achieved by creating standard curves of variable amounts of glucosylceramide standards (N-16:0-, 24:1, and 24:0-glucosylceramides) versus a fixed amount of N-D3-16:0-glucosylceramide (internal standard). The linearity and the correlation coefficients of the standard curves were obtained *via* linear regression analysis. Quantification of sphingolipid molecular species for which there were no standards available was performed using best possible approximation from the closest available analogs.

2.13 Mouse Experiments

All experiments were approved by the IACUC, and animal treatment guidelines were followed. Three month-old female *Smpd1*$^{+/+}$, *Smpd1*$^{+/-}$, or *Smpd1*$^{-/-}$ mice (C57Bl/6 background strain), obtained from Dr. Edward

Schuchman and Dr. Erich Gulbins, were used to harvest perfused lungs, which were snap frozen in liquid nitrogen.[100] Lung tissue was homogenized in the cell lysis buffer used for Western blotting. Homogenized tissue was sonicated for two seconds at 30% power, centrifuged at high speed, and supernatant was removed as whole lung lysate.

2.14 Statistical Analysis

All statistical analyses were performed using GraphPad Prism version 6.00 for Windows, GraphPad Software, La Jolla California USA, www.graphpad.com.

Chapter 3. Results

3.1 ASM is required for homeostatic mTOR signaling

We utilized HPAEC due to their copious ASM activity and dysregulation of it in disease.[101] We first confirmed the presence of baseline ASM activity in primary HPAEC using a fluorometric ASM activity assay (**Figure 21**). Consistent with the literature, we confirmed that ASM activity is profoundly inhibited by imipramine with a fluorescent kinetic assay (50 μM; 4 hours; n = 1) (**Figure 21**).

Since ASM activity influences lysosomal ceramide content, which may contribute to the coalescence of microdomains that may be needed for LYNUS docking and signaling, we decided to see if mTOR (a member of the LYNUS) activity was changed during ASM inhibition by investigating the phosphorylation status of its downstream target, P70S6k.[101] Pharmacological ASM inhibition (50-100 μM; n = 3) significantly decreased the phosphorylation status of P70S6k in as little as one hour, for a sustained duration of up to 24 hours, as visualized by Western blot and quantified by densitometry (**Figure 22A-C**). To rule out nonspecific effects of the pharmacological inhibitor, we targeted the transcript of the sphingomyelin phosphodiesterase gene (*SMPD1*) with specific siRNA (1-3 μM, 48-72 hours), which greatly reduced ASM mRNA (n = 5) levels as well as activity (n = 3) (**Figure 23A and B**). Compared to two non-targeting pools of siRNA, or to fluorescently labeled siRNA (siGLO), ASM knock-down with *SMPD1* siRNA markedly reduced the phosphorylation status of both mTOR and P70S6k proteins, as measured by Western blot and quantified (P70S6k; n = 7) by densitometry (**Figure 24A and B**). Another indicator of LYNUS activation is the

Figure 21.

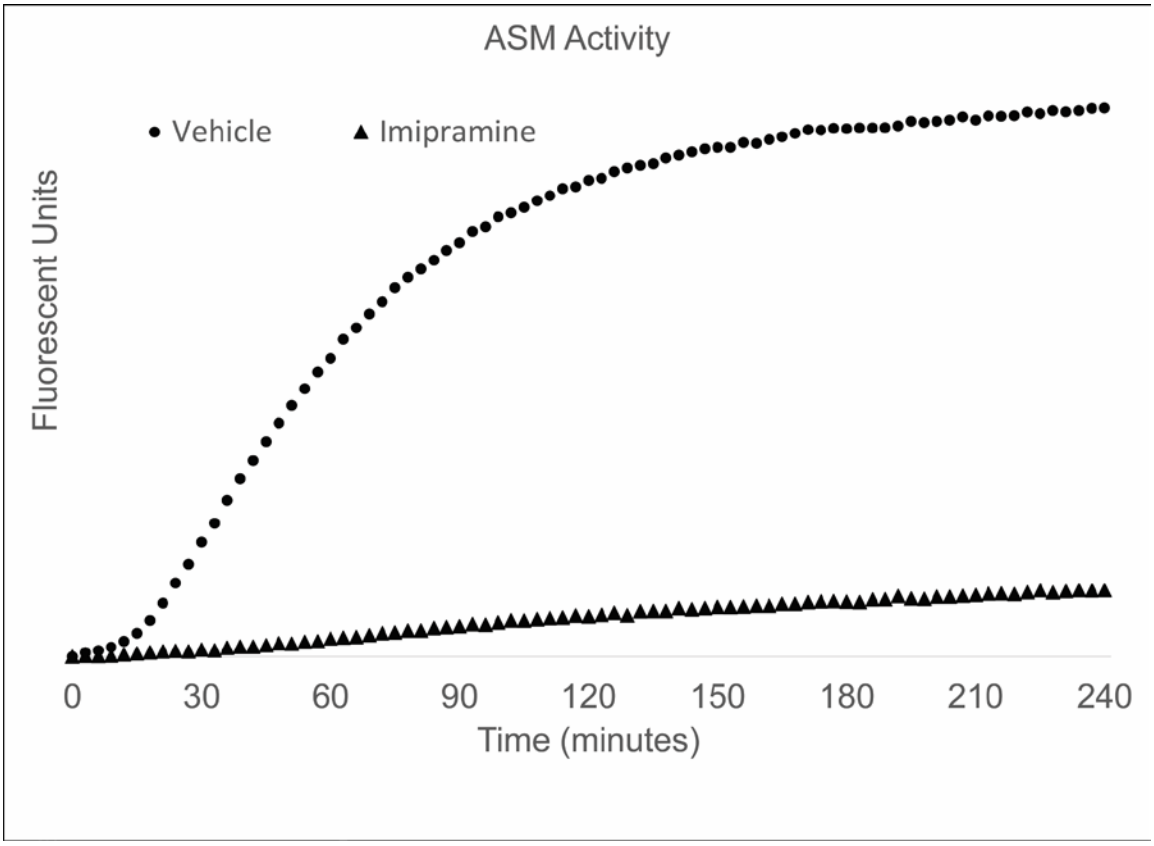

Inhibition of ASM with imipramine.

Kinetics of AmplexRed ASM activity assay in HPAEC exposed to either vehicle (water) or ASM inhibitor imipramine (4 hours; 50 μM) in full growth media. ASM activity is expressed in arbitrary fluorescent units. Confirmatory data is from one experiment.

Figure 22.

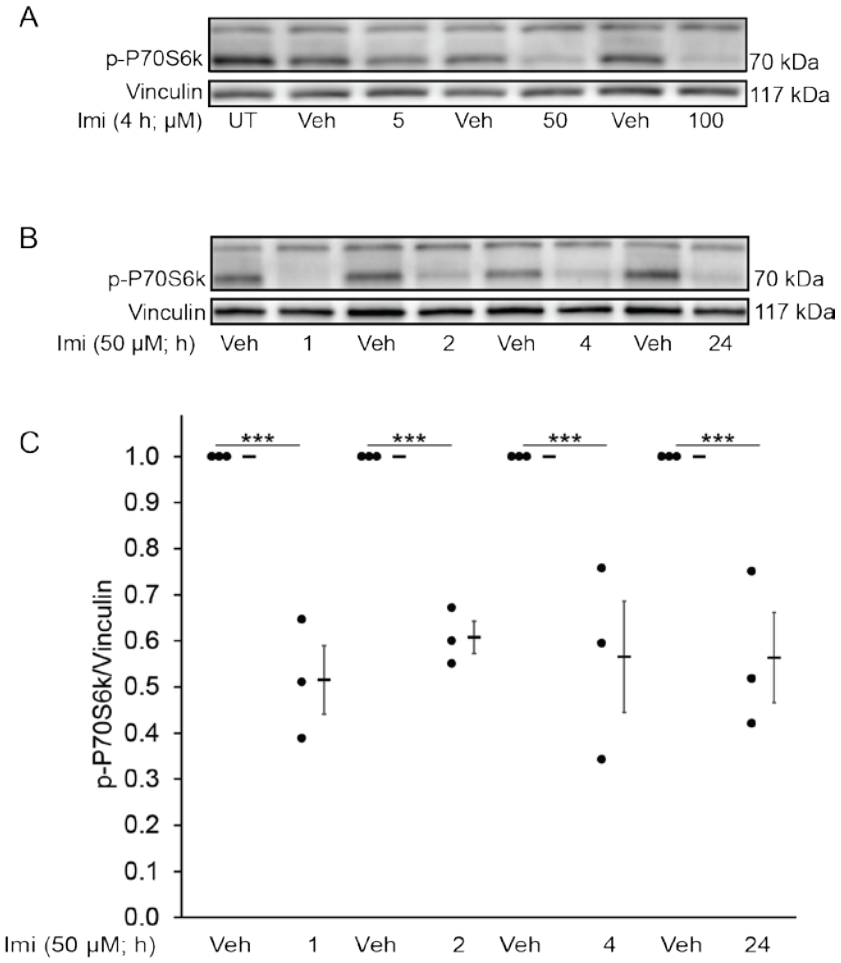

ASM is required for mTOR activity (pharmacological inhibition).

(A) Representative Western blot of phosphorylated P70S6k relative to vinculin (loading control) in HPAEC treated with imipramine (indicated times; 50 µM). (B) Representative Western blot and (C) quantification by densitometry of phosphorylated P70S6k protein expression in HPAEC relative to vinculin (loading control) treated with imipramine (indicated doses; 4 hours). Graph shows individual data points of three independent experiments, as well as means and standard error of the mean, *** = $p \leq 0.001$ (ANOVA with Tukey Post Hoc).

Figure 23.

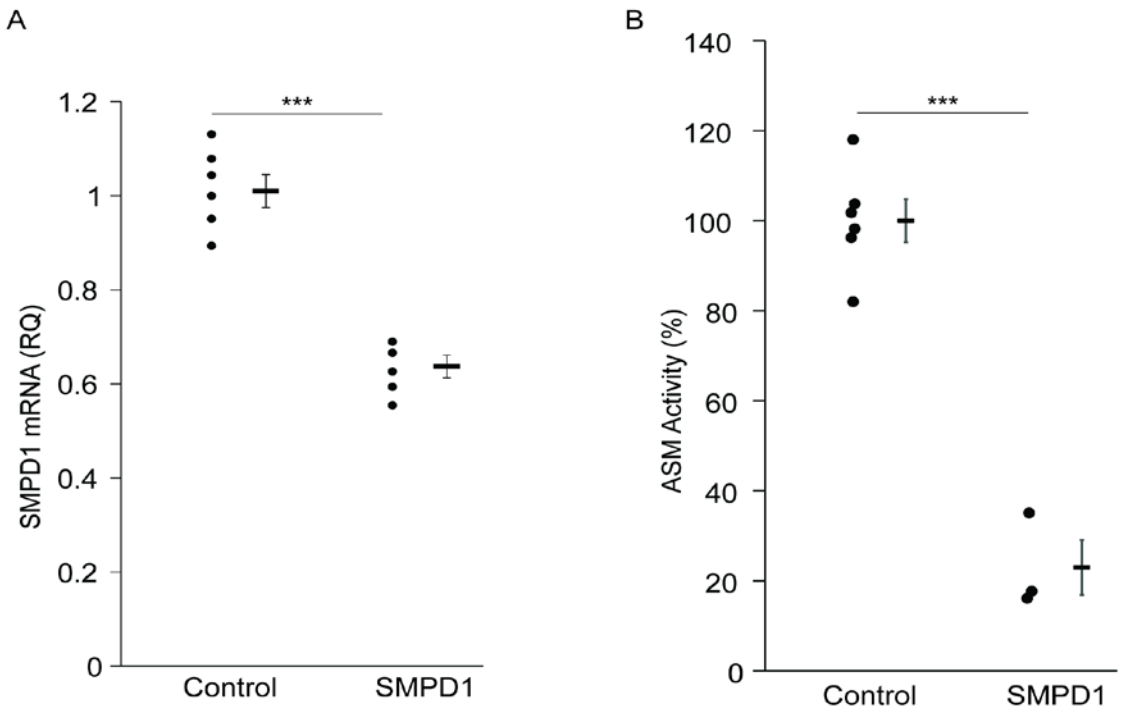

ASM inhibition with siRNA reduces *SMPD1* mRNA and ASM activity.

(A) Relative quantification of *SMPD1* mRNA (ASM gene transcript) by real-time PCR of HPAEC transfected with siGlo (transfection indicator), non-targeting pool 1, pool 2 or *SMPD1* siRNA (1-3 µM; 48-72 hours) (B) ASM activity as determined by Amplex Red fluorescent and radioactive assays in HPAEC transfected with siGlo (transfection indicator), non-targeting pool 1, pool 2 or *SMPD1* siRNA (1-3 µM; 48-72 hours). Graphs show individual data points of five (A) and three (B) independent experiments, as well as means and standard error of the mean, *** = $p \leq 0.001$ (Student's t-test).

Figure 24.

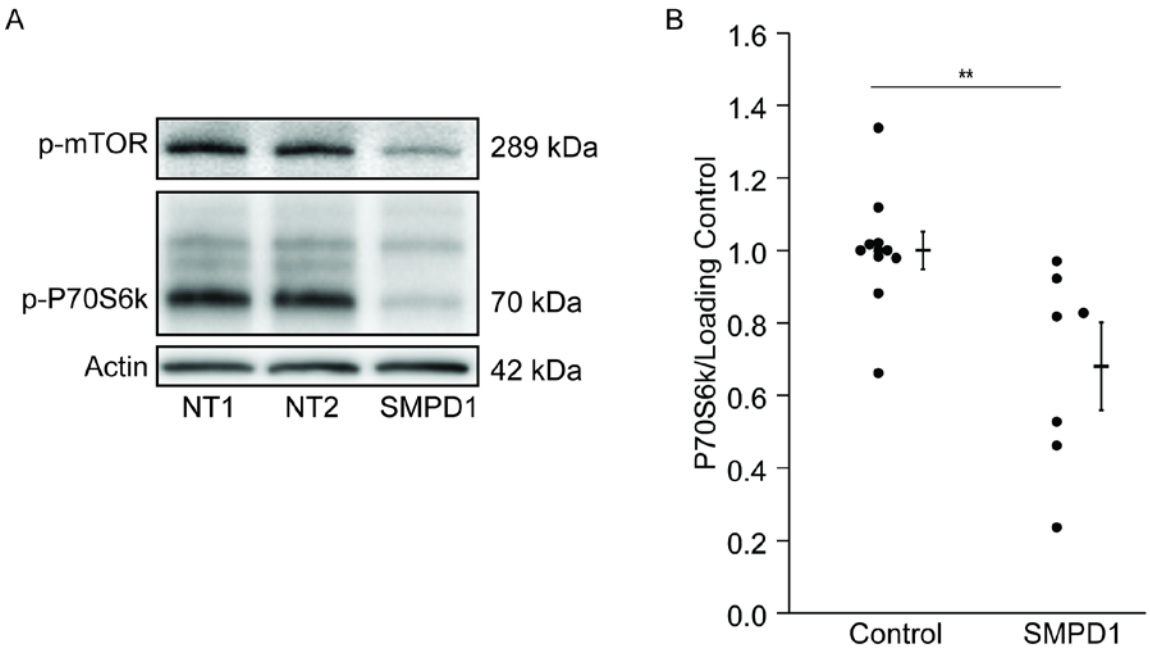

ASM is required for mTOR activity (siRNA inhibition).

(A) Representative Western blot (B) and quantification of p-P70S6k by densitometry in HPAEC transfected with siGlo (transfection indicator), non-targeting pool 1, pool 2 or *SMPD1* siRNA (1-3 µM; 48-72 hours). Graphs show individual data points of seven independent experiments, as well as means and standard error of the mean, ** = $p \leq 0.01$ (Student's t-test).

phosphorylation status of TFEB, which has more than 10 phosphorylation sites.[27] Indeed, ASM inhibition was associated with a distinct TFEB immunoblotting pattern on Western blots (samples were denatured), indicated by loss of the "smear" appearance, which is indicative of TFEB phosphorylation seen in control conditions, and presence of a lower molecular weight and more resolved band, which may indicate a shift in TFEB phosphorylation status (**Figure 25**).[102] This pattern is very similar to that of TFEB when cell were exposed to λ phosphatase.[102] Utilizing immunofluorescence microscopy, we noted translocation of TFEB the nucleus following ASM inhibition with imipramine (50 μM; n = 3) as compared to vehicle-treated cells (**Figure 26**). These images are z-stacks from an epi-fluorescent source that have been projected onto a two-dimensional plane Together, these findings suggest that ASM activity is a requisite for LYNUS function.

3.2 Baseline ASM activity is required for mTOR inhibition of autophagy

Since mTOR is a well-known inhibitor of autophagy by phosphorylating the ULK1 complex, we decided to test the functional impact of baseline ASM activity on autophagy.[25] Autophagosome abundance was inferred by measuring accumulation of LC3B-II. Pharmacological inhibition of ASM with imipramine caused a dose-dependent (50-100 μM; n = 3) increase in LC3B-II as detected by Western blot and quantified by densitometry (**Figure 27A and B**). A time course, with imipramine at the 50 μM dosage, revealed a sustained effect of ASM inhibition on LC3B-II levels for up to 24 hours as detected by Western blot and quantified by densitometry (n = 3) (**Figure 28A and B**). Levels of p62 varied

Figure 25.

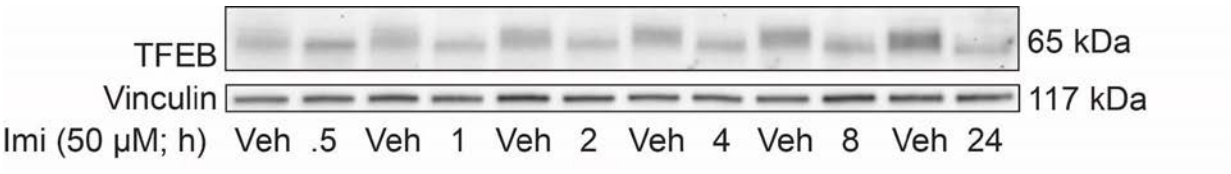

Decreased phosphorylation of TFEB during ASM inhibition.

Representative Western blot of TFEB in HPAEC treated with imipramine (50 μM; indicated amount of time). Note the loss of the “smear” pattern in imipramine-treated cells.

Figure 26.

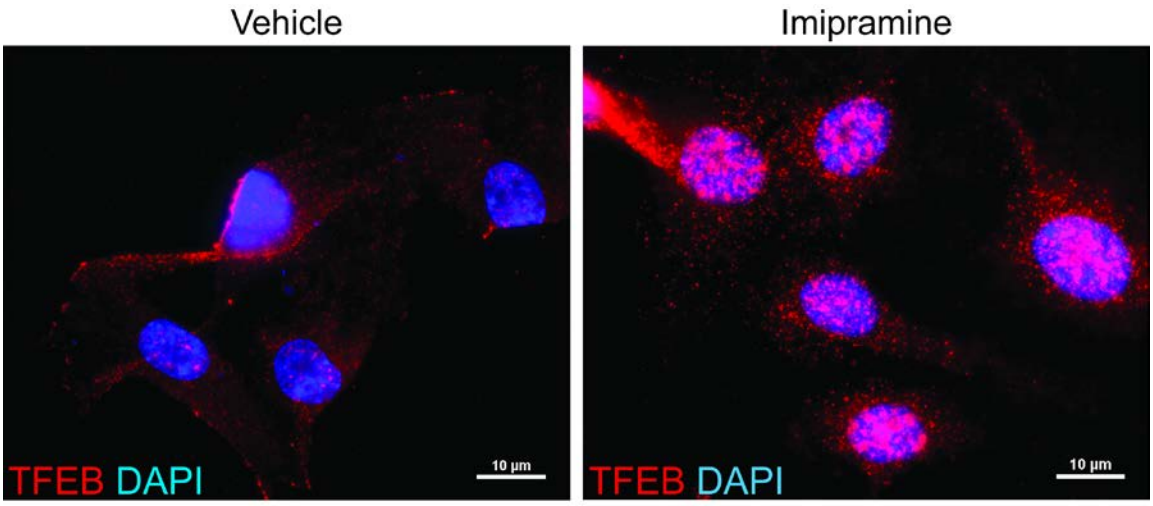

Nuclear translocation of TFEB during ASM inhibition.

TFEB immunofluorescence (red) and nuclear staining in blue (DAPI) in HPAEC following treatment with imipramine (50 µM; 30 minutes). Note the increased abundance of TFEB, both nuclear and cytoplasmic.

Figure 27.

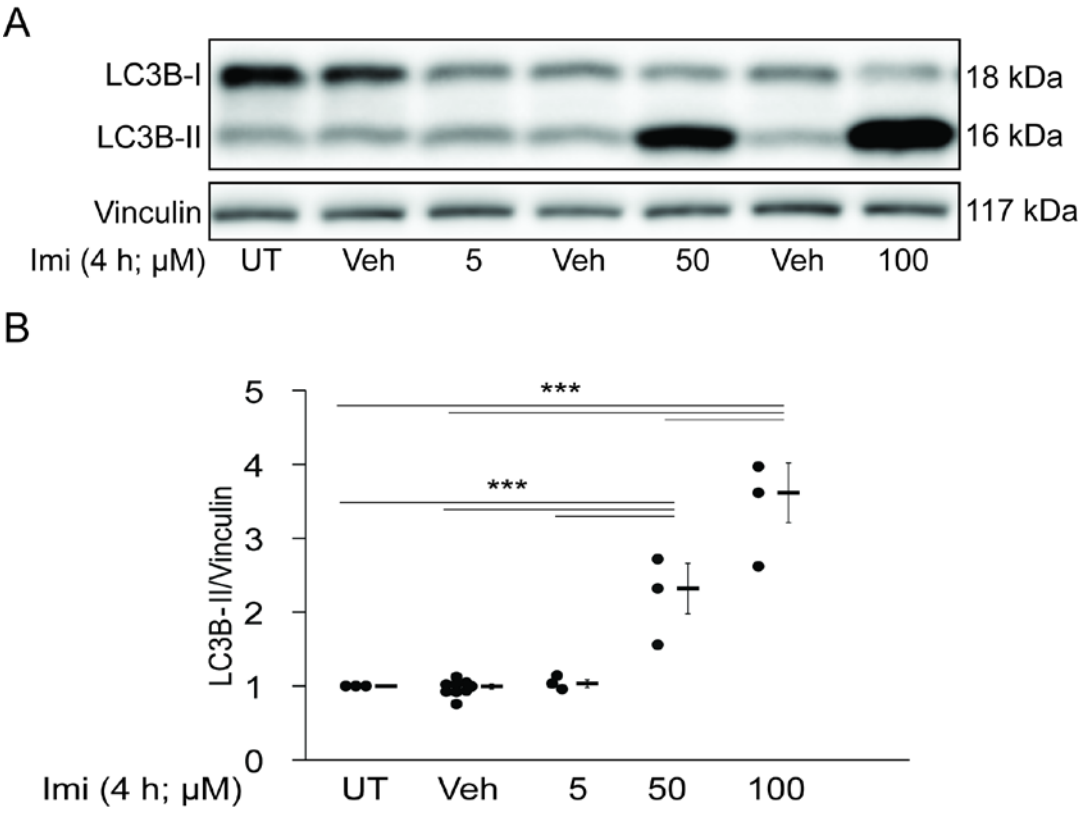

ASM is required for mTOR to inhibit autophagy (pharmacological dose dependence).

(A) Representative Western blot and (B) quantification by densitometry of LC3B-II protein expression in HPAEC relative to vinculin (loading control), following treatment with the ASM inhibitor imipramine (indicated doses; 4 hours), compared to vehicle (water). Graph shows individual data points of three independent experiments, as well as means and standard error of the mean, *** = $p \leq 0.001$ (ANOVA with Tukey Post Hoc).

Figure 28.

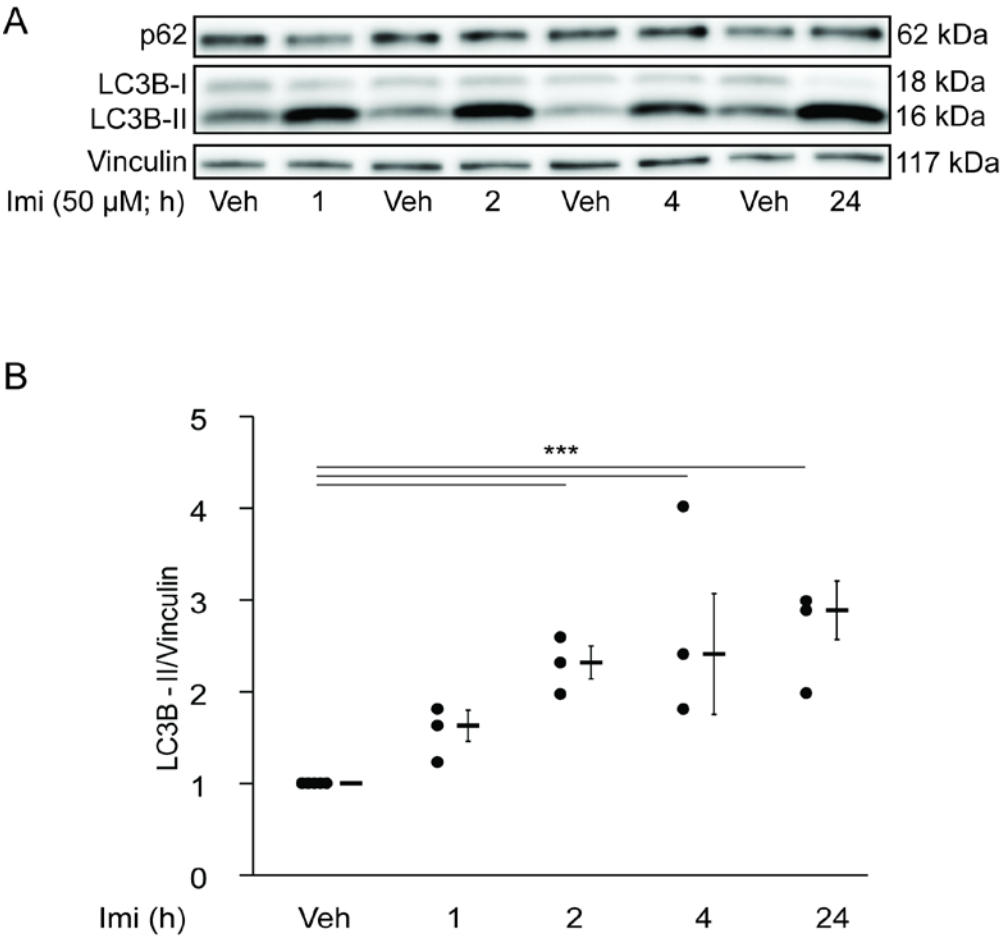

ASM is required for mTOR to inhibit autophagy (pharmacological time dependence).

(A) Representative Western blot and (B) quantification by densitometry of LC3B-II relative to vinculin in HPAEC treated with imipramine (50 µM for indicated amount of time). Graph shows individual data points of three independent experiments, as well as means and standard error of the mean, *** = $p \leq 0.001$ (ANOVA with Tukey Post Hoc).

slightly with no significant differences. Off-target effects were not responsible for this phenomenon as inhibition with siRNA against the ASM gene precursor *SMPD1*, led to variable but significant increases in LC3B-II as detected by Western blot and quantified by densitometry (n = 14) (**Figure 29A and B**). These results indicate that decreasing ASM activity may induce autophagy.

3.3 Autolysosomes exhibit degradative potential during ASM inhibition

The increased LC3B-II abundance following ASM inhibition could be due to increased production of autophagosomes or, conversely, the reduced clearance of these membrane-encapsulated vesicles.[22] To test this point, ASM-inhibition experiments in HPAEC were performed in the presence or absence of chloroquine, which increases lysosomal pH, diminishes the activity of acidic proteases, decreases autophagosome-lysosome fusion, and slows the degradation of LC3B-II associated with autophagosomes.[103-106] When lysosomal degradation was inhibited with chloroquine (50 µM) during ASM-inhibition with imipramine (50 µM), we noted a significant increase in LC3B-II above that seen during treatment of cells with imipramine alone, suggesting that autophagosomal turnover is still occurring and that LC3B-II accumulation is due to increased autophagosome formation rather than blocked autophagic flux, although both may be occurring to different extents (n = 3) (**Figure 30A and B**).[107-109] Consistent with earlier experiments, p62 levels were not significantly increased with imipramine-treated cells (**Figure 30A and C**). We wondered if the lysosomal inhibition by chloroquine (50 µM) was too great to see increases in LC3B-II and p62 levels above that of chloroquine treatment alone, so we decided to perform

Figure 29.

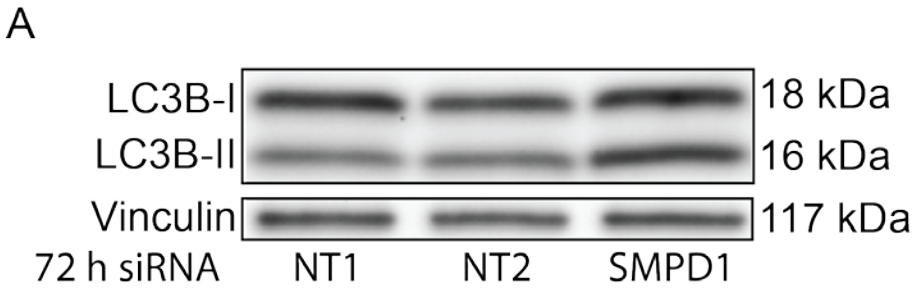

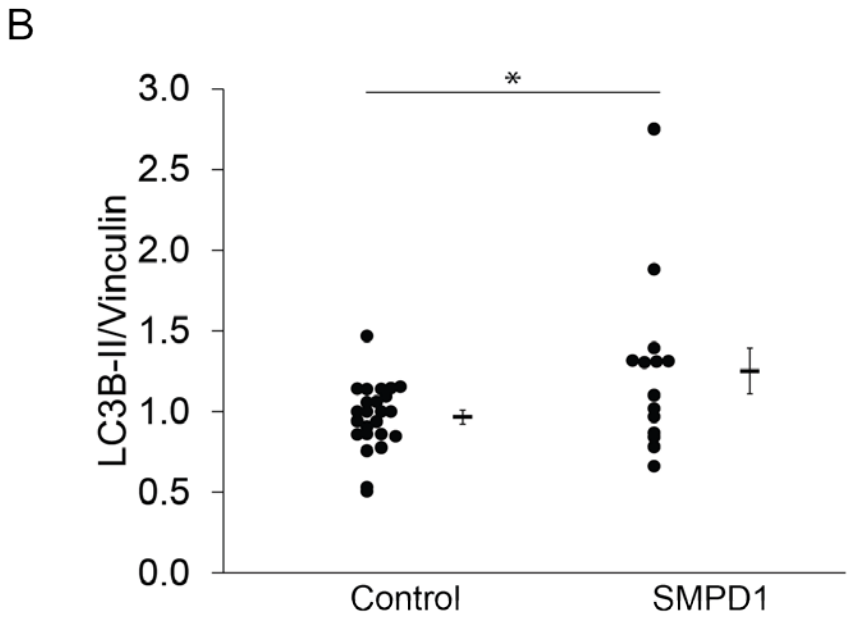

ASM is required for mTOR to inhibit autophagy (siRNA inhibition).

(A) Representative Western blot (B) and quantification of LC3B-II by densitometry in HPAEC transfected with siGlo (transfection indicator), non-targeting pool 1, pool 2 or *SMPD1* siRNA (1-3 µM; 48-72 hours). Graphs show individual data points of 14 independent experiments, as well as means and standard error of the mean, * = $p \leq 0.05$ (Student's t-test).

Figure 30.

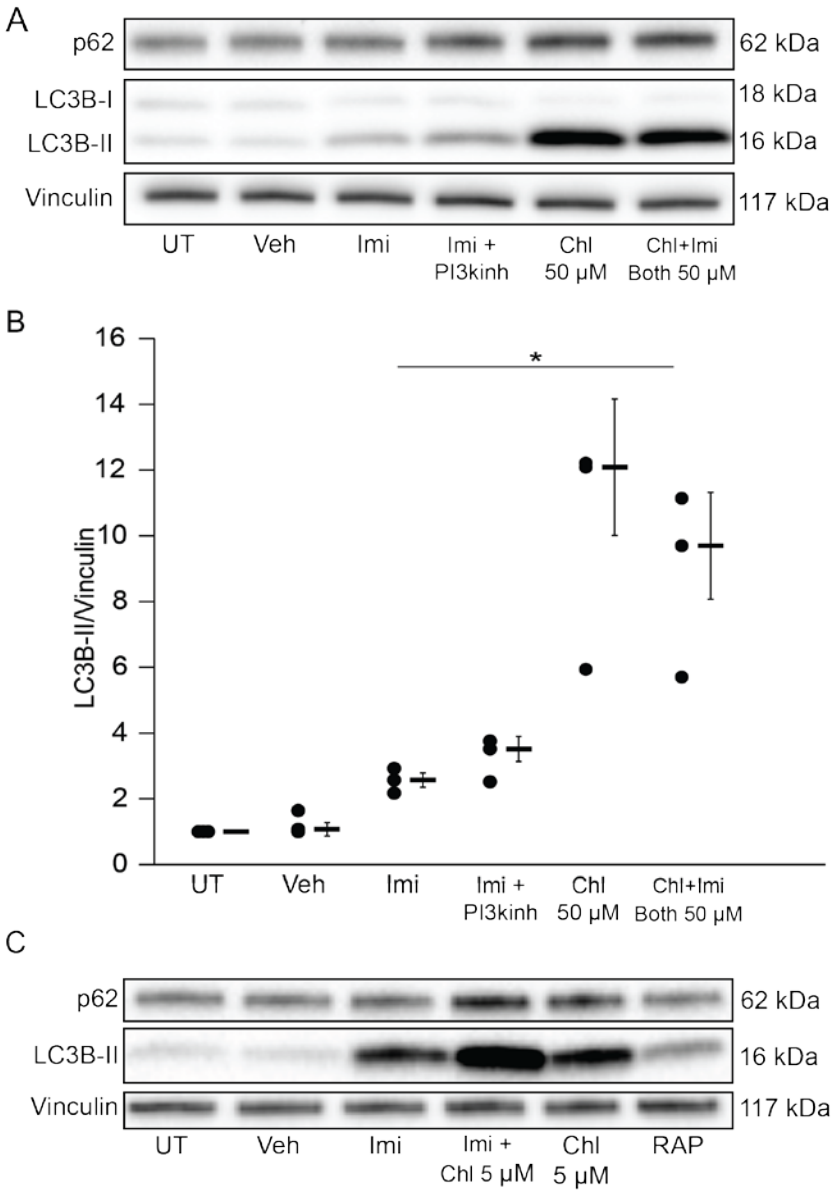

ASM inhibition induces autophagy with degradative potential

(A) Representative Western blot (LC3B-II and p62) and (B) quantification by densitometry of LC3B-II protein expression in HPAEC relative to vinculin (loading control), following treatment with the ASM inhibitor imipramine (50 µM; 4 hours), compared to concomitant treatment with imipramine (50 µM; 4 hours) and

chloroquine (50 μM; 4 hours). LY294002 (100 μM) was administered 1 hour prior to treatment. Graph shows individual data points of three independent experiments, as well as means and standard error of the mean, * = $p \leq 0.05$ (ANOVA with Tukey Post Hoc). (C) Representative Western blot of p62, LC3B-II, and vinculin (loading control), following treatment with the ASM inhibitor imipramine (50 μM; 4 hours) and chloroquine (5 μM; 4 hours).

the same flux experiments using a much lower concentration of chloroquine (5 μM). Imipramine (50 μM) treatment raised LC3B-II levels above that of vehicle, and the co-treatment of imipramine (50 μM) and chloroquine (5 μM) markedly increased LC3B-II levels above that of imipramine or chloroquine treatment alone signifying more LC3B-II was being generated due to ASM inhibition. (**Figure 30C**). Together, these results indicate that ASM is required to inhibit excessive autophagy and that ASM inhibition by imipramine induces autophagy in HPAEC.

We also investigated the autophagic flux in cells with pharmacologically reduced ASM function *via* detection of immunofluorescence in a stable eGFP-LC3B (green) expressing epithelial cell line (BEAS2b) immunostained with LAMP1. Vehicle-treated cells exhibited cytosolic and diffuse green immunofluorescence, as expected due to low levels of autophagy, with various levels of co-localization with LAMP1-positive (red) endolysosomal vesicles (**Figure 31**). Imipramine treatment increased the abundance of punctate, GFP-containing autophagic vesicles, consistent with biochemical analysis of increased LC3B-II abundance in cells, which overlapped with LAMP1 signal suggesting fusion was occurring (**Figure 31**). Co-treatment with imipramine and chloroquine revealed a greater abundance of intracellular GFP punctate vesicles, reflecting an increased number of autophagosomes, consistent with the inhibition of proteolysis using this weak base (**Figure 31**). Overlapping signals in this treatment from LC3B-II and LAMP1 immunofluorescence produced a yellow fluorescence suggestive of intact autophagosome-lysosome fusion in this condition. Chloroquine treatment alone, known to raise lysosomal pH, block

Figure 31.

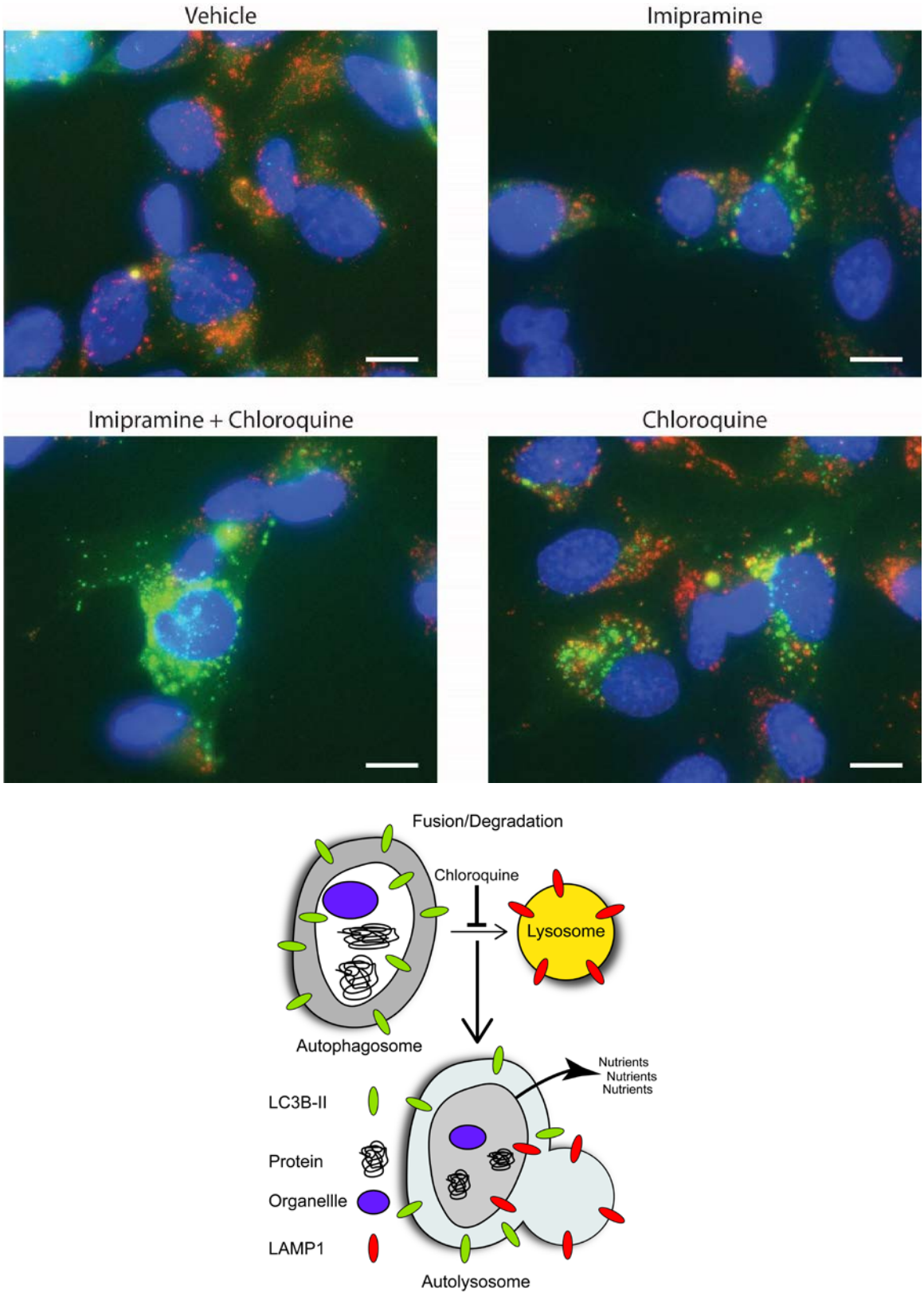
Vehicle
Imipramine
Imipramine + Chloroquine
Chloroquine
Fusion/Degradation
Chloroquine
Lysosome
Autophagosome
Nutrients
Nutrients
Nutrients
LC3B-II
Protein
Organellle
LAMP1
Autolysosome

Autophagosome-lysosome fusion occurs during ASM inhibition.

Immunofluorescence of BEAS2b expressing eGFP-LC3B (green) and LAMP1 immunolabeling (red) following treatment with imipramine (50 µM; 4 hours) and/or chloroquine (50 µM; 4 hours). Note the red-only immunofluorescence in fusion-blocked chloroquine treated cells (lower right), absence of red-only immunofluorescence in ASM-inhibited cells (upper right), and bright yellow in co-treated cells.

fusion, and halt degradation, caused green punctae to form but not to the extent noted in the co-treatment condition (**Figure 31**).[104-106] Different than imipramine alone, the chloroquine alone treatment had many regions of red-only staining, indicating a block in autophagosome-lysosome fusion that was not visualized in the imipramine-alone-treated cells (**Figure 31**). Together, these results suggest that ASM inhibition signals phagophore initiation and induces autophagy that has degradative potential.

3.4 ASM inhibition of autophagy in multiple cell types

To determine whether ASM is required to inhibit autophagy during homeostatic conditions in other cell types, we tested their response to ASM inhibition using similar conditions that triggered autophagy in HPAEC (imipramine, 50 μM, 4 hours). Primary human lung microvascular endothelial cells (HLMVEC), primary human umbilical vein endothelial cells (HUVEC), human monocytic THP-1 cells, and BEAS2b all exhibited similar increases in LC3B-II following ASM inhibition as determined by Western blot and quantified (BEAS2b) by densitometry ($n=6$) (**Figure 32A and B**). We utilized electron microscopy as a complementary method to help understand and visualize morphological changes occurring due to ASM inhibition. BEAS2b, cultured under control conditions, exhibited very few intra-cytoplasmic autolysosomal bodies as determined by small amounts of double membranes (darker) encapsulating cytoplasmic material and fusing with lysosomes (arrow; upper left-hand panel) (**Figure 33**).[22] In contrast, following ASM inhibition with imipramine (6 hours; in low serum), cells accumulated multiple large autolysosomal bodies (**Figure 33**).

Figure 32.

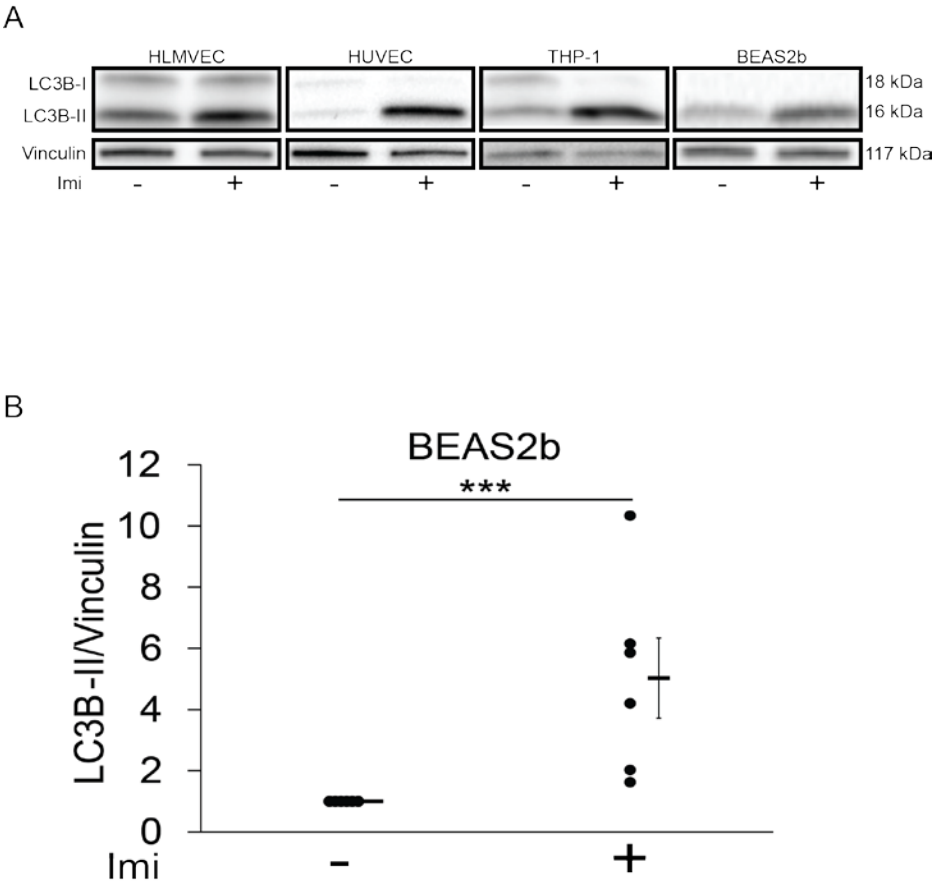

ASM inhibition of autophagy in multiple cell types.

(A) Western blot of LC3B-II and vinculin loading control in primary human lung microvascular endothelial cells (HLMVEC), primary human umbilical vein endothelial cells (HUVEC), human monocytes (THP-1), or immortalized bronchial epithelial cells (BEAS2b) treated with imipramine (4 hours; 50 μM). (B) LC3B-II quantification relative to vinculin (loading control) by densitometry in BEAS2b treated with imipramine (6 h in 2% FBS; 50 μM). Graph shows individual data points of six independent experiments, as well as means and standard error of the mean, *** = $p \leq 0.001$ (ANOVA with Tukey Post Hoc).

Figure 33.

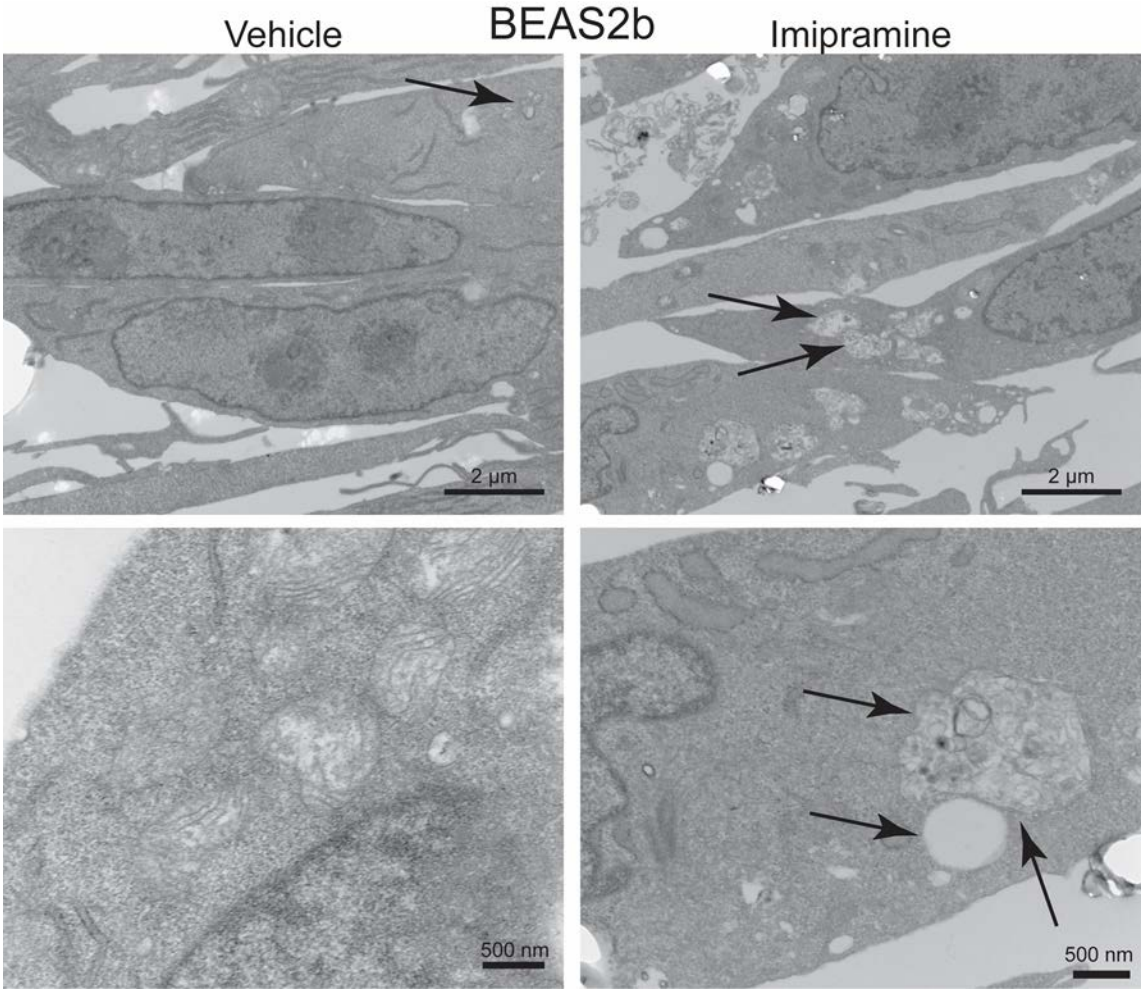

Large autolysosomes are formed during ASM inhibition.

Electron microscopy showing representative images of BEAS2b treated with vehicle (left) or imipramine (50 µM; six hours; low serum) (right). Lower panels are increased magnification images (lower left is different area than upper left; lower right is increased magnification of upper right). Very few autolysosomal bodies, as determined by darker limiting membranes of autophagosome fused with lysosome were detected in vehicle conditions (arrow; upper right panel). Markedly increased amounts of autophagosomes and autolysosomes in various

stages of the autophagic process can be seen in the imipramine-treated cells. The top two arrows in the upper right-hand panel point to an autophagosome that has fused with a lysosome (an autolysosome) and the contents are being degraded. The bottom two arrows in the upper right-hand panel point to an autophagosome and a lysosome that are about to fuse. Increased magnification of the autophagosome about to fuse with a lysosome revealed the actual double membrane structure that defines autophagosomes (arrow that points upward in lower right panel). The autophagosome contains cytoplasmic contents to be degraded while the lysosome is much less electron dense.

Different stages of the autophagic process can be seen (**Figure 33**).[22] The top two arrows in the upper right-hand panel point to an autophagosome that has fused with a lysosome and the contents are being degraded (**Figure 33**). The bottom two arrows in the upper right-hand panel point to an autophagosome and a lysosome that are about to fuse (**Figure 33**). In the lower-right panel, the double membrane of an autophagosome is clearly visible (arrow that points upward) (**Figure 33**).[22] The autophagosome contains cytoplasmic contents to be degraded while the lysosome is much less electron dense (**Figure 33**).[22]

3.5 Rapid autophagosome formation in response to ASM inhibition

To analyze the sphingolipid content of lysosomes of both vehicle-treated and imipramine-treated cells, we inhibited ASM at the shortest time point that gain of TFEB mobility and loss of smear pattern was evident (30 minutes) and performed a subcellular fractionation. We used isopycnic separation because organelles have different ranges of densities thus allowing for the enrichment of certain organelles over others (lightest fraction is one and the densest is six) (**Figure 34**). The technique that was used yielded both the mature form of cathepsin D and LAMP1 in fraction six indicating enrichment for lysosomes in this fraction (**Figure 34**). However, histone h3 (nuclear marker), VDAC (mitochondrial marker), and LC3B-II were also found in this fraction indicating that lysosomes were not the only constituents of this fraction (**Figure 34**). Due to the marked increase in autophagosomes in this fraction, lysosomal sphingolipid assessment was not possible. However, LC3B-II was markedly increased in fraction six and present in all fractions of the imipramine-treated cells but was virtually

Figure 34.

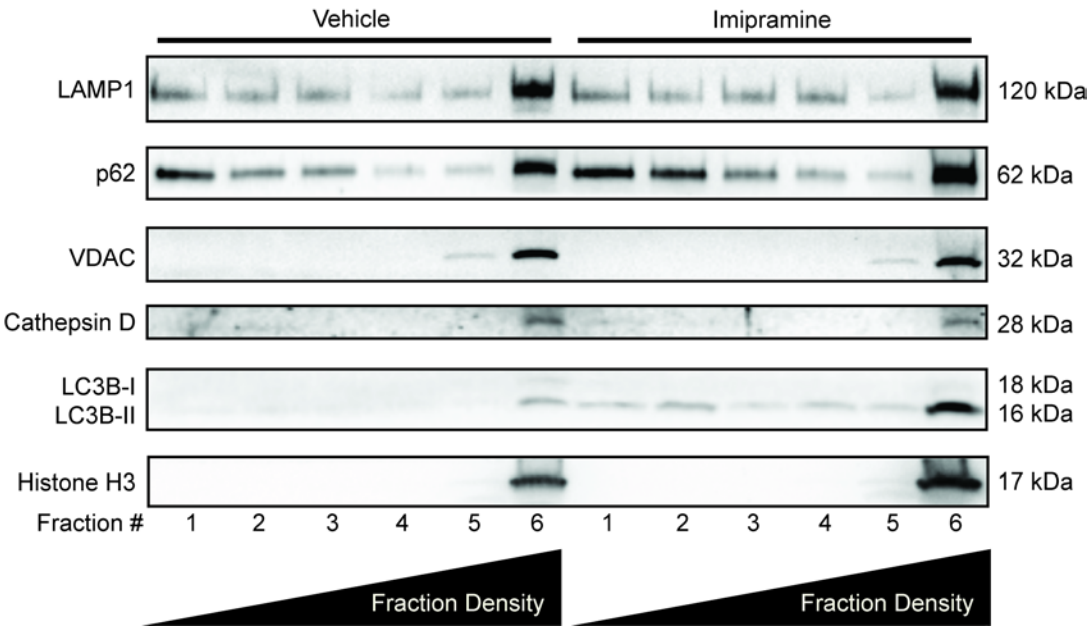

Rapid autophagosome formation due to ASM inhibition.

Western blot of subcellular fractions (Opti-prep, isopycnic separation) of HPAEC treated with ASM inhibitor imipramine (50 μM; 30 minutes). Note the abundance of autophagosomal marker LC3B-II in all imipramine-treated fractions. Fraction one was the lowest density fraction and fraction six the greatest.

undetectable in fractions one through five of the vehicle-treated cells and may be indicative of newly formed or forming autophagosomes (**Figure 34**). This increase in LC3B-II was not due to different amount of protein loaded because LAMP1, a very abundant protein, was found in all fractions with roughly the same pattern and abundance in vehicle-treated samples as in imipramine-treated samples, indicating that roughly the same amount of protein was used for electrophoresis (**Figure 34**).

3.6 Sphingolipid changes due to ASM inhibition

We next used tandem mass spectrometry to measure the effect of ASM inhibition on sphingolipid content in the isolated fractions. Fraction six revealed the same sphingolipid regulation as all of the other fractions, including whole cells and soluble cytosolic portions as determined by LC-MS/MS (n = 4) (**Figures 35 and 36**). Consistent with a manuscript by Elojeimy *et al*. in 2006, which treated DU 145 cancer cells with ASM inhibitor desipramine, primary HPAEC trended towards increased ceramide and decreased sphingosine content when the pharmacological ASM inhibitor was applied as determined by LC-MS/MS(n = 4) (**Figures 35 and 36**).[110] To test if decreased sphingosine abundance was due to the non-specificity of the pharmacological inhibitor or if ASM activity is needed for sphingosine production, we analyzed levels of sphingosine by LC-MS/MS in HPAEC transfected with non-targeting pool 1, pool 2 or *SMPD1* siRNA (1-3 µM; 48-72 hours; n = 3). Specific inhibition of ASM with siRNA reduced sphingosine levels in HPAEC (**Figure 37**). These results suggest the requirement of ASM to maintain appropriate sphingosine levels.

Figure 35.

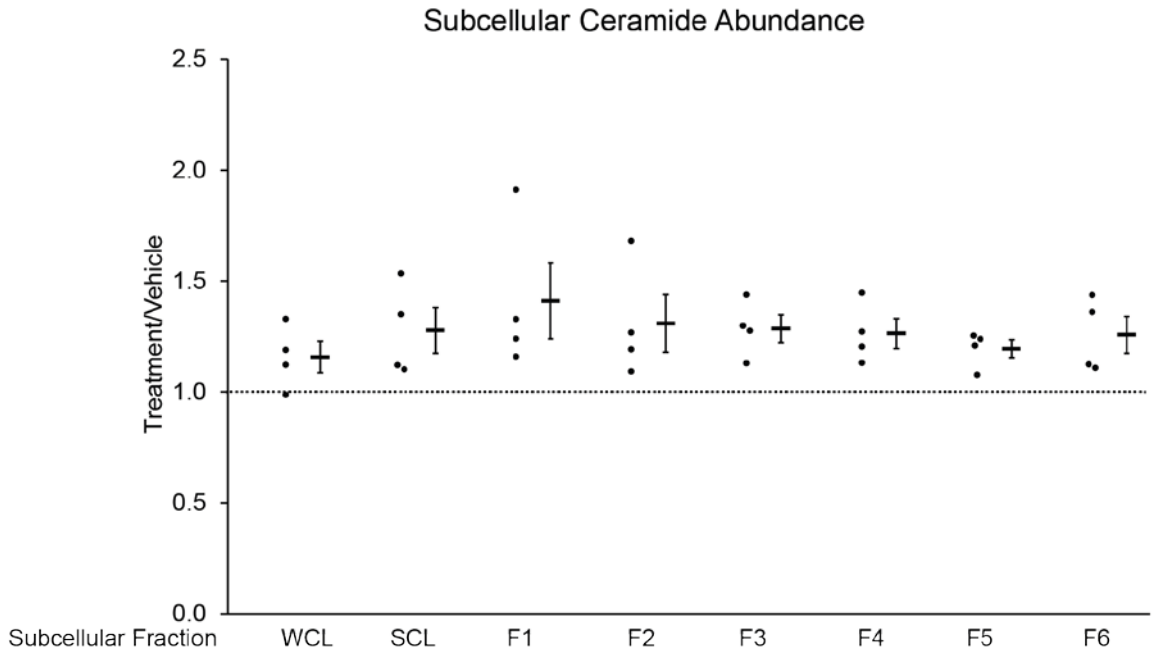

Subcellular ceramides increase due to ASM inhibition.

Total ceramide content of subcellular fractions (Opti-prep, isopycnic separation) of HPAEC treated with ASM inhibitor imipramine (50 µM; 30 minutes). Fraction one was the lowest density fraction and fraction six the greatest. WCL stands for whole cell lipids, and SCL stands for soluble cytosolic lipids. Graph shows data points for four independent experiments.

Figure 36.

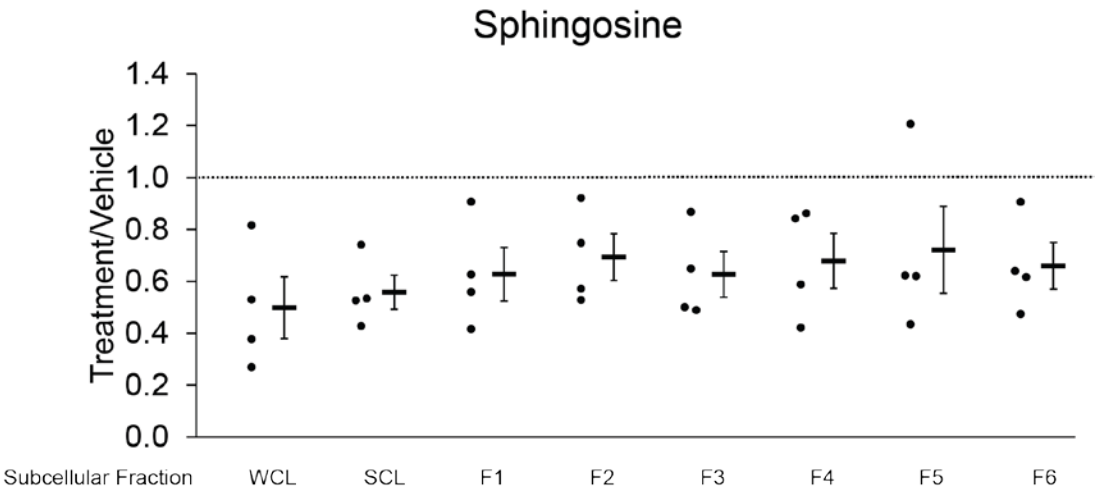

Sphingosine levels trended towards decrease in all subcellular fractions when ASM is inhibited.

Sphingosine content of subcellular fractions (Opti-prep, isopycnic separation) of HPAEC treated with ASM inhibitor imipramine (50 µM; 30 minutes). Fraction one was the lowest density fraction and fraction six the greatest. WCL stands for whole cell lipids, and SCL stands for soluble cytosolic lipids. Graph shows data points for four independent experiments.

Figure 37.

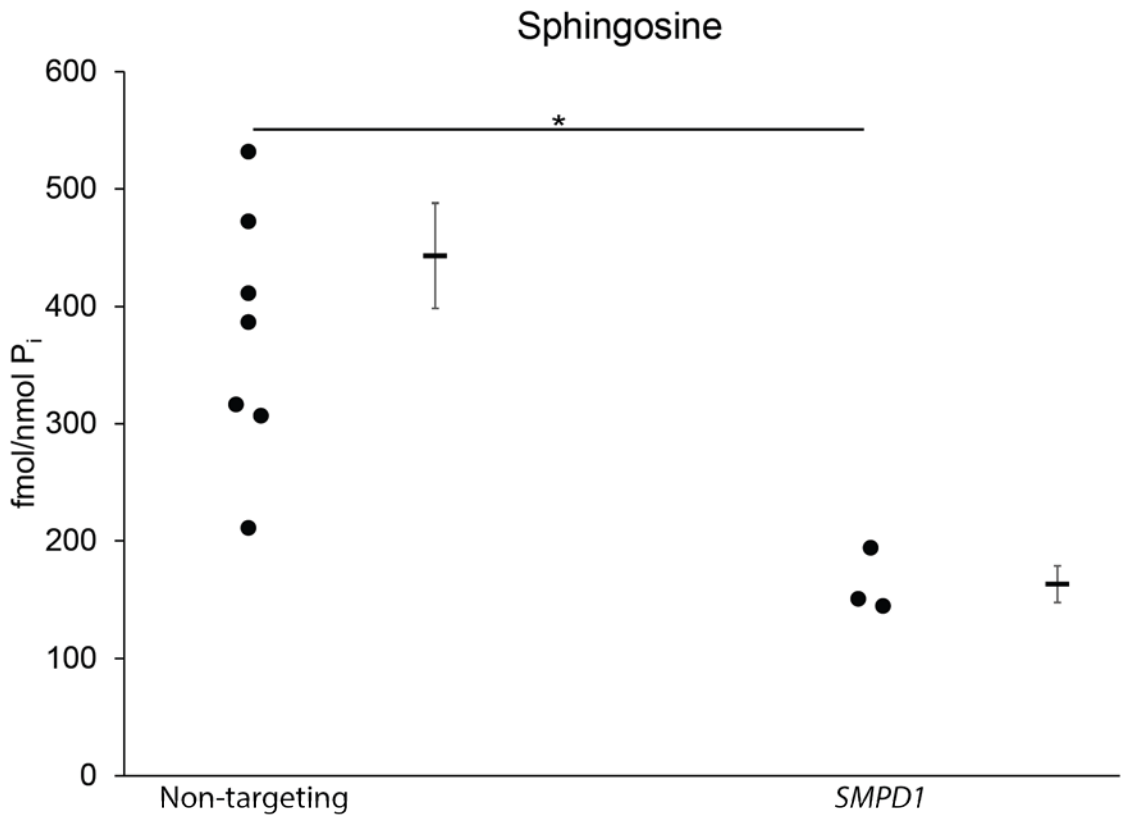

ASM inhibition with siRNA decreases sphingosine levels.

Sphingosine levels in HPAEC transfected with non-targeting pool 1, pool 2 or *SMPD1* siRNA (1-3 µM; 48-72 hours). Graphs show individual data points of three independent experiments, as well as means and standard error of the mean, * = $p \leq 0.05$ (Student's t-test).

3.7 Transgenic knockout of ASM increases LC3B-II levels and decreases sphingosine levels in lungs of mice

To investigate if the marked effects of ASM inhibition on autophagy are recapitulated *in vivo*, we probed whole lung lysates of *Smpd1*$^{+/-}$ mice, which have 50% the ASM activity as wild-type mice, for LC3B-II.[100] These tissues exhibited an increase of LC3B-II protein compared to *Smpd1*$^{+/+}$ littermates, as determined by Western blot and might not be due to the sphingomyelin overload that the *Smpd1*$^{-/-}$ mice exhibit (**Figure 38A**).[1, 111] To test if the known decrease in sphingosine seen in primary cells with pharmacological inhibition was present *in vivo* with genetically modified mice and thus not due to the degradation of acid ceramidase by the pharmacological inhibitor, we analyzed the sphingosine levels in the lungs of the genetically modified mice and compared them to the wildtype mice. The sphingosine content was both significantly decreased in the *Smpd1*$^{+/-}$ mouse and drastically reduced in the *Smpd1*$^{-/-}$ mouse, suggesting that sphingosine abundance depends on ASM activity (n = 7, 6, and 5 for *Smpd1*$^{+/+}$, *Smpd1*$^{+/-}$, and *Smpd1*$^{-/-}$, respectively) (**Figure 38B**).

3.8 Schematic depicting changes due to ASM inhibition

During homeostatic conditions, ASM functions normally and lysosomal homeostasis allows for proper LYNUS signaling that favors protein synthesis (**Figure 39**). ASM inhibition alters LYNUS function by reducing mTOR phosphorylation, reducing phosphorylation of mTOR downstream substrate P70S6k, translocating TFEB to the nucleus, and inducing autophagy with degradative potential (**Figure 39**).

Figure 38.

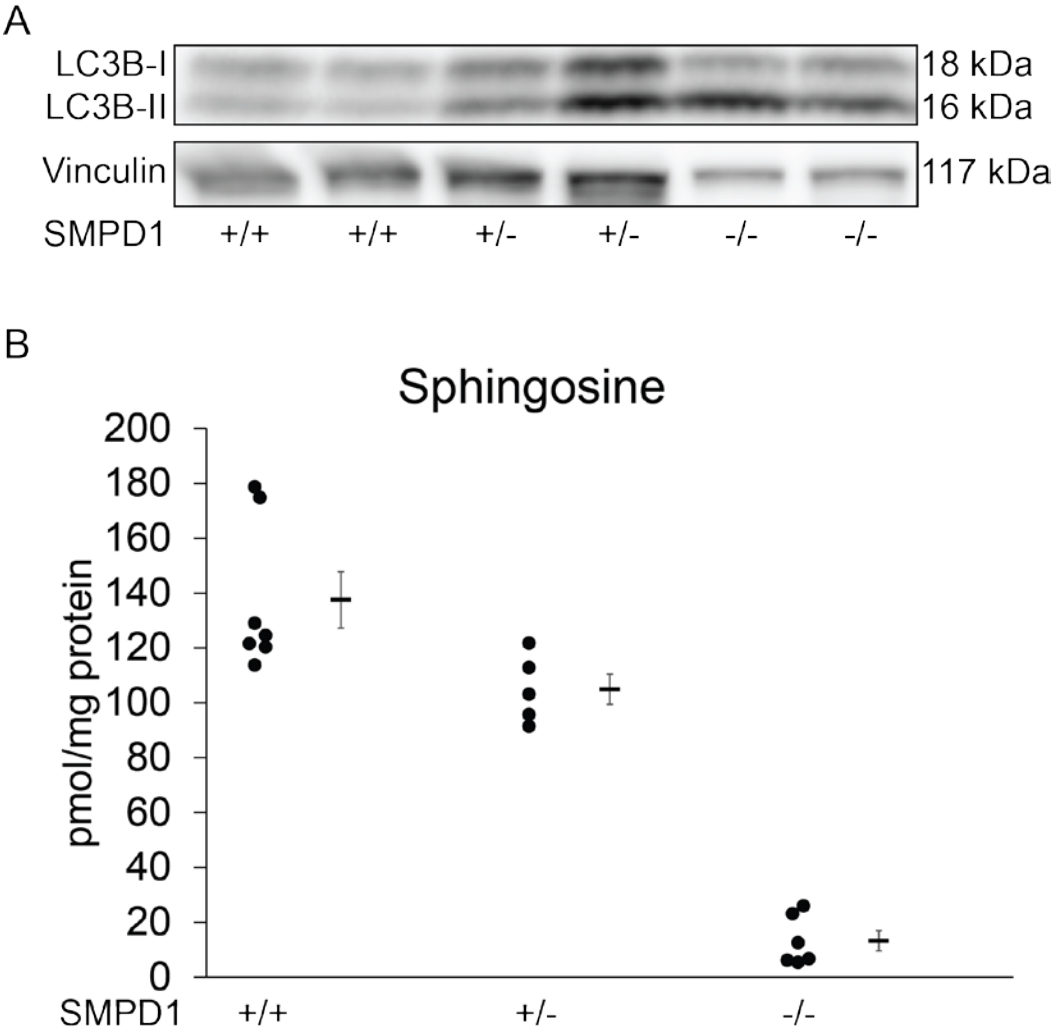

ASM inhibits autophagy in vivo.

(A) Western blot of LC3B-II from whole lung lysates of genetically modified mice (females, three months of age) (B) LC-MS/MS lipid quantification of sphingosine (downstream ceramide metabolite) in whole lungs of genetically modified mice (females, three months of age). Graph shows individual data points from different animals, means and standard error of the mean, * = $p \leq 0.05$, *** = $p \leq 0.001$ (ANOVA with Dunnett's post hoc analysis).

Figure 39.

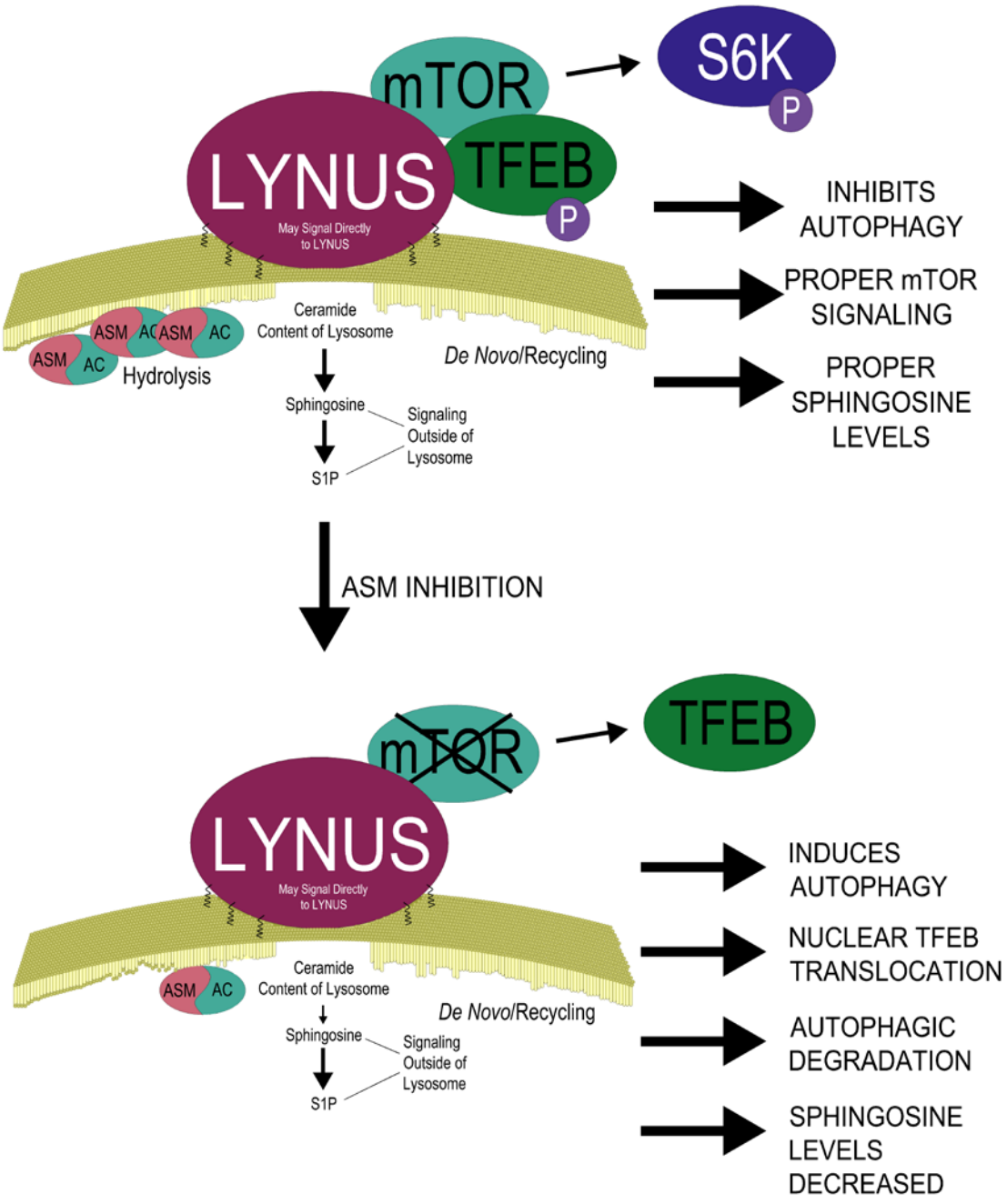
mTOR
S6K
P
LYNUS
May Signal Directly to LYNUS
TFEB
P
INHIBITS AUTOPHAGY
PROPER mTOR SIGNALING
PROPER SPHINGOSINE LEVELS
ASM
AC
ASM
AC
ASM
AC
Hydrolysis
Ceramide Content of Lysosome
De Novo/Recycling
Sphingosine
S1P
Signaling Outside of Lysosome
ASM INHIBITION
mTOR
TFEB
LYNUS
May Signal Directly to LYNUS
INDUCES AUTOPHAGY
NUCLEAR TFEB TRANSLOCATION
AUTOPHAGIC DEGRADATION
SPHINGOSINE LEVELS DECREASED
ASM
AC
Ceramide Content of Lysosome
De Novo/Recycling
Sphingosine
S1P
Signaling Outside of Lysosome

Lysosomal ASM contribution to mTOR signaling and autophagy.

Graphic representation of the lysosomal membrane with LYNUS docked on the cytosolic side of the membrane and ASM forming a complex with acid ceramidase on the luminal side of the membrane. During homeostatic conditions, ASM generates ceramide at a basal rate allowing for proper biophysical characteristics of the lysosomal membrane and signaling from downstream metabolites. ASM inhibition reduces mTOR phosphorylation, reduces P70S6k phosphorylation, translocates TFEB to the nucleus, and induces autophagy with degradative potential.

Chapter 4. Discussion

We set out to investigate the hypothesis that ASM function is required for mTOR signaling and inhibition of autophagy during homeostasis. As a corollary, reduced ASM activity is sufficient to induce autophagy while concomitantly changing lysosomal membrane lipid composition to favor autophagosome-lysosome fusion. With this research, we have discovered a new role for ASM in autophagy due to its baseline activity requirement for mTOR activity. Although the exact mechanism for this effect remains to be elucidated, it may be related to both changes in the lysosomal sphingolipid content and/or reduced sphingosine levels. ASM inhibition manifested itself as TFEB translocation with the induction of autophagy due to loss of mTOR signaling and decreased sphingosine levels. In addition, large, irregular autolysosomes, possibly due to a favorable membrane lipid composition and less autophagosome movement due to decreased calcium efflux from the lysosome because of ASM inhibition likely contributes to the size of these autolysosomal bodies.[4] Furthermore, since inhomogeneity of EM signal was noted both inside and outside of large, irregular autolysosomes, autophagic induction and pleiotropic fusion may be occurring simultaneously.[22] No loss of lysosomal integrity or cell viability occurred, the former assessed by acridine orange staining and the latter measured by thymidine incorporation (data not shown).

One study, by Rossi *et al*. in 2009, that was performed in a cancer cell line that overexpressed LC3-GFP, showed that desmethylclomipramine (DCMI), a metabolite of clomipramine which is very close in structure to imipramine, blocks

autophagic flux.[109] If the increase in LC3B-II due to ASM inhibition in HPAEC was due to a blockage in the autophagic flux, much higher levels of LC3B-II would have been observed over a 72-hour period. Inducing autophagy by inhibiting ASM retains degradative potential in HPAEC. The increase in LC3B-II in the *Smpd1*$^{+/-}$ mice, which have half the ASM activity as their wild type counterparts, is most likely not due the sphingomyelin overload and blockage of autophagic flux that is seen in the *Smpd1*$^{-/-}$ mice, which have little to no ASM activity.[1, 100, 111] One limitation in the present study is that autolysosomal degradation was not tested using a lysosomal protease inhibitor. It has also been shown that autophagosomes move slower without ASM due to decreased calcium efflux from the lysosome when this enzyme is not present.[108] Autophagic induction with less flux may explain the large bodies observed in the electron microscopy images. Along with the observations seen by others, we suggest that ASM is also needed for mTOR activity and autophagy is induced when this enzyme is inhibited both pharmacologically and with siRNA. These effects were also observed in an epithelial cell line, endothelial cells of different origins, other lung endothelial cells, as well as in monocytes, suggesting ASM control of mTOR may be a fundamental mechanism in cells.

The markedly increased presence of autophagosomes did not allow for assessment of lysosomal sphingolipid changes and is another limitation of the present study. Subcellular fractionation revealed the rapid manner in which autophagosome formation occurs due to ablation of mTOR signaling in response to changes in ASM activity. The presence of LC3B-II in the lighter fractions of

ASM-inhibited cells and not in vehicle-treated cells, at a 30 minute time point, is suggestive of newly formed or forming autophagosomes. Since the markers, LAMP1 and mature cathepsin D were present with roughly the same abundance in imipramine-treated cells as in vehicle-treated cells, the trend towards increased ceramide abundance seen in this fraction may be due to the overwhelming presence of autophagosomes. The most profound change in sphingolipid metabolism that was observed in response to pharmacological ASM inhibition, consistent with previous literature, was a global decrease in sphingosine abundance.[112]

Here, we show that HPAEC have significantly decreased sphingosine levels in response to specific ASM inhibition with siRNA, indicating that ASM activity is needed for acid ceramidase to convert ceramide to sphingosine. This effect was recapitulated *in vivo* by significantly and profoundly decreased levels of sphingosine in *Smpd*1$^{+/-}$ and *Smpd1*$^{-/-}$ mice, respectively. It is unknown whether the activity of ASM is needed to produce substrates for acid ceramidase or if its presence is needed to form a complex with acid ceramidase for sphingosine production.[110] It is also unknown if the drop in sphingosine levels is responsible for the reduction in mTOR activity.

Several possibilities exist for the reduction in mTOR signaling due to reduction in sphingosine content. First, sphingosine plays a role in calcium efflux from the lysosome.[113] Hoglinger *et al*. delivered inactive, caged sphingosine to cells and then uncaged the sphingosine with light, which instantly produces higher levels of sphingosine intracellularly.[113] When sphingosine levels were

increased, calcium efflux from the lysosome increased. This led to increased calcineurin, which is phosphatase, activity and subsequent dephosphorylation of TFEB.[114] Also, in cells from Niemann-Pick type C, which mimics Niemann-Pick A and B but has a different mechanism, patients were shown to have increased lysosomal sphingosine content and exhibited less lysosomal calcium efflux upon the uncaging of sphingosine.[113] This suggests that the ratio of sphingosine outside of the lysosome to that inside of the lysosome plays a role in how much calcium exits the lysosome. Acute lowered lysosomal sphingosine and normal cytoplasmic sphingosine content may mimic the uncaging of sphingosine and subsequent dephosphorylation of TFEB seen by this group. Once sphingosine concentrations inside and outside of the lysosome stabilize, the effect may be less or even opposite and might be another reason for occasional lower levels of LC3B-II in samples with ASM inhibited by siRNA, which would indicate a feedback loop. Second, sphingosine itself is known to activate many protein kinases and can act without being further metabolized to S-1-P.[115, 116] It may be possible to decrease mTOR signaling by decreasing sphingosine content—either directly or through an unknown signaling cascade. Last, sphingosine can be metabolized to S-1-P, which has a plethora of signaling effects.[117] The lowered sphingosine content may lead to lower S-1-P levels and decreased mTOR activation through reduced S-1-P receptor three activation.[118]

ASM activity in different human tissues is known to change with age.[119, 120] Both apoptosis and impaired autophagy are associated with ASM hyperactivation, which has been implicated in the pathogenesis of multiple acute

and chronic diseases, including but not limited to Alzheimer's disease, acute lung edema, and pulmonary emphysema. [5, 7, 101, 121, 122] In general, aging and chronic diseases that have hyperactivation of ASM as part of their pathogenesis result, eventually, in excessive apoptosis of an organ, such as the brain in Alzheimer's disease or the lung in COPD. This thesis inadvertently contains a translational component because it suggests that diseases which have blocked autophagic flux as part of the pathogenesis may benefit from therapeutics that inhibit ASM. Once tissue loss in the brain of an Alzheimer's patient or in the lungs of emphysema patient occurs, these tissues cannot be regenerated. Blocked autophagic flux is part of the pathogenesis of both of these diseases and occurs before loss of tissue. It is unknown whether accumulation of autophagosomes is the triggering mechanism for tissue loss in either of these diseases, however, induction of autophagy with degradative potential may be able to abrogate this effect if it is. Administration of tricyclic anti-depressants, with well-known side effects that have already been approved by the Food and Drug Administration might be able to extend the lives of patients with early signs of these diseases. More experiments testing this theory should be performed.

.

Chapter 5. Conclusion

Our study demonstrates for the first time an important, homeostatic functional relationship between ASM and LYNUS in HPAEC. These results indicate a requirement for baseline ASM activity in order to maintain sphingosine levels and for homeostatic mTOR signaling to occur, inhibiting excessive autophagy during normal conditions. These findings, which provide a new link between ASM and homeostatic lysosomal function, complement our knowledge of the role of ASM hyperactivation during stress. Given the marked effects of ASM inhibition on triggering autophagy with degradative potential and blocking mTOR activity, our results could be leveraged in clinical conditions before irreversible loss of tissue occurs. Reducing ASM activity as a means of triggering fluxing autophagy would be pertinent to diseases such as COPD and Alzheimer's disease, where blocked autophagic flux is part of the pathogenesis that occurs before permanent tissue loss.[7, 87]

The mechanisms by which ASM maintains lysosomal homeostasis remain somewhat elusive and can only be postulated. We hypothesize these effects may be due to biophysical sphingolipid membrane perturbations that may change microdomain characteristics such that LYNUS docking is less favorable and fusion of autophagosome and lysosome is more favorable, altered ceramide signaling directly to LYNUS *via* short time scale ceramide flip-flop may be happening, indirect signaling by sphingosine itself, or signaling cascades that depend on sphingosine, may not be happening in the proper manner. Further

studies that can better tease out the lysosomal ceramide content and the effects associated with it have to be performed.

In conclusion, our study indicates that lysosomal ASM is an important determinant of homeostatic mTOR signaling and LYNUS function, making this sphingolipid metabolic enzyme an important regulator of protein synthesis and autophagy inhibition. The clinical implications of these results relate to the widespread use of antidepressants that inhibit lysosomal ASM production and may give them application in other settings. Furthermore, it may be of interest to alter ASM activity to control autophagic induction for therapeutic purposes in conditions where these outcomes are desirable.

References

1. Gabande-Rodriguez E, Boya P, Labrador V, Dotti CG, Ledesma MD. High sphingomyelin levels induce lysosomal damage and autophagy dysfunction in Niemann Pick disease type A. Cell death and differentiation 2014; 21:864-75.

2. Schuchman EH. The pathogenesis and treatment of acid sphingomyelinase-deficient Niemann-Pick disease. Int J Clin Pharmacol Ther 2009; 47 Suppl 1:S48-57.

3. Mizushima N. Autophagy: process and function. Genes & development 2007; 21:2861-73.

4. Xu M, Zhang Q, Li PL, Nguyen T, Li X, Zhang Y. Regulation of dynein-mediated autophagosomes trafficking by ASM in CASMCs. Front Biosci (Landmark Ed) 2016; 21:696-706.

5. Perrotta C, Cervia D, De Palma C, Assi E, Pellegrino P, Bassi MT, Clementi E. The emerging role of Acid Sphingomyelinase in autophagy. Apoptosis : an international journal on programmed cell death 2015; 20:635-44.

6. Garcia-Ruiz C, Mato JM, Vance D, Kaplowitz N, Fernandez-Checa JC. Acid sphingomyelinase-ceramide system in steatohepatitis: a novel target regulating multiple pathways. J Hepatol 2015; 62:219-33.

7. Lee JK, Jin HK, Park MH, Kim BR, Lee PH, Nakauchi H, Carter JE, He X, Schuchman EH, Bae JS. Acid sphingomyelinase modulates the autophagic process by controlling lysosomal biogenesis in Alzheimer's disease. J Exp Med 2014; 211:1551-70.

8. Cervia D, Assi E, De Palma C, Giovarelli M, Bizzozero L, Pambianco S, Di Renzo I, Zecchini S, Moscheni C, Vantaggiato C, et al. Essential role for acid sphingomyelinase-inhibited autophagy in melanoma response to cisplatin. Oncotarget 2016; 7:24995-5009.

9. Settembre C, Fraldi A, Medina DL, Ballabio A. Signals from the lysosome: a control centre for cellular clearance and energy metabolism. Nat Rev Mol Cell Bio 2013; 14:283-96.

10. Lin X, Li Z, Gorfe AA. Reversible Effects of Peptide Concentration and Lipid Composition on H-Ras Lipid Anchor Clustering. Biophysical journal 2015; 109:2467-70.

11. Klionsky DJ. Autophagy revisited: a conversation with Christian de Duve. Autophagy 2008; 4:740-3.

12. Mizushima N, Yoshimori T, Ohsumi Y. The role of Atg proteins in autophagosome formation. Annual review of cell and developmental biology 2011; 27:107-32.

13. Boya P, Reggiori F, Codogno P. Emerging regulation and functions of autophagy. Nat Cell Biol 2013; 15:713-20.

14. Li WW, Li J, Bao JK. Microautophagy: lesser-known self-eating. Cellular and molecular life sciences : CMLS 2012; 69:1125-36.

15. Sattler T, Mayer A. Cell-free reconstitution of microautophagic vacuole invagination and vesicle formation. J Cell Biol 2000; 151:529-38.

16. Schuck S, Gallagher CM, Walter P. ER-phagy mediates selective degradation of endoplasmic reticulum independently of the core autophagy machinery. J Cell Sci 2014; 127:4078-88.

17. Cuervo AM, Wong E. Chaperone-mediated autophagy: roles in disease and aging. Cell Res 2014; 24:92-104.

18. Tooze SA, Yoshimori T. The origin of the autophagosomal membrane. Nature cell biology 2010; 12:831-5.

19. Hailey DW, Rambold AS, Satpute-Krishnan P, Mitra K, Sougrat R, Kim PK, Lippincott-Schwartz J. Mitochondria supply membranes for autophagosome biogenesis during starvation. Cell 2010; 141:656-67.

20. Kimura S, Noda T, Yoshimori T. Dynein-dependent movement of autophagosomes mediates efficient encounters with lysosomes. Cell structure and function 2008; 33:109-22.

21. Mauvezin C, Nagy P, Juhasz G, Neufeld TP. Autophagosome-lysosome fusion is independent of V-ATPase-mediated acidification. Nature communications 2015; 6:7007.

22. Klionsky DJ, Abdelmohsen K, Abe A, Abedin MJ, Abeliovich H, Acevedo Arozena A, Adachi H, Adams CM, Adams PD, Adeli K, et al. Guidelines for the use and interpretation of assays for monitoring autophagy (3rd edition). Autophagy 2016; 12:1-222.

23. Laplante M, Sabatini DM. mTOR signaling in growth control and disease. Cell 2012; 149:274-93.

24. Dunlop EA, Hunt DK, Acosta-Jaquez HA, Fingar DC, Tee AR. ULK1 inhibits mTORC1 signaling, promotes multisite Raptor phosphorylation and hinders substrate binding. Autophagy 2011; 7:737-47.

25. Kim J, Kundu M, Viollet B, Guan KL. AMPK and mTOR regulate autophagy through direct phosphorylation of Ulk1. Nature cell biology 2011; 13:132-41.

26. Shimobayashi M, Hall MN. Multiple amino acid sensing inputs to mTORC1. Cell Res 2016; 26:7-20.

27. Settembre C, Zoncu R, Medina DL, Vetrini F, Erdin S, Erdin S, Huynh T, Ferron M, Karsenty G, Vellard MC, et al. A lysosome-to-nucleus signalling mechanism senses and regulates the lysosome via mTOR and TFEB. The EMBO journal 2012; 31:1095-108.

28. Buerger C, DeVries B, Stambolic V. Localization of Rheb to the endomembrane is critical for its signaling function. Biochemical and biophysical research communications 2006; 344:869-80.

29. Castro AF, Rebhun JF, Clark GJ, Quilliam LA. Rheb binds tuberous sclerosis complex 2 (TSC2) and promotes S6 kinase activation in a rapamycin- and farnesylation-dependent manner. The Journal of biological chemistry 2003; 278:32493-6.

30. Clark GJ, Kinch MS, Rogers-Graham K, Sebti SM, Hamilton AD, Der CJ. The Ras-related protein Rheb is farnesylated and antagonizes Ras signaling and transformation. The Journal of biological chemistry 1997; 272:10608-15.

31. Bar-Peled L, Schweitzer LD, Zoncu R, Sabatini DM. Ragulator is a GEF for the rag GTPases that signal amino acid levels to mTORC1. Cell 2012; 150:1196-208.

32. Sancak Y, Bar-Peled L, Zoncu R, Markhard AL, Nada S, Sabatini DM. Ragulator-Rag complex targets mTORC1 to the lysosomal surface and is necessary for its activation by amino acids. Cell 2010; 141:290-303.

33. Settembre C, Di Malta C, Polito VA, Garcia Arencibia M, Vetrini F, Erdin S, Erdin SU, Huynh T, Medina D, Colella P, et al. TFEB links autophagy to lysosomal biogenesis. Science 2011; 332:1429-33.

34. Zheng X, Liang Y, He Q, Yao R, Bao W, Bao L, Wang Y, Wang Z. Current models of mammalian target of rapamycin complex 1 (mTORC1) activation by growth factors and amino acids. International journal of molecular sciences 2014; 15:20753-69.

35. Chiang GG, Abraham RT. Phosphorylation of mammalian target of rapamycin (mTOR) at Ser-2448 is mediated by p70S6 kinase. The Journal of biological chemistry 2005; 280:25485-90.

36. Klionsky DJ, Abdalla FC, Abeliovich H, Abraham RT, Acevedo-Arozena A, Adeli K, Agholme L, Agnello M, Agostinis P, Aguirre-Ghiso JA, et al. Guidelines for the use and interpretation of assays for monitoring autophagy. Autophagy 2012; 8:445-544.

37. Klionsky DJ, Abeliovich H, Agostinis P, Agrawal DK, Aliev G, Askew DS, Baba M, Baehrecke EH, Bahr BA, Ballabio A, et al. Guidelines for the use and interpretation of assays for monitoring autophagy in higher eukaryotes. Autophagy 2008; 4:151-75.

38. van Meer G, Voelker DR, Feigenson GW. Membrane lipids: where they are and how they behave. Nature reviews Molecular cell biology 2008; 9:112-24.

39. Haimovitz-Friedman A, Kolesnick RN, Fuks Z. Ceramide signaling in apoptosis. Br Med Bull 1997; 53:539-53.

40. Kitatani K, Idkowiak-Baldys J, Hannun YA. The sphingolipid salvage pathway in ceramide metabolism and signaling. Cellular signalling 2008; 20:1010-8.

41. Siow DL, Anderson CD, Berdyshev EV, Skobeleva A, Natarajan V, Pitson SM, Wattenberg BW. Sphingosine kinase localization in the control of sphingolipid metabolism. Advances in enzyme regulation 2011; 51:229-44.

42. Levy M, Futerman AH. Mammalian ceramide synthases. IUBMB life 2010; 62:347-56.

43. Goni FM, Alonso A. Sphingomyelinases: enzymology and membrane activity. FEBS letters 2002; 531:38-46.

44. Orii T, Nakamura F, Kudoh T, Tsuchihashi K, Nakao T. A profound deficiency of (CH3-14C)choline sphingomyelin-cleaving enzyme in Niemann-Pick disease type B. Tohoku J Exp Med 1975; 117:193-5.

45. Wu BX, Rajagopalan V, Roddy PL, Clarke CJ, Hannun YA. Identification and characterization of murine mitochondria-associated neutral sphingomyelinase (MA-nSMase), the mammalian sphingomyelin phosphodiesterase 5. The Journal of biological chemistry 2010; 285:17993-8002.

46. Poirier C, Berdyshev EV, Dimitropoulou C, Bogatcheva NV, Biddinger PW, Verin AD. Neutral sphingomyelinase 2 deficiency is associated with lung anomalies similar to emphysema. Mammalian genome : official journal of the International Mammalian Genome Society 2012; 23:758-63.

47. Krut O, Wiegmann K, Kashkar H, Yazdanpanah B, Kronke M. Novel tumor necrosis factor-responsive mammalian neutral sphingomyelinase-3 is a C-tail-anchored protein. The Journal of biological chemistry 2006; 281:13784-93.

48. Moylan JS, Smith JD, Wolf Horrell EM, McLean JB, Deevska GM, Bonnell MR, Nikolova-Karakashian MN, Reid MB. Neutral sphingomyelinase-3 mediates TNF-stimulated oxidant activity in skeletal muscle. Redox Biol 2014; 2:910-20.

49. Gorter E, Grendel F. On Bimolecular Layers of Lipoids on the Chromocytes of the Blood. The Journal of experimental medicine 1925; 41:439-43.

50. Dewey MM. The ultrastructure of mammalian cell membranes. Med Bull (Ann Arbor) 1959; 25:132-47.

51. Singer SJ, Nicolson GL. The fluid mosaic model of the structure of cell membranes. Science 1972; 175:720-31.

52. Nadal M, Gold SE. Assessment of Autophagosome Formation by Transmission Electron Microscopy. Plant Fungal Pathogens: Methods and Protocols 2012; 835:481-9.

53. Parsegian AV, Ninham BW. Application of the Lifshitz theory to the calculation of Van der Waals forces across thin lipid films. Nature 1969; 224:1197-8.

54. Lis LJ, McAlister M, Fuller N, Rand RP, Parsegian VA. Interactions between neutral phospholipid bilayer membranes. Biophysical journal 1982; 37:657-65.

55. Bai J, Pagano RE. Measurement of spontaneous transfer and transbilayer movement of BODIPY-labeled lipids in lipid vesicles. Biochemistry 1997; 36:8840-8.

56. Eckford PD, Sharom FJ. The reconstituted P-glycoprotein multidrug transporter is a flippase for glucosylceramide and other simple glycosphingolipids. The Biochemical journal 2005; 389:517-26.

57. Justice MJ, Petrusca DN, Rogozea AL, Williams JA, Schweitzer KS, Petrache I, Wassall SR, Petrache HI. Effects of lipid interactions on model vesicle engulfment by alveolar macrophages. Biophysical journal 2014; 106:598-609.

58. Brown MF, Ribeiro AA, Williams GD. New view of lipid bilayer dynamics from 2H and 13C NMR relaxation time measurements. Proceedings of the National Academy of Sciences of the United States of America 1983; 80:4325-9.

59. Wassall SR, McCabe MA, Wassall CD, Adlof RO, Feller SE. Solid-state (2)H NMR and MD simulations of positional isomers of a monounsaturated phospholipid membrane: structural implications of double bond location. J Phys Chem B 2010; 114:11474-83.

60. Jenkins RW, Canals D, Hannun YA. Roles and regulation of secretory and lysosomal acid sphingomyelinase. Cellular signalling 2009; 21:836-46.

61. Jenkins RW, Idkowiak-Baldys J, Simbari F, Canals D, Roddy P, Riner CD, Clarke CJ, Hannun YA. A novel mechanism of lysosomal acid sphingomyelinase maturation: requirement for carboxyl-terminal proteolytic processing. The Journal of biological chemistry 2011; 286:3777-88.

62. Jenkins RW, Canals D, Idkowiak-Baldys J, Simbari F, Roddy P, Perry DM, Kitatani K, Luberto C, Hannun YA. Regulated secretion of acid sphingomyelinase: implications for selectivity of ceramide formation. The Journal of biological chemistry 2010; 285:35706-18.

63. Ni X, Morales CR. The lysosomal trafficking of acid sphingomyelinase is mediated by sortilin and mannose 6-phosphate receptor. Traffic 2006; 7:889-902.

64. Schissel SL, Keesler GA, Schuchman EH, Williams KJ, Tabas I. The cellular trafficking and zinc dependence of secretory and lysosomal sphingomyelinase, two products of the acid sphingomyelinase gene. The Journal of biological chemistry 1998; 273:18250-9.

65. Lehmann HE, Cahn CH, De Verteuil RL. The treatment of depressive conditions with imipramine (G 22355). Canadian Psychiatric Association journal 1958; 3:155-64.

66. Hurwitz R, Ferlinz K, Sandhoff K. The tricyclic antidepressant desipramine causes proteolytic degradation of lysosomal sphingomyelinase in human fibroblasts. Biological chemistry Hoppe-Seyler 1994; 375:447-50.

67. Kornhuber J, Tripal P, Reichel M, Terfloth L, Bleich S, Wiltfang J, Gulbins E. Identification of new functional inhibitors of acid sphingomyelinase using a structure-property-activity relation model. Journal of medicinal chemistry 2008; 51:219-37.

68. Albouz S, Hauw JJ, Berwald-Netter Y, Boutry JM, Bourdon R, Baumann N. Tricyclic antidepressants induce sphingomyelinase deficiency in fibroblast and neuroblastoma cell cultures. Biomedicine / [publiee pour l'AAICIG] 1981; 35:218-20.

69. Valencia-Sanchez MA, Liu J, Hannon GJ, Parker R. Control of translation and mRNA degradation by miRNAs and siRNAs. Genes & development 2006; 20:515-24.

70. Villanueva Paz M, Cotan D, Garrido-Maraver J, Cordero MD, Oropesa-Avila M, de La Mata M, Delgado Pavon A, de Lavera I, Alcocer-Gomez E, Sanchez-Alcazar JA. Targeting autophagy and mitophagy for mitochondrial diseases treatment. Expert Opin Ther Targets 2016; 20:487-500.

71. Zhang L, Xie L. [The relationship between autophagy and ocular diseases]. Zhonghua Yan Ke Za Zhi 2016; 52:391-5.

72. Zeki AA, Yeganeh B, Kenyon NJ, Post M, Ghavami S. Autophagy in airway diseases: a new frontier in human asthma? Allergy 2016; 71:5-14.

73. Jiang P, Mizushima N. Autophagy and human diseases. Cell research 2014; 24:69-79.

74. Jing K, Lim K. Why is autophagy important in human diseases? Experimental & molecular medicine 2012; 44:69-72.

75. Lee JA, Yue Z, Gao FB. Autophagy in neurodegenerative diseases. Brain research 2016; 1649:141-2.

76. Zhang Z, Miah M, Culbreth M, Aschner M. Autophagy in Neurodegenerative Diseases and Metal Neurotoxicity. Neurochem Res 2016; 41:409-22.

77. Vij N. Nano-based rescue of dysfunctional autophagy in chronic obstructive lung diseases. Expert Opin Drug Deliv 2016:1-7.

78. Liu N, Shi Y, Zhuang S. Autophagy in Chronic Kidney Diseases. Kidney Dis (Basel) 2016; 2:37-45.

79. Li L, Chen X, Gu H. The signaling involving in autophagy machinery in keratinocytes and therapeutic approaches for skin diseases. Oncotarget 2016.

80. De Rechter S, Decuypere JP, Ivanova E, van den Heuvel LP, De Smedt H, Levtchenko E, Mekahli D. Autophagy in renal diseases. Pediatr Nephrol 2016; 31:737-52.

81. Carneiro LA, Travassos LH. Autophagy and viral diseases transmitted by Aedes aegypti and Aedes albopictus. Microbes Infect 2016; 18:169-71.

82. Aggarwal S, Mannam P, Zhang J. Differential regulation of autophagy and mitophagy in pulmonary diseases. American journal of physiology Lung cellular and molecular physiology 2016; 311:L433-52.

83. Zhang N, Li L, Wang J, Cao M, Liu G, Xie G, Yang Z, Li Y. Study of autophagy-related protein light chain 3 (LC3)-II expression levels in thyroid diseases. Biomed Pharmacother 2015; 69:306-10.

84. Elleder M. Niemann-Pick disease. Pathology, research and practice 1989; 185:293-328.

85. Savic R, Schuchman EH. Use of acid sphingomyelinase for cancer therapy. Advances in cancer research 2013; 117:91-115.

86. Swerdlow RH. Pathogenesis of Alzheimer's disease. Clin Interv Aging 2007; 2:347-59.

87. Monick MM, Powers LS, Walters K, Lovan N, Zhang M, Gerke A, Hansdottir S, Hunninghake GW. Identification of an autophagy defect in smokers' alveolar macrophages. Journal of immunology 2010; 185:5425-35.

88. Petrache I, Natarajan V, Zhen L, Medler TR, Richter AT, Cho C, Hubbard WC, Berdyshev EV, Tuder RM. Ceramide upregulation causes pulmonary cell apoptosis and emphysema-like disease in mice. Nature medicine 2005; 11:491-8.

89. Kim HP, Wang X, Chen ZH, Lee SJ, Huang MH, Wang Y, Ryter SW, Choi AM. Autophagic proteins regulate cigarette smoke-induced apoptosis: protective role of heme oxygenase-1. Autophagy 2008; 4:887-95.

90. Bizzozero L, Cazzato D, Cervia D, Assi E, Simbari F, Pagni F, De Palma C, Monno A, Verdelli C, Querini PR, et al. Acid sphingomyelinase determines melanoma progression and metastatic behaviour via the microphtalmia-associated transcription factor signalling pathway. Cell death and differentiation 2014; 21:507-20.

91. Clarke R, Cook KL, Hu R, Facey CO, Tavassoly I, Schwartz JL, Baumann WT, Tyson JJ, Xuan J, Wang Y, et al. Endoplasmic reticulum stress, the unfolded protein response, autophagy, and the integrated regulation of breast cancer cell fate. Cancer research 2012; 72:1321-31.

92. Patel AS, Morse D, Choi AM. Regulation and functional significance of autophagy in respiratory cell biology and disease. American journal of respiratory cell and molecular biology 2013; 48:1-9.

93. Chatelut M, Leruth M, Harzer K, Dagan A, Marchesini S, Gatt S, Salvayre R, Courtoy P, Levade T. Natural ceramide is unable to escape the lysosome, in contrast to a fluorescent analogue. FEBS letters 1998; 426:102-6.

94. Goni FM, Alonso A. Biophysics of sphingolipids I. Membrane properties of sphingosine, ceramides and other simple sphingolipids. Biochimica et biophysica acta 2006; 1758:1902-21.

95. Bligh EG, Dyer WJ. A rapid method of total lipid extraction and purification. Canadian journal of biochemistry and physiology 1959; 37:911-7.

96. Berdyshev EV, Gorshkova IA, Usatyuk P, Zhao Y, Saatian B, Hubbard W, Natarajan V. De novo biosynthesis of dihydrosphingosine-1-phosphate by sphingosine kinase 1 in mammalian cells. Cellular signalling 2006; 18:1779-92.

97. Vaskovsky VE, Kostetsky EY, Vasendin IM. A universal reagent for phospholipid analysis. Journal of chromatography 1975; 114:129-41.

98. Berdyshev EV, Gorshkova IA, Garcia JG, Natarajan V, Hubbard WC. Quantitative analysis of sphingoid base-1-phosphates as bisacetylated derivatives by liquid chromatography-tandem mass spectrometry. Analytical biochemistry 2005; 339:129-36.

99. Clarke NG, Dawson RM. Alkaline O leads to N-transacylation. A new method for the quantitative deacylation of phospholipids. The Biochemical journal 1981; 195:301-6.

100. Horinouchi K, Erlich S, Perl DP, Ferlinz K, Bisgaier CL, Sandhoff K, Desnick RJ, Stewart CL, Schuchman EH. Acid sphingomyelinase deficient mice: a model of types A and B Niemann-Pick disease. Nature genetics 1995; 10:288-93.

101. Smith EL, Schuchman EH. The unexpected role of acid sphingomyelinase in cell death and the pathophysiology of common diseases. FASEB journal : official publication of the Federation of American Societies for Experimental Biology 2008; 22:3419-31.

102. Pena-Llopis S, Vega-Rubin-de-Celis S, Schwartz JC, Wolff NC, Tran TA, Zou L, Xie XJ, Corey DR, Brugarolas J. Regulation of TFEB and V-ATPases by mTORC1. The EMBO journal 2011; 30:3242-58.

103. Ohkuma S, Poole B. Fluorescence probe measurement of the intralysosomal pH in living cells and the perturbation of pH by various agents. Proceedings of the National Academy of Sciences of the United States of America 1978; 75:3327-31.

104. Shintani T, Klionsky DJ. Autophagy in health and disease: a double-edged sword. Science 2004; 306:990-5.

105. Kawai A, Uchiyama H, Takano S, Nakamura N, Ohkuma S. Autophagosome-lysosome fusion depends on the pH in acidic compartments in CHO cells. Autophagy 2007; 3:154-7.

106. Yoon YH, Cho KS, Hwang JJ, Lee SJ, Choi JA, Koh JY. Induction of lysosomal dilatation, arrested autophagy, and cell death by chloroquine in cultured ARPE-19 cells. Investigative ophthalmology & visual science 2010; 51:6030-7.

107. Mizushima N, Yoshimori T. How to interpret LC3 immunoblotting. Autophagy 2007; 3:542-5.

108. Li X, Xu M, Pitzer AL, Xia M, Boini KM, Li PL, Zhang Y. Control of autophagy maturation by acid sphingomyelinase in mouse coronary arterial smooth muscle cells: protective role in atherosclerosis. Journal of molecular medicine 2014; 92:473-85.

109. Rossi M, Munarriz ER, Bartesaghi S, Milanese M, Dinsdale D, Guerra-Martin MA, Bampton ET, Glynn P, Bonanno G, Knight RA, et al. Desmethylclomipramine induces the accumulation of autophagy markers by blocking autophagic flux. J Cell Sci 2009; 122:3330-9.

110. Elojeimy S, Holman DH, Liu X, El-Zawahry A, Villani M, Cheng JC, Mahdy A, Zeidan Y, Bielwaska A, Hannun YA, et al. New insights on the use of desipramine as an inhibitor for acid ceramidase. FEBS letters 2006; 580:4751-6.

111. Corcelle-Termeau E, Vindelov SD, Hamalisto S, Mograbi B, Keldsbo A, Brasen JH, Favaro E, Adam D, Szyniarowski P, Hofman P, et al. Excess sphingomyelin disturbs ATG9A trafficking and autophagosome closure. Autophagy 2016; 12:833-49.

112. Park JH, Schuchman EH. Acid ceramidase and human disease. Biochimica et biophysica acta 2006; 1758:2133-8.

113. Hoglinger D, Haberkant P, Aguilera-Romero A, Riezman H, Porter FD, Platt FM, Galione A, Schultz C. Intracellular sphingosine releases calcium from lysosomes. Elife 2015; 4.

114. Medina DL, Di Paola S, Peluso I, Armani A, De Stefani D, Venditti R, Montefusco S, Scotto-Rosato A, Prezioso C, Forrester A, et al. Lysosomal calcium signalling regulates autophagy through calcineurin and TFEB. Nature cell biology 2015; 17:288-99.

115. Pushkareva M, Khan WA, Alessenko AV, Sahyoun N, Hannun YA. Sphingosine activation of protein kinases in Jurkat T cells. In vitro phosphorylation of endogenous protein substrates and specificity of action. The Journal of biological chemistry 1992; 267:15246-51.

116. Ma Y, Pitson S, Hercus T, Murphy J, Lopez A, Woodcock J. Sphingosine activates protein kinase A type II by a novel cAMP-independent mechanism. The Journal of biological chemistry 2005; 280:26011-7.

117. Mendelson K, Evans T, Hla T. Sphingosine 1-phosphate signalling. Development 2014; 141:5-9.

118. Taniguchi M, Kitatani K, Kondo T, Hashimoto-Nishimura M, Asano S, Hayashi A, Mitsutake S, Igarashi Y, Umehara H, Takeya H, et al. Regulation of autophagy and its associated cell death by "sphingolipid rheostat": reciprocal role of ceramide and sphingosine 1-phosphate in the mammalian target of rapamycin pathway. The Journal of biological chemistry 2012; 287:39898-910.

119. Eisenberg S, Stein Y, Stein O. Phospholipases in arterial tissue. IV. The role of phosphatide acyl hydrolase, lysophosphatide acyl hydrolase, and sphingomyelin choline phosphohydrolase in the regulation of phospholipid composition in the normal human aorta with age. The Journal of clinical investigation 1969; 48:2320-9.

120. Yamamura T, Tezuka T. Change in sphingomyelinase activity in human epidermis during aging. Journal of dermatological science 1990; 1:79-83.

121. Zhang D, Li C, Zhou J, Song Y, Fang X, Ou J, Li J, Bai C. Autophagy protects against ischemia/reperfusion-induced lung injury through alleviating blood-air barrier damage. J Heart Lung Transplant 2015; 34:746-55.

122. Mizumura K, Cloonan SM, Haspel JA, Choi AM. The emerging importance of autophagy in pulmonary diseases. Chest 2012; 142:1289-99.

Curriculum Vitae

Matthew J. Justice

I. Education

Indiana University, South Bend IN – BS 05/2006 Physics
Purdue University, Indianapolis IN – MS 08/2009 Physics
Indiana University, Indianapolis IN – MS 12/2013 Biochemistry & Molecular Biology
Indiana University, Indianapolis IN – PhD 04/2017 Biochemistry & Molecular Biology

II. Research Experience/Professional Positions

2005-2006, Undergraduate Student – University of Notre Dame, Joint Institute for Nuclear Astrophysics, South Bend IN. Design, optimize, and begin implementation of the focal plane for a recoil mass separator.

2006-2007, Quality Control Supervisor – Patrick Aluminum Extrusions, Mishawaka, IN. Quality assurance of custom aluminum parts. (Allowed spouse to complete her graduate education before attending graduate school in Indianapolis).

2007-2009, Graduate Student–Purdue University, Physics, Indianapolis, IN. Bio-membrane Sciences Laboratory. Investigated lipid-lipid and lipid-protein systems with small-angle X-ray scattering and solid state deuterium NMR.

2009-2012, Research Technician–Indiana University School of Medicine, Indianapolis. Studied sphingolipid metabolism in emphysema.

2012-2017, Graduate Student–Indiana University, Biochemistry & Molecular Biology, Indianapolis, IN. Studied the role of acid sphingomyelinase in mammalian target of rapamycin signaling and autophagy.

2017-Present, Postdoctoral Fellow–University of Colorado, Anschutz Medical Campus, Pharmacology, Aurora, CO. Studying the role of autophagy in cell death mechanisms.

III. Awards/Honors

2014 Recipient – Southeastern Regional Lipid Conference Travel Award
2014 Co-runner-up – Indiana University School of Medicine Research Day Best Presentation Award
2015 Co-organizer – 2nd Midwest Membrane Signaling & Trafficking Symposium

IV. Societies Membership

2008-2009	Indiana Academy of Science
2009-2013	Biophysical Society
2012-Present	American Thoracic Society
2014	American Heart Association
2015-Present	American Society for Cell Biology

VIII. Teaching Experience

Fall 2013-Spring 2015 Adjunct Professor, Butler University, Physics Department, Indianapolis, Indiana

IX. Grants Funded

A. CURRENT FUNDING:
Novel Endogenous Regulation of Lysosomal Stress Response in Lung Endothelium, National Heart, Lung, and Blood Institute, 3 years of funding, Primary Investigator – Matthew Justice, Mentor – Irina Petrache F31 HL126459

X. Publications

Peer Reviewed Research Manuscripts

1. Brownholland DP, Longo GS, Struts AV, **Justice MJ**, Szleifer I, Petrache HI, Brown MF, Thompson DH. Phase Separation in Binary Mixtures of Bipolar and Monopolar Lipid Dispersions Revealed by 2H NMR Spectroscopy, Small Angle X-Ray Scattering, and Molecular Theory. **Biophys J.** 2009 November 15; 97(10): 2700-9. doi: 10.1016/j.bpj.2009.06.058.PMCID:PMC2776299

2. Mallikarjunaiah KJ, Leftin A, Kinnun JJ, **Justice MJ**, Rogozea AL, Petrache HI, Brown MF. Solid-State 2H NMR Shows Equivalence of Dehydration and Osmotic Pressures in Lipid Membrane Deformation. **Biophys J**. 2011 January 5; 100(1): 98-107. doi: 10.1016/j.bpj.2010.11.010.PMCID:PMC3010004

3. Xu F, Zhang H, Ilavsky J, Stanciu L, Ho D, **Justice MJ**, Petrache HI, Xie J. Investigation of a catalyst ink dispersion using both ultra-small-angle X-ray scattering and cryogenic TEM. **Langmuir**. 2010 Dec 21;26(24):19199-208. doi: 10.1021/la1028228. Epub 2010 Nov 19. PMID:21090580[PubMed - indexed for MEDLINE]

4. Schweitzer KS, Hatoum H, Brown MB, Gupta M, **Justice MJ**, Beteck B, Van Demark MJ, Gu Y, Presson RG, Hubbard WC , Petrache I. Mechanisms of lung endothelial barrier disruption induced by cigarette smoke: role of oxidative stress and ceramides. **Am J Physiol Lung Cell Mol Physiol**. 2011 December; 301(6): L836-L846. Published online 2011 August 26. doi: 10.1152/ajplung.00385.2010.PMCID:PMC3233827

5. Lahm T, Albrecht M, Fisher AJ, Selej M, Patel NG, Brown JA, **Justice MJ**, Brown MB, Van Demark MJ, Trulock KM, Dieudonne D, Reddy JG, Presson RG, Petrache I. 17β-Estradiol Attenuates Hypoxic Pulmonary Hypertension via Estrogen Receptor-mediated Effects. **Am J Respir Crit Care Med**. 2012 May 1; 185(9): 965-80. Published online 2012 May 1. doi: 10.1164/rccm.201107-1293OC.PMCID:PMC3359941

6. Green LA, Petrusca D, Rajashekhar G, Gianaris T, Schweitzer KS, Wang L, **Justice MJ**, Petrache I, Clauss M. Cigarette smoke-induced CXCR3 receptor up-regulation mediates endothelial apoptosis. **Am J Respir Cell Mol Biol**. 2012 Dec;47(6):807-14. doi: 10.1165/rcmb.2012-0132OC. Epub 2012 Aug 30. PMID:22936405[PubMed - indexed for MEDLINE]

7. Bardita C, Predescu D, **Justice MJ**, Petrache I, Predescu S. In vivo knockdown of intersectin-1s alters endothelial cell phenotype and causes microvascular remodeling in the mouse lungs. **Apoptosis**. 2013 January; 18(1): 57-76. Published online 2012 October 7. doi: 10.1007/s10495-012-0762-x. PMCID:PMC3543613

8. Petrache I, Kamocki K, Poirier C, Pewzner-Jung Y, Laviad EL, Schweitzer KS, Van Demark MJ, **Justice MJ**, Hubbard WC, Futerman AH. Ceramide Synthases Expression and Role of Ceramide Synthase-2 in the Lung: Insight from Human Lung Cells and Mouse Models. **PLoS One**. 2013; 8(5): e62968. Published online 2013 May 14. doi: 0.1371/journal.pone.0062968.PMCID: PMC3653891

9. **Justice MJ**, Petrusca DN, Wassall S, Petrache I, Petrache HI. Effects of Lipid Interactions on Model Membrane Engulfment by Macrophages. **Biophysical J**. 2014 Feb 4;106(3):598-609. Doi: 10.1016/j.bpj.2013.12.036

10. Petrusca DN, Van Demark MJ, Gu Y, **Justice MJ**, Rogozea A, Hubbard WC, Petrache I. Smoking Exposure Induces Human Lung Endothelial Cell Adaptation to Apoptotic Stress. **Am. J. Respir. Cell Mol. Biol**. 2014 Mar;50(3):513-25.doi:10.1165/rcmb.2013-0023OC.

11. Cruickshank-Quinn CI, Mahaffey S, **Justice MJ**, Hughes G, Armstrong M, Bowler RP, Reisdorph R, Petrache I, Reisdorph N. Transient and persistent metabolomic changes in plasma following chronic cigarette smoke exposure in a mouse model. **PLoS One**. 2014 Jul 9;9(7):e101855. doi: 10.1371/journal.pone.0101855.

12. Xie J, Broxmeyer HE, Feng D, Schweitzer KS, Yi R, Cook TG, Chitteti BR, Barwinska D, Traktuev DO, Van Demark MJ, **Justice MJ**, Ou X, Srour EF, Prockop DJ, Petrache I, March KL. **Stem Cells**. 2015 Feb;33(2):468-78. doi: 10.1002/stem.1851.

13. Schweitzer KS, Chen SX, Law S, Van Demark MJ, Poirier C, **Justice MJ**, Hubbard WC, Kim ES, Lai X, Wang M, Kranz WD, Carroll CJ, Ray BD, Bittman R, Goodpaster J, Petrache I. **Am J Physiol Lung Cell Mol Physiol**. 2015 May 15:ajplung.00411.2015. doi: 10.1152/ajplung.00411.2014.

14. Lockett AD, Petrusca DN, **Justice MJ**, Poirier C, Serban KA, Rush NI, Kamocka M, Predescu D, Predescu S, Petrache I, **AM J Physiol Lung Cell Mol Physiol**. 2015 Jun 19: doi: 10.1152/ajplung.00376.2014.

15. Klionsky *et al* (**Justice MJ**). Guidelines for the use and interpretation of assays for monitoring autophagy (3rd edition). **Autophagy**. 2016 Jan 2;12(1): 1-222

16. Serban K, Rezania S, Petrusca D, Poirier C, Cao D, **Justice MJ,** Patel M, Tsvetkova I, Kamocki K, Mikosz A, Schweitzer KS, Jacobson S, Cardoso A, Carlesso N, Hubbard WC, Kechris K, Dragnea B, Berdyshev E, McClintick J, and Petrache I. Structural and functional characterization of endothelial microparticles released by cigarette smoke. **Nature Scientific Reports**. Sci Rep. 2016 Aug 17;6:31596.

17**. Justice MJ**, Kelly S. Schweitzer, Christophe Poirier, Irina Bronova, Evgeny V. Berdyshev, Janice Blum, and Irina Petrache. Acid Sphingomyelinase is Required for Homeostatic LYNUS Signaling and mTOR Inhibition of Autophagy. **Journal of Lipid Research**, *Submitted*, January 2017.

18. **Justice MJ**, Kenji Mizumura, Kelly S. Schweitzer, Sheila Krishnan, Evgeny V. Berdyshev, Walter C. Hubbard, Yael Pewzner-Yung, Anthony Futerman, Augustine M.K. Choi, and Irina Petrache, *In Preparation*.

Abstracts

1. **Matthew J. Justice**, Carina Poltera, Horia I. Petrache, Electrostatic interactions in membrane systems. Symposium on Frontiers in Biological Membranes, Purdue University, West Lafayette, 2008.

2. **Matthew J. Justice**, Carina M. Poltera, Horia I. Petrache, Measurements of Electrostatic Interactions between Charged Membranes. 53rd Biophysical Society Meeting. Boston. Biophysical Journal 96(3) pp. 459a, 2009.

3. **Matthew J. Justice**, Adriana L. Rogozea, Daniela N. Petrusca, Irina Petrache, Stephen R. Wassall, Horia I. Petrache, The Effect of Ceramide on Model Membranes and Apoptotic Cells Determined by X-Ray Scattering, Solid State NMR, and Flow Cytometry. 54th Biophysical Society Meeting. San Francisco. Biophysical Journal 98(3) pp. 465a-466a, 2010.

4. **Matthew J. Justice**, Adriana L. Rogozea, Daniela N. Petrusca, Kelly Schweitzer, Irina Petrache, Stephen R. Wassall, Horia I. Petrache. The Role of Ceramide in the Clearence of Apoptotic Cells. 55th Biophysical Society Meeting. Baltimore. Biophysical Journal 100(3) pp. 409a, 2011.

5. **Matthew J. Justice**, Daniela N. Petrusca, Justin Williams, Kelly S. Schweitzer, Irina Petrache, Stephen R. Wassall, Horia I. Petrache. Engulfment of Model Membranes by Alveolar Macrophages. 56th Biophysical Society Meeting. San Diego. Biophysical Journal 102(3) pp. 502a, 2012.

6. **Matthew J. Justice**, K. Schweitzer, D.N. Petrusca, I. Petrache. Control of Cigarette Smoke-Induced Apoptosis or Autophagy by Acid Sphingomyelinase. American Thoracic Society International Conference. Philadelphia. American Journal of Respiratory and Critical Care Medicine 187; 2013: A5180, 2013.

7. **Matthew J. Justice**, Christophe Poirier, Kelly Schweitzer, Jacob Saliba, Irina Petrache. Acid Sphingomyelinase Involvement in mTOR Signaling. Gordon Research Conference–Lysosomes & Endocytosis. Andover, New Hampshire, 2014.

8. **Matthew J. Justice**, Christophe Poirier, Kelly Schweitzer, Jacob Saliba, Irina Petrache. Acid Sphingomyelinase Regulation of Autophagy and Autophagic Flux in Emphysema. Keystone Autophagy Meeting. Breckinridge, CO, 2015.

9. **Matthew J. Justice**, Christophe Poirier, Kelly Schweitzer, Jacob Saliba, Irina Petrache. Acid Sphingomyelinase is a Novel Regulator of LYNUS and Autophagy. American Thoracic Society International Conference. San Francisco. American Jurnal of Respiratory and Critical Care Medicine C67, A5787. 2016.

Coauthor Abstracts

1. Avigdor Leftin, **Matthew J. Justice**, Jacob G. Kinnun, Horia I. Petrache, Michael F. Brown, Structural and Dynamic Markers of Membrane Osmotic Stress from X-Ray Scattering and Solid-State 2H NMR. 53rd Biophysical Society Meeting. Boston. Biophysical Journal 96(3) pp. 356a, 2009.

2. Andrey Struts, David P. Holland, Gabriel Longo, **Matthew J. Justice**, Igal Szleifer, Avigdor Leftin, Horia I. Petrache, Michael F. Brown, David H. Thompson, Phase Separation in Binary Mixtures of Bipolar and Monopolar Lipid Dispersions Revealed by Solid-State 2H NMR Spectroscopy and Small Angle X-ray Scattering. 53rd Biophysical Society Meeting. Boston. Biophysical Journal 96(3) pp. 355a, 2009.

3. Adriana L. Rogozea, **Matthew J. Justice**, Horia I. Petrache, Molecular Hydration Investigated using Extended Membrane Surfaces. 54th Biophysical Society Meeting. San Francisco. Biophysical Journal 98(3) pp. 689a, 2010.

4. K.J. Mallikarjunaiah, Avigdor Leftin, Jacob J. Kinnun, **Matthew J. Justice**, Adriana L. Rogozea, Horia I. Petrache, Michael F. Brown, Osmotic Membrane Deformation Revealed by Solid-State 2H NMR and Small-Angle X-Ray Scattering. 54th Biophysical Society Meeting. San Francisco. Biophysical Journal 98(3) pp. 282a, 2010.

5. Megan M. Koerner, **Matthew J. Justice**, Bruce D. Ray, Horia I. Petrache, Buffer Properties Revealed with Model Lipid Membranes. 54th Biophysical Society Meeting. San Francisco. Biophysical Journal 98(3) pp. 273a-274a, 2010.

6. K.J. Mallikarjunaiah, Jacob J. Kinnun, Avigdor Leftin, Luis A. Palacio, **Matthew J. Justice**, Horia I. Petrache, Michael F. Brown. Area Deformation of Membranes from the Perspective of 2H NMR and X-ray Scattering. 55th Biophysical Society Meeting. Baltimore. Biophysical Journal100 (3) pp. 173a, 2011.

7. Kelly S. Schweitzer, **Matthew J. Justice**, Margie Albrecht, Mary Van Demark, Yuan Gu, Yong Gao, Krzysztof Kamocki, Robert Bittman, Irina Petrache. Therapeutic Potential of FTY720-Analogs in Cigarette-Smoke Induced Lung Injury that is Dependent upon Sphingosine-1 Phosphate Receptor-1, S1PR1. American Thoracic Society International Conference. San Francisco. 2012.

8. Daniela N. Petrusca, **Matthew J. Justice**, Robert Bittman, Kelly Schweitzer, Walter C. Hubbard, Homer L. Twigg, and Irina Petrache. FTY720 Analogs Improve Alveolar Macrophages Efferocytosis During Cigarette Smoking. American Thoracic Society International Conference. San Francisco. 2012.

9. Matthias Clauss, Gangaraju Rajashekhar, Robert Voswinckel, Kelly Schweitzer, **Matthew J. Justice**, and Irina Petrache. Involvement of Monocytes in EMAP II Induced Alveolar Airspace Enlargement. American Thoracic Society International Conference. San Francisco. 2012.

10. Kelly Schweitzer, **Matthew J. Justice**, Margie Albrecht, Mary Van Demark, Jordan Wood, Krzysztof Kamocki, Mariam Qureshi, Zorina Galis, Irina Petrache. Role of EMMPRIN in Cigarette-Smoke Induced Emphysema. American Thoracic Society International Conference. Philadelphia. 2013.

11. Karina A. Serban, Daniela N. Petrusca, Angelia D. Lockett, **Matthew J. Justice**, Irina Petrache. Alpha 1 Antitrypsin Effect on Alveolar Macrophages Engulfment of Apoptotic and Phagocytic Targets. American Thoracic Society International Conference. Philadelphia. 2013.

12. Christophe Poirier, **Matthew J. Justice**, Mary Van Demark, Yuan Gu, Walter Hubbard, Irina Petrache. The Importance of Constitutive Acid Sphingomyelinase (aSMase) for the Maintenance of Lung Function during Development and Exposure to Cigarette Smoke (CS). American Thoracic Society International Conference. Philadelphia. 2013.

13. Matthias Clauss, Gangaraju Rajashekhar, Robert Voswinckel, Kelly Schweitzer, **Matthew J. Justice**, Irina Petrache. Involvement of Monocytes In EMAP II-Induced Alveolar Airspace Enlargement. American Thoracic Society International Conference. Philadelphia. 2013.

14. Daniela N. Petrusca, Mary Van Demark, Yuan Gu, **Matthew J. Justice**, Adriana Rogozea, Walter C. Hubbard, Irina Petrache. Smoking Exposure Induces Human Lung Endothelial Cell Adaptation to Apoptotic Stress. American Thoracic Society International Conference. San Diego. 2014.

15. Kelly Schweitzer, **Matthew J. Justice**, Mary Van Demark, Irina Petrache. The Effect Of Nicotine On The Lung Endothelial Barrier Function. American Thoracic Society International Conference. San Diego. 2014.

16. Kenji Mizumura, **Matthew J. Justice**, Evgeny Berdyshev, Augustine M.K. Choi, Irina Petrache. Involvement of Sphingolipids in Cigarette Smoke Induced Lung Epithelial Cell Mitophagy and Necroptosis. American Thoracic Society International Conference. Denver. 2015.

17. Matthew Landrigan, Jordan Wood, **Matthew J. Justice**, Christophe Poirier, Mary Van Demark, Jake Walker, Kelly Schweitzer, Irina Petrache. Human Bone Marrow Concentrate Improves Lung Function and Exercise Tolerance in a Mouse Model of Cigarette Smoke-Induced Emphysema. American Thoracic Society International Conference. Denver. 2015.

18. Karina A. Serban, Daniela N. Petrusca, Angelia D. Lockett, **Matthew J. Justice**, Lauren Saint, Homer L. Twigg, Michael A. Campos, Irina Petrache. Alpha-1 Antitrypsin (AAT) Enhances Alveolar Macrophages Scavenging During Conditions Simulating COPD Exacerbation. American Thoracic Society International Conference. Denver. 2015.

19. Danting Cao, **Matthew J. Justice**, Irina Petrache, Karina A. Serban. Effect of Endothelial Cell Microparticles on Macrophage Efferocytosis. American Thoracic Society International Conference. Denver. 2015.

20. Catherine R. Sears, George E. Sandusky, Marjorie Albrecht, Christophe Poirier, **Matthew J. Justice**, Irina Petrache. The Role of XPC in DNA Damage, Oxidative Stress and Metaplasia During Chronic Cigarette Smoke Exposure. American Thoracic Society International Conference. Denver. 2015.

21. Erica Beatman, Christophe Poirier, Karina A. Serban, Evgeny Berdyshev, Jacob Saliba, **Matthew J. Justice**, Tamas Ovarecz, David J. Zambrowicz, Kelly Schweitzer, Irina Petrache. Targeting Sphingosine-1-Phosphate Lyase to Enhance Lung S1P and Reduce Experimental Cigarette Smoke-Induced Chronic Lung Injury and Remodeling. San Francisco 2016.

22. Kengo Koike, Erica Beatman, **Matthew J. Justice**, Brian Johnstone, Matthias Clauss, Kelly Schweitzer, Irina Petrache. Preclinical Development of an Antibody Against EMAP II to Treat Cigarette-Smoke (CS)-Induced Emphysema. San Francisco 2016.

23. Kevin Ni, Muhammad U. Mukhtar, Catherine Meador, Danting Cao, **Matthew J. Justice**, Kelly Schweitzer, Keith L. March, Irina Petrache. Priming Adipose Stromal Cells for Enhanced Paracrine Anti-Elastase Activity. San Francisco 2016.

24. Andrew M. Mikosz, Robinah K. Maasa, Seth Winfree, **Matthew J. Justice**, Kenneth Dunn, Irina Petrache, Karina A. Serban. Alpha-1 Antitrypsin Decreases Pro-Inflammatory Monocyte-Endothelial Cells Interactions Via Fractalkine Axis. San Francisco 2016.

Oral Presentations

1. **Matthew J. Justice**, Horia I. Petrache, Measurements of Electrostatic Interactions between Charged Membranes, Indiana Academy of Science, University of Evansville, 2008

2. **Matthew J. Justice**, Horia I. Petrache, X-ray Measurements of Multilamellar Lipid Structures, IUPUI Biomembrane Sciences Center, 2008.

3. **Matthew J. Justice**, Horia I. Petrache, Ceramide inhibits apoptotic cell clearance by affecting cell membrane fusion, IUPUI Biomembrane Sciences Center, 2009.

4. **Matthew J. Justice**, Effects of lipid interactions on model vesicle engulfment by alveolar macrophages. International Ceramide Conference. Montauk, NY, 2013.

5. **Matthew J. Justice**, Lysosomal acid sphingomyelinase regulation of autophagy. Southeastern Regional Lipid Conference. Cashiers, NC, 2014.

6. **Matthew J. Justice**, Lysosomal acid sphingomyelinase regulation of autophagy. Biochemistry Research Day, Indianapolis, IN, 2014.

7. **Matthew J. Justice**, Lysosomal acid sphingomyelinase regulation of autophagy. Indiana University School of Medicine Pulmonary Conference, Indianapolis, IN, 2014.